THE NATURE OF CHAIN-PLANE COUPLING IN $YBa_2Cu_3O_7$

by

WILLIAM A. ATKINSON

B.Sc. (Queen's) 1989
M.Sc. (Alberta) 1991

A Thesis
Submitted to the School of Graduate Studies
in Partial Fulfilment of the Requirements
for the Degree
Doctor of Philosophy

McMaster University

DOCTOR OF PHILOSOPHY (1995)
(Physics)

McMaster University
Hamilton, Ontario

TITLE: The Nature of Chain-Plane Coupling in $YBa_2Cu_3O_7$

AUTHOR: William A. Atkinson

SUPERVISOR: Dr. J. P. Carbotte

NUMBER OF PAGES: viii, 96

THE NATURE OF CHAIN-PLANE COUPLING IN $YBa_2Cu_3O_7$

Abstract

The work in this thesis revolves around a simple model of the high temperature superconductor $YBa_2Cu_3O_{7-\delta}$. Of all of the high temperature materials, $YBa_2Cu_3O_{7-\delta}$ is by far the most widely studied. Despite this, relatively little is understood about it. Although the structure of the unit cell has been known since the discovery of the material, its electronic structure is still a subject of intense controversy. Theories of the electronic structure range from the conventional theories of metallic systems with complicated band structures, to exotic theories of strongly correlated electron systems. Exotic theories are, necessarily, difficult to work with, and we adopt the attitude that it is more fruitful to understand the strengths and weaknesses of the simplest models before pursuing more complicated approaches. For this reason, no attempt is made to provide a comprehensive theory of high temperature superconductivity. Instead a model is chosen which captures the few features of the structure of $YBa_2Cu_3O_{7-\delta}$ which we wish to study.

The main focus of the model is the link between two structural elements within the unit cell—the so called copper-oxide "planes" and "chains". Both the chains and planes are believed to play an active role in determining the highly unusual properties of $YBa_2Cu_3O_{7-\delta}$. At the moment, relatively little is known about the chains, since the planes are suspected to be the more interesting of the two elements and have been more carefully studied. Recently, though, attention has begun to shift towards the chains.

In the chapters which follow, several physical properties of the model are calculated. The calculations allow us to interpret a number of experiments, such as penetration depth, and $YBa_2Cu_3O_7$/Pb Josephson junction experiments. As a result of comparing the theory with experiment, we are able to make a few fairly broad statements about the electronic structure of $YBa_2Cu_3O_7$ in both the normal and superconducting states.

Acknowledgements

First of all, I would like to thank my supervisor, Jules Carbotte, for his patience and guidance. Thanks should also go to the students and post docs making up the condensed matter theory group. It is a wonderful thing to be a part of an active and vibrant group. In particular, I should thank Dwayne Branch and Chris O'Donovan for many helpful discussions over the years. Dimitri Basov has also played an important role in my education, and I would like to thank him for explaining experimental physics to me.

I would like to thank Tamara Hoogerdyk for her patience and persistent cheerfulness throughout the writing of my thesis. Finally, I must thank my parents, Karen and Gerald, for encouraging me in everything that I have tried.

Preface

There are two included papers in this thesis. contained in chapters 4 and 5. These papers were published in the journal *Physical Review B* and have been reprinted here with their permission.

Both of the included papers were written by me. The calculations contained within the papers were also performed by me. although many were checked by J. P. Carbotte. The ideas contained within the papers are the results of lengthy discussions with J. P. Carbotte and others who are acknowledged in the papers. The motivation to do the calculations in the first place came largely from J. P. Carbotte.

Contents

List of Figures

Chapter 1

Introduction

When it was first announced in 1986. high temperature superconductivity caught the imagination of both the public and the scientific conmunity. A Nobel prize was promptly awarded to Bednorz and Müller for their discovery(1986) of the first superconductor ($La_{2-x}Ba_xCuO_4$) with a transition temperature higher than 30 K. Less than a year later, $YBa_2Cu_3O_7$ (Wu et al. 1987)(for which the onset of superconductivity occurs at a temperature more than twice that of $La_{2-x}Ba_xCuO_4$) was discovered. Suddenly, the small (but nonetheless spectacular) demonstration of a piece of supeconductor hovering over a magnet enshrouded in the mist of boiling liquid nitrogen became a part of the standard science demonstration. Euphoria was high. The ease with which $YBa_2Cu_3O_7$ had been discovered could only mean that even higher transition temperatures were just around the corner. It seemed only a matter of time before the Holy Grail of superconductivity—a room temperature superconductor—was discovered.

Theorists were busy. The high temperature materials posed a new problem containing new physics. The theory of conventional superconductivity could not explain these new materials. and there were few hints as to what mechanism could possibly produce such high temperatures. Not surprisingly. under these conditions an incredibly diverse assortment of theories sprang up. And every theory. with a few obvious exceptions. had to be given serious consideration. For theorists. high temperature superconductivity presented an opportunity to become contemplative and re-examine the basic principles of condensed matter physics. and to exercise creative spirit.

Experimentalists were also busy. The initial drive to produce a room temperature superconductor led to the development of hundreds of different materials. In the quest for the key experiment which would unlock the heart of the superconductors. experimentalists

refined their techniques to new levels of precision and sensitivity. and developed new and beautiful techniques. Important experimental results were being produced regularly. and these were carefully digested by theorists. who then fitted them to their models.

At the time of writing this thesis. it has been nearly ten years since the discovery of the first superconductor. The euphoria has faded. The number of superconductivity articles appearing monthly in *Physical Review B* is beginning to decline. The mood is taking on a tone of grimness which is suggestive of a long and torturous path ahead. No elegant model has been discovered. The highest transition temperatures found so far are still only half of room temperature. And while it is fair to say that some real progress towards an understanding has been made by experimentalists. many experiments have been limited in their usefulness by the lack of a theory with which to interpret them. It is beginning to appear as though the next Nobel prize to come out of the high temperature superconductors will not be coming soon.

The work contained in this thesis is one small step towards understanding the high temperature superconductors. No attempt is made to produce a comprehensive theory. Such a theory would likely be quite complicated and difficult to interpret. Instead. the simplest possible model containing the few features of the high T_c materials in which we are interested is studied. The model is relatively easy to work with. and its value is that we are able to calculate a number of experimentally observable quantities with it. The real importance of this model is that it provides a conceptual framework within which experiments may be interpreted and conceived.

1.1 Materials

The work presented in this thesis is primarily concerned with descriptions of the high temperature superconductor $YBa_2Cu_3O_{7-\delta}$ (Y-123) which is one member of the family of Y-Ba-Cu-O (YBCO) superconductors. Y-123 and its related compounds form the most widely studied family of high T_c superconductors. Discovered in 1987 by Wu *et. al.*. the first YBCO compound was found to superconduct at a critical temperature of $T_c = 93$ K. This remarkably high temperature represented an important advance over the only other known class of high T_c materials at the time [the lanthanum family—known generically as La-214—which contains the prominent members $La_{2-x}Ba_xCuO_{4-\delta}$ ($T_c \sim 34$ K) (Bednorz and Müller 1986) and $La_{2-x}Sr_xCuO_{4-\delta}$ ($T_c \sim 37$ K) (van Dover et al. 1987)]. since it could

be made to superconduct at liquid nitrogen temperatures. The accessibility of YBCO to labs without expensive refrigeration equipment has since led to an incredible proliferation of articles.

Since 1987, a vast number of high T_c materials has been discovered, many with critical temperatures much higher than that of Y-123. For example, $Tl_2Ba_2Ca_2Cu_3O_{10}$ has $T_c \sim 125$ K and $HgBa_2Ca_3Cu_4O_{10+\delta}$ has $T_c \sim 120$ K. Relatively little work has been done with these materials for a number of reasons, one of which is the difficulty of working with them: both thallium and mercury are poisonous. Perhaps a bigger reason, however, is that there seems to be an inertia within the research community. The technical aspects of working with YBCO are better developed than with other materials, making it more attractive for experiments.

High T_c materials are produced in a number of forms. Powders are easily produced but generally have poor superconducting properties. Annealing the powders leads to ceramics with large densities of grain boundaries and defects. High quality single crystals of a small number of the high T_c materials have been succesfully grown, and have been the subject of all of the most important experiments to be performed over the last few years. Thin films are also manufactured in large numbers, but tend to have very high densities of twins. Much of the interest in thin films comes from industry.

1.2 Comparison of Y-Ba-Cu-O and Bi-Sr-Ca-Cu-O

Experiments involving single crystals have proved, in general, to be the only experiments in which external factors do not consistently mar results. The two most widely studied groups of materials are the bismuth cuprates [known generically as BSCCO and containing widely studied compound $Bi_2Sr_2CaCu_2O_8$ (Bi-2212)] and the YBCO family. Both of these materials can be grown as single crystals, and the technology of working with these materials is fairly well developed. The two families of compound have proven suitable for different types of experiments. BSCCO can be cleaved to form surfaces of atomic smoothness and is therefore suitable for tunneling and angle resolved photoemission (ARPES) experiments. A single YBCO sample, on the other hand, can be reproducibly hole doped to different levels by annealing in atmospheres of varying oxygen content, making it suitable for studies of superconducting properties as a function of hole density. Furthermore, the quality of the Y-123 thin films and single crystals which are made is substantially higher

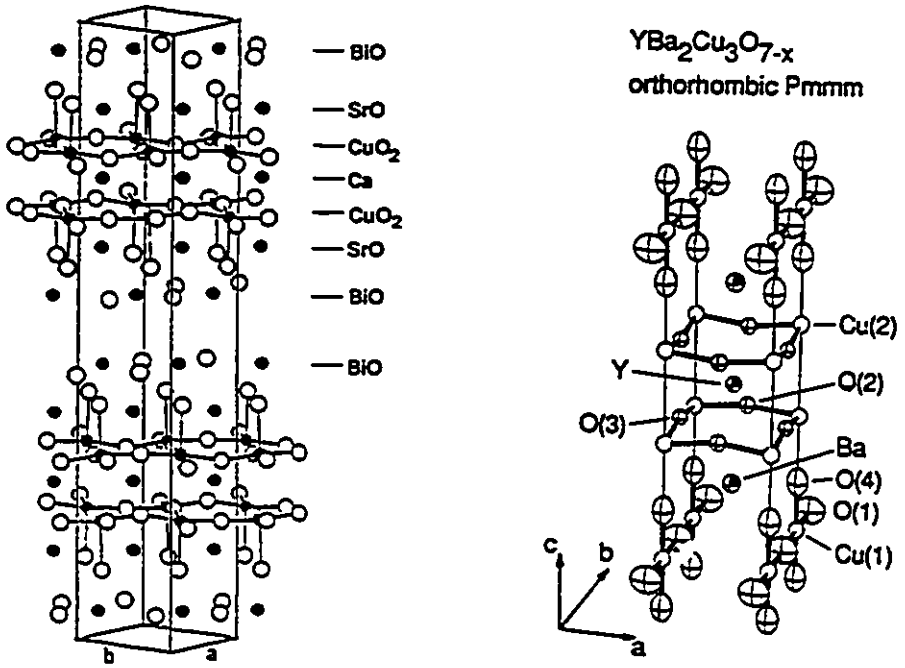

Figure 1.1: Unit cells of BSCCO and YBCO.
Unit cells of (a) $Bi_2Sr_2CaCu_2O_{8+x}$ (Bi-2212) (Hazen 1990) and (b) $YBa_2Cu_3O_{7-\delta}$ (Y-123) (Jorgensen et al. 1990) are shown.

than all of the other cuprate superconductors.

In Fig. 1.1. the unit cells of Bi-2212 and Y-123 are shown. Both of these crystals are based on a layered structure: the Bi-2212 unit cell consists of the stack of layers BiO/SrO/CuO_2/Ca/CuO_2/SrO/BiO while the Y-123 unit cell consists of CuO/BaO/-CuO_2/Y/CuO_2/BaO/CuO. In both of these materials. the CuO_2 planes are conducting and. at optimal doping. display metallic behaviour. The remaining layers are insulating. with the important exception of the CuO "chains" (made up of the Cu(1) and O(1) ions) and possibly the BiO planes. Images taken with a scanning tunneling microscope (STM) of the surface of a BSCCO crystal suggest that there is a semiconducting gap in the BiO layers (Hasegawa and Kitazawa 1990). making them insulating. while ARPES experiments are contradictory as to whether the BiO layer has a Fermi surface (Aebi et al. 1994: Wells et al. 1990). Evidence that the CuO chains are metallic can be found in electron-positron annihilation experiments (Pankaluoto et al. 1994: Haghighi et al. 1991: Manuel et al. 1993)

and photoemission experiments (Tobin et al. 1992; Liu et al. 1992), which map out a Fermi surface which is in agreement with first principles band structure calculations (Pickett et al. 1990; Pickett et al. 1992; Yu et al. 1993). In untwinned crystals, it is common to separate the chain conductivity from the plane conductivity by assuming that the difference between the a (perpendicular to the chains) and b (parallel to the chains) axis conductivities comes from the chains. In dc resistivity (Gagnon et al. 1994; Friedmann et al. 1990), penetration depth measurements (Zhang et al. 1994) and optical conductivity measurements (Basov et al. 1995) it has been found that the conductivity of the chains is approximately equal to the conductivity of the planes.

If the effects of the chains are accounted for, then the behaviour of the CuO_2 planes in Bi-2212 and Y-123 are fairly similar. The real difference lies in the c axis transport properities. dc resistivity measurements in the normal state have found that while the resistivity parallel to the CuO_2 planes ρ_{ab} is very similar in both BSCCO and YBCO, the resistivity ρ_c along the c axis is dramatically different, both in magnitude and in temperature dependence. For Y-123, $\rho_c/\rho_{ab} \sim O(50)$ and both ρ_c and ρ_{ab} increase linearly with temperature, T. While this temperature dependence suggests an unconventional scattering mechanism, it is nonetheless metallic. For $Bi_2Sr_2CuO_6$ (Bi-2201), on the other hand, $\rho_c/\rho_{ab} \sim O(10^4)$ at 100 K and, although ρ_{ab} still varies linearly with T, $\rho_c \propto 1/T$ for $T < 100$ K (Iye 1992). The behaviour of ρ_c in BSCCO has been described as "semiconducting".

Further evidence of the nonmetallic nature of BSCCO in the c direction can be found in measurements of an intrinsic Josephson effect. In 1962 Josephson (1962) showed that a current may flow through a superconductor-insulator-superconductor (SIS) junction due to pair tunneling through the junction. There is no voltage drop across the junction provided that the supercurrent through the junction is less than the *critical current* I_c. If the critical current is small enough that it does not generate a significant magnetic field, it will vary in an applied magnetic field according to

$$I_c(H) = I_c(0)\left|\frac{\sin(\pi H/H_0)}{\pi H/H_0}\right|.$$

where H is the applied magnetic field and H_0 is the magnetic field at which one flux quantum is enclosed by the junction. A simple test for Josephson coupling, then, is to look for this Fraunhoffer pattern in the field dependence of I_c. This has been done for Bi-2212 in a series of careful and fairly convincing experiments (Kleiner and Müller 1994), and it seems clear that one of the layers within each unit cell acts as an insulating layer through which

electrons must tunnel in order to travel along the c axis. Until very recently, measurements done on Y-123 have not revealed any Josephson coupling. Ling *et al.* (1995), now claim to have measured an intrinsic Josephson effect, although their results should be viewed with caution as there are a number of serious difficulties which they had to overcome in order to perform the experiment.

Based on the structure of the Bi-2212 and Y-123 unit cells, it seems possible that the source of the differences in the c axis transport properties stems from the differences between the BiO and CuO layers. The differences are probably not due to the Sr and Ba ions since substitution of Sr for Ba in Y-123 does not change its superconducting properities significantly (Veal et al. 1987; Wada and Mihara 1987). A reasonable picture of the c axis charge transport in both YBCO and BSCCO is that it occurs through the O(4) ("apical") oxygens. These ions are nominally part of the SrO and BaO layers, although they are much more closely bound to the adjacent Cu ions along the c axis. One obvious possibility, then, is that the BiO layer may form an insulating barrier through which electrons must tunnel in order to move along the c axis. Another possibility is that the Ca ion which lies sandwiched between the CuO_2 layers may act as some kind of barrier to c axis transport. A summary of the various speculations concerning interlayer coupling can be found in Ref. (Cooper and Gray 1994).

It is important to stress that the above discussion applies only to optimally doped $YBa_2Cu_3O_{7-\delta}$ (for which $\delta \sim 0.05$). In the underdoped regime ($\delta > 0.15$), Y-123 begins to display semiconducting behaviour along the c axis similar to that of BSCCO.

1.3 Comparison with Conventional Superconductors

1.3.1 Theory of Conventional Superconductors

In this section, we will review some of the most important aspects of the conventional theory of superconductivity. There are a number of texts which give excellent reviews of the theory (Rickayzen 1965; Parks 1969) for any reader who is interested in learning more. The purpose of this section is provide some background as an introduction to the high T_c superconductors.

In 1956, Cooper showed that the ground state of a normal metal is unstable to the formation of "Cooper pairs" at zero temperature. He showed that a small attractive

interaction between the electrons is sufficient to cause a transition to a new phase—the superconducting phase. In 1957, Bardeen, Cooper and Schrieffer (BCS) (1957) were able to find the ground state wavefunction of a superconducting system:

$$\Psi_{BCS} = \prod_k [u_k + v_k c^\dagger_{k\uparrow} c^\dagger_{-k\downarrow}]|0\rangle.$$

where $|0\rangle$ is the vacuum state and $c^\dagger_{k\uparrow}$ creates a spin-up electron with momentum k. The coefficients u_k and v_k indicate respectively the probability amplitude that a state k is unoccupied or occupied by a pair. They are

$$u_k^2 = \frac{1}{2}\left[1 - \frac{\xi_k}{E_k}\right]$$
$$v_k^2 = \frac{1}{2}\left[1 + \frac{\xi_k}{E_k}\right].$$

In the above equations ξ is the normal state energy dispersion, written so that the zero of energy is at the Fermi surface. For a free electron gas it is

$$\xi_k = \frac{\hbar^2 k^2}{2m} - \mu.$$

where μ is the chemical potential and m is the electron mass. The excitation spectrum in the superconducting state is

$$E_k = \sqrt{\xi_k^2 + \Delta^2}. \tag{1.1}$$

where Δ is the superconducting order parameter or "gap". The term "gap" arises because the minimum excitation energy in the superconducting state is $|\Delta|$. The gap in the excitation spectrum is one of the remarkable predictions of BCS theory, and it is responsible for, among other things, the infinite conductivity in the superconducting state.

The BCS wavefunction is the ground state of the well known BCS Hamiltonian

$$H_{BCS} = \sum_{k,\sigma} c^\dagger_{k\sigma} c_{k\sigma} \xi_k - \frac{1}{\Omega} \sum_{k,k'} V_{kk'} c^\dagger_{k\uparrow} c^\dagger_{-k\downarrow} c_{-k'\downarrow} c_{k'\uparrow}. \tag{1.2}$$

in which σ is a spin index, Ω is the volume of the crystal and $V_{kk'}$ is the pairing interaction.

In conventional superconductors, the pairing interaction is due to the exchange of phonons between electrons. The pairing interaction is modelled by

$$V_{kk'} = \begin{cases} V & |\xi_k|, |\xi_{k'}| < \hbar\omega_D \\ 0 & \text{otherwise.} \end{cases} \tag{1.3}$$

where ω_D is the Debye frequency and V is the strength of the electron-phonon coupling. In this form for $V_{kk'}$, the pairing is restricted to electrons within $\hbar\omega_D$ of the Fermi surface. The Debye energy is the characteristic energy of the phonons which are exchanged and therefore represents the maximum change in energy of an electron which is scattered by a phonon. In a conventional superconductor, $\hbar\omega_D \sim 10$ meV, while the Fermi energy is $\epsilon_F \sim 10$ eV. Scattering events are therefore effectively restricted to the Fermi surface.

In order to solve the BCS Hamiltonian, it is usual to make a *mean field approximation* (Rickayzen 1965; Parks 1969). The order parameter is defined by

$$\Delta = \frac{V}{\Omega}\sum_k \langle c_{-k\downarrow} c_{k\uparrow}\rangle. \tag{1.4}$$

where $\langle\ \rangle$ represents a thermal average, and the mean field Hamiltonian is

$$H_{MF} = \sum_{k,\sigma} c^\dagger_{k\sigma} c_{k\sigma}\xi_k - \frac{1}{\Omega}\sum_k \left[c^\dagger_{k\uparrow} c^\dagger_{-k\downarrow}\Delta + c_{-k\downarrow}c_{k\uparrow}\Delta^*\right]. \tag{1.5}$$

Diagonalization of this Hamiltonian leads to the quasiparticle spectrum of Eq. (1.1). Once the Hamiltonian is diagonalized, Eq. (1.4) can be solved self consistently for Δ. Equation (1.4) yields two types of solution: above a certain *critical temperature* T_c, the only solution is $\Delta = 0$ while below the critical temperature Δ will be nonzero. Δ will be temperature dependent, having its maximum value at $T = 0$ and decreasing monotonically to zero at T_c. The critical temperature is given by

$$T_c = 1.13\hbar\omega_D e^{-1/N(0)V}. \tag{1.6}$$

where $N(0)$ is the density of states at the Fermi surface in the normal state. There is a universal relationship between $\Delta(T = 0)$ and T_c in BCS theory:

$$\frac{2\Delta(T = 0)}{k_B T_c} = 3.53 \tag{1.7}$$

Equations (1.6) and (1.7) rarely apply exactly to real materials and definitely do *not* apply to high T_c superconductors. They are useful, however, as they provide a standard against which to compare later work.

1.3.2 Coherence Length

The most striking difference between the high T_c materials and the conventional superconductors is the difference in transition temperature. Most conventional materials

become superconducting at temperatures of the order 1–10 K. Transition temperatures in the cuprate superconductors typically range from 30 K in the lanthanum compounds to as high as 150 K for certain mercury based compounds.

One result of the large critical temperature is an extremely small coherence length ξ_0. The coherence length is the distance scale over which the superconducting order parameter Δ may vary spatially. In the BCS theory it is [see. *eg.* Rickayzen (1965)]

$$\xi_0 = \frac{\hbar v_f}{\pi \Delta}.$$

where v_f is the electron Fermi velocity. and Δ is the magnitude of the BCS order parameter (also known as the "gap"). For a BCS superconductor with $T_c = 100$ K. $\Delta = 15$ meV [*cf.* Eq. (1.7)]. The Fermi velocity can be estimated from the bandwidth of the conduction band. and since the high T_c materials are highly anisotropic. there will be substantial differences between v_f in the various directions. The coherence length will therefore be anisotropic as well. In the a and b directions (parallel to the CuO_2 planes) the CuO_2 bandwidth is $t_{\|} \sim 1$ eV. The Fermi velocity can be estimated as

$$v_{fa} \sim v_{fb} \sim \frac{a t_{\|}}{\hbar \pi}$$

where a is the lattice constant in the a direction. For the BSCCO compounds. $a \sim 5\mathring{A}$. The coherence length in the planes is therefore

$$\xi_a \sim \xi_b \sim \frac{a t_{\|}}{\pi^2 \Delta} \sim 25\mathring{A}.$$

The bandwidth along the c axis is considerably smaller than in the CuO_2 planes. In the BSCCO compounds. it is typically $t_{\perp} \sim 10$ meV. Since the unit cell size along the c axis is $c \sim 30\mathring{A}$. the coherence length in BSCCO is

$$\xi_c \sim \frac{c t_{\perp}}{\pi^2 \Delta} \sim 2\mathring{A}.$$

These values are typical for most of the high T_c materials and distinguish them from the conventional materials in one important way: the fact that ξ_c is substantially less than the length of the unit cell along the c axis allows the order parameter to vary spatially *over the unit cell.* In the conventional materials. where the coherence lengths are 10^3 or $10^4\mathring{A}$. the structure of the unit cell is invisible to Δ. In the high T_c materials. the value of Δ may depend on the layer type.

In YBCO, the coherence lengths in the CuO_2 planes are very similar to those of BSCCO. The c axis coherence length, however, is somewhat larger since the bandwidth along the c axis is $t_\perp \sim 100$ meV and $c \sim 11.6\mathring{A}$:

$$\xi_c \sim 8\mathring{A}.$$

The coherence length is still smaller than the c axis lattice constant, although this estimate suggests that the spatial variation of the order parameter on the length scale of the unit cell will be suppressed somewhat. It should be noted, however, that estimates of ξ_c based on the upper critical magnetic field suggest that $\xi_c \sim 3\mathring{A}$, and therefore support the idea the Δ might vary within the unit cell.

1.3.3 Isotope Effect

In conventional superconductors, T_c has been found to shift when different isotopes of the same ion are substituted for one another. The change in T_c is related to the change in the mass of the isotope and the relationship is given by

$$T_c \propto M^{-\alpha}.$$

where M is the mass of the isotope. The reason that the mass of the ions in the crystal has an effect on the superconducting properties is that the superconductivity is mediated by phonons. In Eq. (1.6), we showed that, for a BCS superconductor, T_c is proportional to ω_D, the characteristic phonon frequency. If the ions are assumed to move in a harmonic potential, then the phonon frequency is inversely proportional to the ion mass:

$$\omega_D \propto M^{-0.5}.$$

For BCS superconductors, therefore, $\alpha = 0.5$, although it may be reduced from this substantially by the Coulomb repulsion between electrons (Carbotte 1990). Generally, there is a correlation between T_c and α, since Coulomb repulsions also tend to reduce T_c. For example, Cd ($T_c = 0.56$ K), Zn ($T_c = 0.875$ K) and Hg ($T_c = 4.1$ K) have $\alpha = 0.32$, $\alpha = 0.45$ and $\alpha = 0.5$ respectively (Kittel 1986). In some cases, (such as Ru and Zr, for which $T_c = 0.5$ K) α can vanish.

The high T_c materials are rather strange in comparison to the conventional materials (see, for example, the review by Franck (1994)). Most experiments have measured the

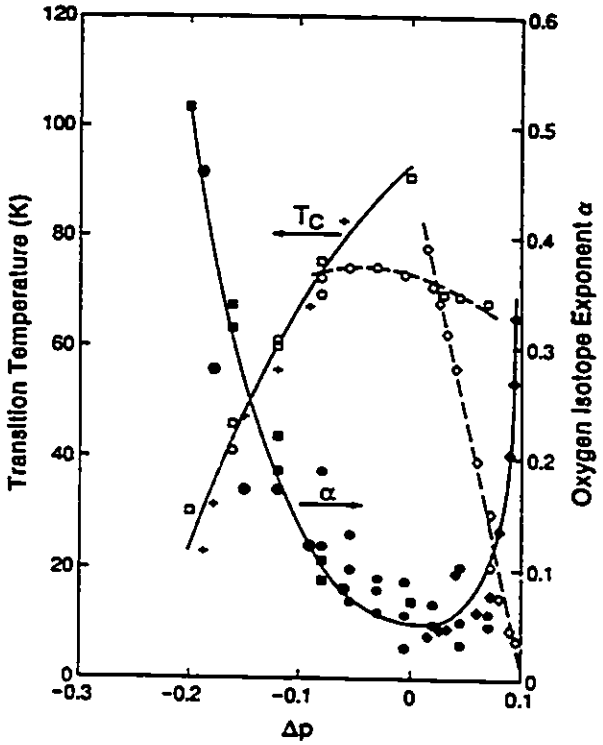

Figure 1.2: Correlation between the isotope effect and T_c.
The oxygen isotope exponent α (filled symbols). and transition temperature T_c (open symbols) are shown as a function of mobile hole concentration per CuO plane. relative to the optimal hole concentration. Squares $(Y_{1-x}Pr_x)Ba_2Cu_3O_7$: Circles $(Y_{0.8-x}Pr_{0.2}Ca_x)Ba_2Cu_3O_7$: Diamonds $YBa_2(Cu_{1-x}Zn_x)O_7$: Crosses $YBa_2(Cu_{1-x}Co_x)O_7$. The hole concentration is varied though impurity doping. Reprinted from Ref. (Franck 1994).

oxygen isotope effect (the change in T_c induced by substituting ^{18}O for ^{16}O). In all cases. the optimally doped materials have a small ($\alpha < 0.05$) or zero isotope effect. This cannot be the result of Coulomb interactions. however. as the critical temperatures are far too high to be accounted for in a manner which is consistent with such small α. This has been taken as evidence that phonons are not the pairing mechanism responsible for the superconductivity. This is not a convincing argument. though. because the high T_c materials have substantial isotope effects away from optimal doping. In fact. doping experiments show a correlation between the concentration of charge carriers (holes) and α. In Fig. 1.2. the isotope effect is shown for a number of doped members of the YBCO family. The data shows quite clearly

that in general, the YBCO compounds *do* have an isotope effect which is comparable to that of the conventional materials, *except* for materials which are near optimal doping. The important question, then, is whether the absence of an isotope effect in materials with the highest T_c's indicates that phonons are not the interaction responsible for the superconductivity or whether it indicates that the phonons are unconventional. Certainly, the phonons cannot be conventional. Calculations of T_c based on the conventional (Eliashberg) theory of superconductivity cannot account for the high critical temperatures found in Y-123 (de Wette et al. 1988).

The possibility that the pairing interaction is electronic in origin has been widely examined. The most popular theories [spin fluctuations (Monthoux and Pines 1993), resonating valence bond theories (Kotliar 1988; Lee and Nagaosa 1992) and many variations of the Hubbard model (Dagotto 1994)] have all attempted to use strong Coulomb repulsions as the source of their pairing interaction. The failure of these models to explain high T_c superconductivity convincingly, coupled with the growing evidence of large electron coupling to certain phonon modes, has recently lead to a resurgence of unconventional phonon theories (Song and Annett 1995; Kresin and Wolf 1994; Plakida 1995; Nazarenko and Dagotto).

1.3.4 Symmetry of the Order Parameter

One of the features of the BCS theory of superconductivity is that the order parameter Δ has no internal structure. The order parameter can, in a loose sense, be thought of as the wavefunction of a Cooper pair. Since the two electrons in a Cooper pair can be described in terms of a centre of mass coordinate R and a relative coordinate r, Δ is generally a function of both coordinates. In BCS theory, however, the translational invariance of the Hamiltonian eliminates the dependence of Δ on R. Problems in which the translational invariance is interrupted (say, by a grain boundary) are usually handled in the phenomenological theory of Ginzburg and Landau (Rickayzen 1965; deGennes 1966), where the dependence of Δ on R is retained.

The internal structure of the order parameter can be directly traced to the form of the pairing interaction in the BCS Hamiltonian. In Eq. (1.2), for example, it can be seen that momentum k in the pairing potential is the relative momentum of the pair $c_{-k\downarrow}c_{k\uparrow}$. The momentum label k is conjugate to the relative coordinate r, so that the internal structure (including the size) of the pair is determined by $V_{kk'}$. Since, in BCS theory, the ansatz is

made that the pairing interaction is isotropic, the resulting order parameter is independent of k and has an "isotropic s wave symmetry".

In the high T_c materials, it is generally (although not universally) believed that the pairing interaction $V_{kk'}$ is *not* isotropic, and that Δ is actually a function of the relative momentum k. Although the actual symmetry of Δ_k remains undetermined at this point, the most popular point of view is that it has d wave symmetry. A function with d wave symmetry has the property that under a rotation of $\pi/2$ about the c axis ($k_x \rightarrow k_y$, $k_y \rightarrow -k_x$, $k_z \rightarrow k_z$), the function changes sign. Two forms of the order parameter which exhibit d wave symmetry are

$$\Delta_k = \Delta_0[\cos(k_x) - \cos(k_y)].$$

and

$$\Delta_k = \Delta_0 \cos(2\phi).$$

where ϕ is the angular variable in cylindrical coordinates (*ie.* $k_x = k\cos(\phi)$, $k_y = k\sin(\phi)$), and $-\pi < k_x, k_y \leq \pi$. Both versions of Δ_k have the same nodal structure as the function $k_x^2 - k_y^2$ (*ie.* $\Delta_k = 0$ when $k_x = \pm k_y$), and are therefore known as $d_{x^2-y^2}$ order parameters.

One of the first indications that the order parameter might not be isotropic came from penetration depth measurements (Hardy et al. 1993) of single crystals of Y-123. These experiments indicated that the quasiparticle spectrum of Y-123 has a finite number of excitations at all energies. This result is incompatible with conventional BCS theory since the minimum excitation energy in BCS theory is Δ. It has been shown, however, that the low T behaviour of the penetration depth is compatible with any anisotropic order parameter Δ_k which vanishes at one or more lines along the Fermi surface (Annett et al. 1991). As a simple example, both of the order parameters given above will vanish on a cylindrical Fermi surface of radius k_f along the lines $k_x = \pm k_y$, $k_f^2 = k_x^2 + k_y^2$.

Probably the most compelling evidence in favour of unconventional pairing comes from a series of recent experiments which measure interference patterns of Josephson junctions (see chapter 5 for a description of Josephson tunneling). Josephson (1962) showed that a finite supercurrent may flow through a thin insulating barrier which separates two superconductors. The current is the result of pair tunneling through the barrier and it differs from the tunneling current in the normal state by the fact that the current is not driven by a voltage drop across the junction. Instead, the current is driven by the *phase*

difference between the order parameters on either side of the junction:

$$I(\phi) = I_c \sin(\phi).$$

where ϕ is the phase difference between Δ on either side of the junction. and I_c is the maximum (*critical*) current through the junction. Because the current is driven by a phase difference, it is possible to construct "two-slit" experiments in which the phase differences in Δ_k for different values of k will interfere.

The most straightforward kind of experiments look for interference in the tunneling current through pairs of Josephson junctions on a single crystal. The junctions are designed to allow pairs with either large k_x or k_y components of momentum to tunnel. If the current of the two junction is combined. then the total current will not simply be the sum of the two magnitudes. but will be the sum of the *(complex) amplitudes* of the two currents. In exactly the same way as in a two slit experiment. the currents may interfere constructively or destructively. In a superconductor with an isotropic s wave order parameter Δ. there is no phase difference between pairs of different momenta and the currents interfere constructively. In a d wave superconductor there is a relative phase of π in Δ_k between $k = (0.\kappa)$ and $k = (\kappa.0)$. and there will be total destructive interference of the current through the two junctions. Of the experiments designed to look for the interference effects most (Wollman et al. 1993: Wollman et al. 1995: Tsuei et al. 1994: Brawner and Ott 1994: Miller et al. 1995: Mathai et al. 1995) are consistent with a d wave order parameter. There are some exceptions to these findings (Chaudhari and Lin 1994: Sun et al. 1994). however. and some criticism that the interference experiments are susceptible to stray magnetic fields and trapped flux. Nevertheless. the experiments provide a relatively convincing argument in favour of a d wave order parameter.

1.3.5 Spatial Variation of Δ

It is generally accepted that the source of the pairing interaction in the high T_c materials lies in the CuO_2 planes. The short coherence length along the c axis ($\xi_c \sim 3\mathring{A}$) means that there can be a large variation of the superfluid wavefunction between adjacent planes within the unit cell. In other words. the translational invariance which exists in the conventional superconductors (where the microscopic structure of the lattice is invisible to pairs whose coherence lengths are typically of the order of $10^3\mathring{A}$) does not exist in the high T_c materials so that Δ is generally a function of the centre of mass coordinate R. For this

reason, it is common practice to associate an order parameter with each layer separately in the high T_c materials. Most theories, in fact, only consider a single CuO_2 plane and ignore the coupling to adjacent layers. We stress here that this point of view is only possible because the short coherence length allows one to define an order parameter within each of the CuO_2 layers separately.

Despite the popular view that the secret to high temperature superconductivity lies within a single CuO_2 plane, there have been some simple theoretical models which examine the spatial structure of Δ between the various planes. One of the most common models is the S/N model, in which there is an intrinsically superconducting layer (S) and an intrinsically normal layer (N) in the unit cell. The word "intrinsic" refers to the behaviour of the the layer in isolation. In other words, the S layers contain a pairing interaction which causes a superconducting transition while the N layers do not.

The layered S/N model is reminiscent of the original proximity effect models (McMillan 1968; deGennes 1966) which were used to describe the effect of placing a normal metal in contact with a superconductor. There, it was found that the S/N system differs from the isolated S and N systems in two ways: the critical temperature of the combined system is lower than that of the isolated S system, and the N system is driven superconducting near the junction by its proximity to the S system. Although the S and N halves of the S/N system have the same T_c, the size of the gap is quite different in each, with the gap in the S layer being depressed slightly from its value in isolation, and the induced gap in the N system being quite small.

The behaviour of the layered S/N model for the high T_c materials is very similar: there is an induced gap in the N layers, and the T_c of the system is depressed by the coupling. This is discussed in more detail in chapters 2 and 3, as well as in Atkinson and Carbotte (1995a). One of the main differences between the layered S/N models and the original proximity effect models is the treatment of the coupling. In the microscopic system it is possible to treat the coupling exactly (provided it is coherent), while in the macroscopic system it is treated as a perturbation.

Most layered S/N models have been geared towards explaining the apparent nodal structure of the order parameter while retaining the s wave symmetry of the order parameter (Bulaevskii and Zyskin 1990; Abrikosov 1991; Abrikosov and Klemm 1992; Simonov 1993; Tachiki et al. 1992; Takahashi and Tachiki 1990; Buzdin et al. 1992a; Buzdin et al. 1992b). In other words, the nodes in the gap seen by experiment are conjectured to be

the result of variations of the pair wavefunction as a function of the centre of mass coordinate R, rather than of the relative coordinate r (*cf.* Sec. 1.3.4). These models have had some success in explaining some simple properties(Atkinson and Carbotte 1995b: Klemm and Liu 1995), such as the penetration depth experiment of Hardy *et al.*(1993), but have failed to account for a number of important experiments, such as the Josephson tunneling experiments described in Sec. 1.3.4. Furthermore, the layered S/N models are really only applicable to YBCO, since there is no clear evidence that any of the other materials contains a metallic layer which is not a CuO_2 layer.

A related model is the layered S/S′ model, in which the unit cell has two distinct superconducting layers. Early interest in the model (Liu and Klemm 1992: Schneider et al. 1989: Kettemann and Efetov 1992: Liu and Klemm 1993) was concerned with the differences between intralayer coupling (which favoured singlet pairing) and interlayer coupling (which could favour either singlet or triplet pairing). More recently, studies of the S/S′ model have been revived in an attempt to understand the internal structure of the CuO_2 bilayers (Kuboki and Lee 1995: Liu et al. 1995: Tikofsky 1995).

1.4 Overview

The electronic structure of the high T_c materials is poorly understood, both in the normal and superconducting states. The work in this thesis is an attempt to describe the superconducting state. As we have shown in this chapter, there is strong evidence that the superconducting state is unconventional. We discussed a number of experiments, for example, which seem to indicate that the Cooper pairs have an internal structure. In this work, we will adopt the ansatz that this internal structure has a $d_{x^2-y^2}$ symmetry. There have been a number of calculations of the properties of a single CuO_2 plane with a $d_{x^2-y^2}$ order parameter (Zhou and Schulz 1992: Fedro and Koelling 1993: Jiang and Carbotte 1993: Bulut and Scalapino 1992), and these models have been fairly successful at explaining, at least qualitatively, many of the properties of the high T_c materials.

In the work presented here, a model is used in which there is both a CuO_2 plane and a CuO chain in the unit cell. One of the goals of this work is to understand how the chains will change the results of calculations involving a single plane. A second goal is to calculate c axis transport properties, which cannot be found from the single layer models. The third goal of this work is to learn more about the nature of the chain-plane coupling

by comparing our calculations with experiment. This last goal is the most interesting since it is also the most fundamental.

In chapter 2, the chain-plane model will be introduced. In chapter 3, the density of states (DOS) will be discussed and interpreted in terms of two experiments—the low temperature heat capacity and the Knight shift. In chapter 4, a published paper will be included in which the penetration depth is caclulated for the chain-plane model. In chapter 5, the model will be used to provide a possible explanation of tunneling experiments which are in apparent contradiction with the d wave model. Finally, in chapter 6, there will be a discussion of the conclusions which can be drawn from our work with the chain-plane model.

Chapter 2

A Simple Model for $YBa_2Cu_3O_{7-\delta}$

2.1 Motivation

In this chapter we will introduce a simple model Hamiltonian for $YBa_2Cu_3O_{7-\delta}$ which is designed to capture a few of the essential features of the electronic structure. To begin with, we will assume that at optimal doping Y-123 can be reasonably described by a Fermi liquid model.

Whether or not optimally doped high T_c materials can be described by a Fermi liquid is a point of controversy. It is generally agreed that the parent compound $YBa_2Cu_3O_6$ is not a Fermi liquid, as band structure calculations predict that it is metallic, while it is, in fact, an antiferromagnetic insulator. The discrepancy stems from the Coulomb repulsions, which are treated at the mean field level in band structure calculations. The Coulomb repulsions between electrons tend to localize the electrons at the copper sites in the CuO_2 planes. With the removal of electrons from the CuO_2 planes, however, the Coulomb repulsion becomes less important. The hole-doped compound $YBa_2Cu_3O_{6+x}$ becomes conducting at $x \sim 0.3$. The conductivity is extremely anisotropic [$\rho_\perp/\rho_\parallel \sim 10^3$ (Cooper and Gray 1994)] and is largest in the CuO_2 planes. The planes are not metallic, however, as we can show from a simple estimate of the mean free path based on the dc resistivity.

In the semiclassical model, the resistivity ρ is related to the mean free path l by

$$l = \frac{v_f m^*}{ne^2\rho} \tag{2.1}$$

where m^* and v_f are the effective mass and Fermi velocity of the conduction electrons respectively and n is the density of charge carriers. For the in-plane mean free path, we can

estimate m^* and v_f from the bandwidth $t_\parallel$:

$$v_f \sim \frac{t_\parallel a}{\hbar\pi}$$
$$m^* \sim \frac{\hbar^2\pi^2}{t_\parallel a^2}.$$

where $a = 3.8\mathring{A}$ is the lattice constant in the plane. The density of carriers can be estimated by assuming that there are two carriers per unit cell. Then $n \sim 1.4 \times 10^{22}$ cm^{-3}. Near the metal-insulator transition ($x \sim 0.4$. for example). the resistivity is $\rho_\parallel \sim 1$ mΩ·cm $= 1.1 \times 10^{-15}$ s (Cooper and Gray 1994). From this it follows that

$$l \sim 3\mathring{A}.$$

The planes are not metallic. therefore. since the mean free path must be several unit cells in length for coherent Bloch states to form.

Superconductivity also becomes possible for $x \sim 0.3$. and T_c increases with increasing x thereafter. The highest T_c occurs at $x \sim 0.95$. at which point Y-123 is *optimally doped*. For $x < 0.95$. Y-123 is *underdoped*. As optimal doping is approached. the dc conductivity improves. both within the CuO_2 planes and along the c axis. At optimal doping. the mean free paths can be estimated from Eq. (2.1) to be $l_\parallel \sim 30\mathring{A}$ and $l_\perp \sim 1\mathring{A}$. The in-plane mean free path is roughly 10 lattice spacings. and whether or not the planes are metallic will depend on whether the estimate is too high or too low. There is a qualitative difference in dc and optical conductivities for $x = 0.95$ and $x < 0.8$. however. which suggests that the in-plane behaviour is metallic for $x = 0.95$ (Cooper and Gray 1994). Although it is not generally possible to *overdope* Y-123. it is possible to overdope another high T_c material $La_{2-x}Sr_xCuO_4$ (LSCO). In the overdoped regime $x > 0.15$. LSCO is known to be a true metal (Iye 1992). There is some direct evidence that the optimally doped high T_c materials are Fermi liquids from angle resolved photoemission (ARPES) and positron annihilation experiments (Shen et al. 1993a: Shen et al. 1993b: Hwu et al. 1991: Kelley et al. 1993) which have found a Fermi surface in a number of high T_c materials. In this work. we will take the point of view that both the CuO_2 planes and the CuO chains are Fermi liquids. Electrons in the chains and planes are therefore assumed to be in (coherent) Bloch states.

Since the above estimate of the c axis mean free path suggests that coherent Bloch states do not form along the c axis. it is somewhat surprising that the temperature dependence of the dc resistivity (at optimal doping) appears "metallic". Optical conductivity

measurements (Homes et al. 1995a) have also found that for $x > 0.85$. the c axis conductivity appears weakly metallic, but with an enormously broad Drude peak. The source of the scattering along the c axis is unkown. Recently (Ling et al. 1995) there has been some suggestion that the Yttrium ion. which is sandwiched between two CuO_2 layers. may be a source of incoherence. Another suggestion (Leggett 1992) is that the coupling between adjacent unit cells along the c axis is not sufficient to overcome thermal fluctuations within the CuO_2 layers, leading to a "dephasing" of the unit cells. The term "dephasing" refers to the destruction of the phase coherence between adjacent unit cells which is necessary for a Bloch state to form. A third possibility has been proposed by Anderson (1992). in which the CuO_2 planes are in a non-Fermi liquid state. Transport of charge along the c axis involves the removal (or insertion) of single electrons from (or into) the strongly correlated many-body wavefunctions describing each plane. leading to incoherence. A short review of the various theories of c axis transport is contained in Cooper and Gray (1994).

As of yet. there are no theories of c axis transport which include a description of the CuO chains in Y-123. This is because they present an added level of complication to the model. The important question which must be addressed—and which forms the basis of much of the work presented in this thesis—is what is the nature of the coupling between the chains and the planes? At first glance it may seem that c axis transport properties hold the key to understanding the chain-plane coupling. Certainly the nature of the coupling between the chains and planes will be reflected in the c axis dc and optical conductivities. but to include both the incoherence and the chain-plane coupling in a single theory would introduce an unnecessary level of complication. In this work we will ignore the c axis incoherence. and will. instead discuss experiments in which in is possible to extract information about the chain-plane coupling without looking at c axis transport properties.

Since relatively little is known about the chain-plane coupling. we will take the simplest possible case. in which the chains and planes are coupled *coherently* (*ie.* the wavevector k is conserved when electrons hop between chains and planes). Furthermore. the model is simplified by assuming that a unit cell contains a single CuO_2 plane and a single CuO chain. Since there is no source of incoherence in this model. the electrons also form Bloch states along the c axis.

2.2 Microscopic Model

2.2.1 Normal state

In second quantised notation, the Hamiltonian for a Bloch metal is

$$H_0 = \int d^3r \Psi^\dagger(r)\, h_0 \Psi(r) \tag{2.2}$$

where $\Psi(r)$ are the field operators and h_0 is the first quantised Hamiltonian for an electron moving in a periodic potential $U(r)$:

$$h_0 = -\frac{\hbar^2\nabla^2}{2m} + U(r).$$

The high T_c superconductors are generally treated as tight binding materials in which there is a weak overlap between copper d orbitals and adjacent oxygen p orbitals. In such a case, it is advantageous to expand the field in terms of Wannier states:

$$\Psi(r) = \sum_{i,n,\sigma} c_{in\sigma}\phi_i(r - R_{in}). \tag{2.3}$$

The state $\phi_i(r - R_{in})$ is the Wannier state associated with the i^{th} ion in the n^{th} unit cell. The wavefunction is centred about R_{in}, the location of the ion. In the case of tight binding materials, the Wannier state is localised about the site and closely resembles the atomic wavefunction of the isolated ion. The operator $c_{in\sigma}$ annihilates an electron in the state $\phi_i(r - R_{in})$ with spin σ. The Hamiltonian can now be written

$$\begin{aligned} H_0 &= \sum_{i,n,\sigma}\sum_{j,m} c^\dagger_{in\sigma} c_{jm\sigma} \int d^3r\, \phi_i^*(r - R_{in}) h_0 \phi_j(r - R_{jm}) \\ &= -\sum_{i,n,\sigma}\sum_{j,m,\sigma} t_{in;jm} c^\dagger_{in\sigma} c_{jm\sigma} \end{aligned} \tag{2.4}$$

Now, in the case of a tight binding model, the states $\phi_i(r - R_{in})$ are localised about the ion sites R_{in} so that the leading order contributions to H_0 are

$$H_0 = -\sum_{i,n,\sigma} t_{in;in} c^\dagger_{in\sigma} c_{in\sigma} - \sum_{\langle in,jm\rangle}\sum_{\sigma} t_{in;jm} c^\dagger_{in\sigma} c_{jm\sigma}. \tag{2.5}$$

where the angle brackets indicate that the sum is over nearest neighbour pairs. This is the nearest neighbour tight binding Hamiltonian. It can be written in momentum space using

$$c_{in\sigma} = \frac{1}{\sqrt{N}} \sum_k c_{ik\sigma} e^{ik\cdot R_{in}}. \tag{2.6}$$

where $c_{ik\sigma}$ are the annihilation operators for the tight binding Bloch states and N is the total number of unit cells within the crystal. The factor of $1/\sqrt{N}$ ensures that the anti-commutators $\{c_{jm\sigma}, c_{in\sigma'}\}$ and $\{c_{jk\sigma}, c_{ik\sigma'}\}$ are both normalised to unity. Equation (2.5) becomes

$$H_0 = -\sum_{i,k,\sigma} t_{ii} c^\dagger_{ik\sigma} c_{ik\sigma} - \frac{1}{N} \sum_{\langle i,j \rangle} \sum_{n,k,q,\sigma} t_{ij} e^{i(q-k)\cdot R_{in}} e^{iq\cdot d_{ji}} c^\dagger_{ik\sigma} c_{jq\sigma}.$$

A shorthand notation has been used here. For the most part, nearest neighbour ions will be in the same unit cell, so that $n = m$, $d_{ji} = R_{jn} - R_{in}$ and $t_{ij} = t_{in;jn}$. If the ions are not in the same unit cell, however, then d_{ji} is understood to mean $R_{jm} - R_{in}$ and t_{ij} to mean $t_{ij;jm}$. The sum over n can be performed using

$$\frac{1}{N} \sum_n e^{i(k-q)\cdot R_{in}} = \delta_{k,q} \tag{2.7}$$

so that

$$H_0 = -\sum_{i,k} t_{ii} c^\dagger_{ik\sigma} c_{ik\sigma} - \sum_{\langle i,j \rangle} \sum_{k,\sigma} t_{ij} e^{ik\cdot d_{ji}} c^\dagger_{ik\sigma} c_{jk\sigma}. \tag{2.8}$$

The unit cell for YBCO contains 13 different ions. The inclusion of all of these ions in Eq. (2.8) would be overwhelming. Instead, an extremely simplified model is used in which there are only two ions in the unit cell. One of the ions belongs to the "plane" layer, while the other belongs to the "chain" layer. Furthermore, the simplifying assumption is made that the chain and plane layers are evenly spaced. We take the unit cell to be of length 1 along each edge. The chain-plane distance is therefore 1/2. The Hamiltonian is,

$$H_0 - \mu N = \sum_{i,k,\sigma} \xi_i(k) c^\dagger_{ik\sigma} c_{ik\sigma} + \sum_{k,\sigma} t(k) [c^\dagger_{2k\sigma} c_{1k\sigma} + c^\dagger_{1k\sigma} c_{2k\sigma}] \tag{2.9}$$

where the sum over i is restricted to $i = 1, 2$. The energies ξ_i are the dispersions of the isolated planes and chains. The plane states are given by

$$\xi_1 = -2\sigma_1[\cos(k_x) + \cos(k_y)] - \mu_1. \tag{2.10}$$

and the chain states by

$$\xi_2 = -2\sigma_2 \cos(k_y) - \mu_2. \tag{2.11}$$

where $-\pi < k_x, k_y \leq \pi$. The "chemical potentials" μ_1 and μ_2 are actually the overall chemical potential μ, renormalised by the first term in Eq. (2.8). In other words $\mu_1 = \mu + t_{11}$ and $\mu_2 = \mu + t_{22}$. The dispersion perpendicular to the planes is

$$t(k) = -2t_\perp \cos(k_z/2). \tag{2.12}$$

$-\pi < k_z < \pi$.

It is possible to write H_0 in matrix form

$$H_0 = \sum_k C_k^\dagger Q_0 C_k \tag{2.13}$$

where

$$C_k = \begin{bmatrix} c_{1k} \\ c_{2k} \end{bmatrix}. \tag{2.14}$$

and

$$Q_0 = \begin{bmatrix} \xi_1 & t \\ t & \xi_2 \end{bmatrix}. \tag{2.15}$$

The spin index has been suppressed for simplicity.

The effect of the chain plane coupling t is to mix the plane and chain states. The energies of the resultant bands are given by $\epsilon_\pm$. the eigenvalues of Q_0:

$$\epsilon_\pm = \frac{\xi_1 + \xi_2}{2} \pm \sqrt{\left(\frac{\xi_1 - \xi_2}{2}\right)^2 + t^2} \tag{2.16}$$

and the matrix which diagonalises Q_0 is

$$U(k) = \frac{1}{[(\xi_1 - \xi_2)^2 + 4t^2]^{1/4}} \begin{bmatrix} \frac{t}{\sqrt{\epsilon_+ - \xi_1}} & \frac{t}{\sqrt{\xi_1 - \epsilon_-}} \\ \sqrt{\epsilon_+ - \xi_1} & -\sqrt{\xi_1 - \epsilon_-} \end{bmatrix}. \tag{2.17}$$

so that

$$\begin{bmatrix} \epsilon_+(k) & 0 \\ 0 & \epsilon_-(k) \end{bmatrix} = U^\dagger(k) Q_0(k) U(k).$$

The band structure for a typical set of band parameters is shown in Fig. 2.1. As can be seen in Eq. (2.16). the band energies are shifted from their decoupled ($t_\perp = 0$) values by an amount which depends on the relative sizes of t^2 and $(\xi_1 - \xi_2)^2$. The effect of the plane-chain coupling is largest where $\xi_1 = \xi_2$, at which point there is an *avoided band crossing*. Figure 2.2 shows clearly how the Fermi surfaces are pushed apart by the plane-chain coupling. and that the distortion of the Fermi surfaces depends on their proximity. The band parameters are chosen to qualitatively match some of the results of band structure calculations(Pickett et al. 1992: Yu et al. 1993). Band structure calculations find a Fermi

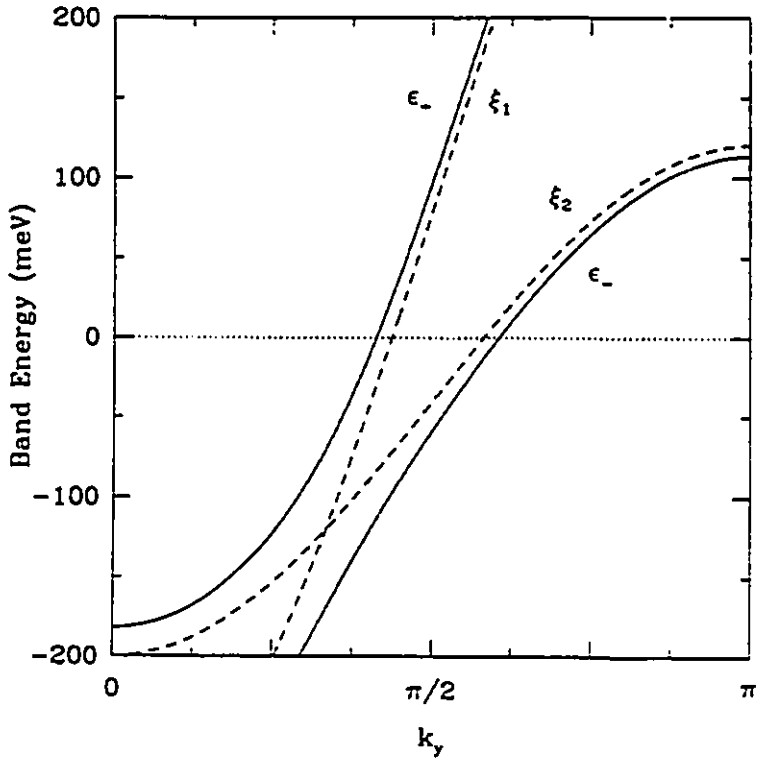

Figure 2.1: Energy dispersions in the normal state.
Energy dispersions along the line $k_y = k_x$ for $k_z = 0$. There is an avoided crossing at $\xi_1 = \xi_2$. The band parameters are typical for the work done in this thesis. They are $\sigma_1 = 100$ meV. $\sigma_2 = 80$ meV. $\mu_1 = -80$ meV. $\mu_2 = 40$ meV and $t_\perp = 25$ meV.

surface which has four pieces. of which two come from the CuO_2 bilayer. one comes from the chains and one is a mixture of chain and plane states. This last piece of Fermi surface is small and is ignored here. Furthermore. we treat the bilayer as a single layer which yields a single piece of Fermi surface.

2.2.2 Superconducting State

The description of the superconducting state will be done in terms of a BCS-like theory. We will begin with the assumption that the pairing interaction is localised to the CuO_2 planes. This seems like a reasonable guess given both the strongly two-dimensional nature of the high T_c materials and the fact that the CuO_2 layer is the only element common

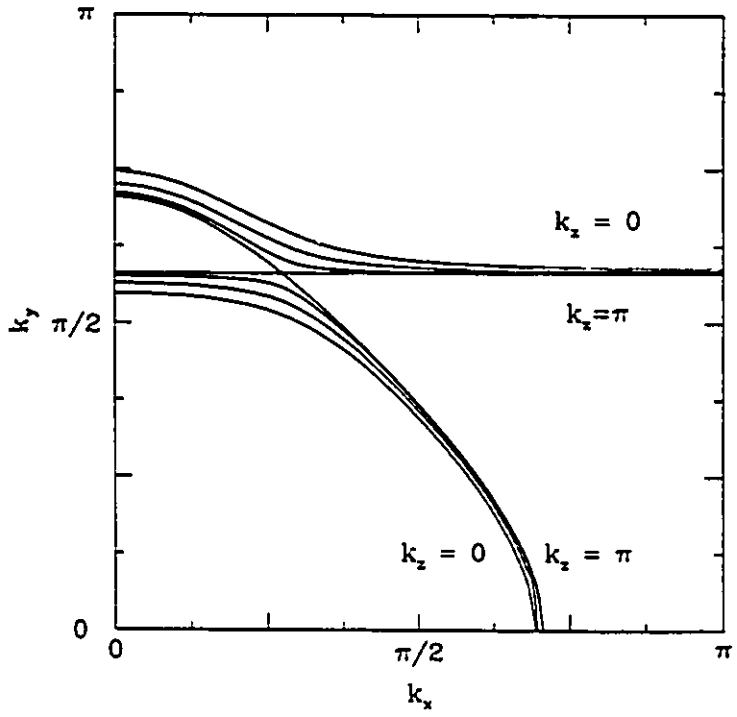

Figure 2.2: The Fermi surface for the model Hamiltonian

The Fermi surface is shown for a range of k_z between $k_z = 0$ and $k_z = \pi$. When $k_z = \pi$, the chain–plane coupling vanishes and the two pieces of Fermi surface are those of the isolated chains and planes. As the chain–plane coupling increases, the Fermi surfaces hybridize and are pushed apart. The amount of hybridization at a given k depends on the relative sizes of t^2 and $(\xi_1 - \xi_2)^2$. There is an avoided crossing of the Fermi surfaces when $\xi_1 = \xi_2 = 0$.

to all of the materials.

The pairing is known to be singlet so that the pairing interaction can be written

$$V = \int d^3r\, d^3r'\, \Psi^\dagger_\uparrow(r)\Psi^\dagger_\downarrow(r')V(r-r')\Psi_\downarrow(r')\Psi_\uparrow(r). \tag{2.18}$$

As before, this can be written in terms of Wannier states

$$V = \sum_{n_1,n_2,n_3,n_4} c^\dagger_{1n_1\uparrow}c^\dagger_{1n_2\downarrow}c_{1n_3\downarrow}c_{1n_4\uparrow} \times \int d^2r\, d^2r'\, \phi_1^*(r-R_{1n_1})\phi_1^*(r'-R_{1n_2})V(r-r')\phi_1(r'-R_{1n_3})\phi_1(r-R_{1n_4}). \tag{2.19}$$

Since the pairing interaction is between electrons in the same CuO_2 plane. it is necessary to make the restriction on the sum over lattice sites that $R_{1n1}.....R_{1,n4}$ must all be in the same plane. For a tight binding system. the leading order contribution comes from $n_1 = n_4$ and $n_2 = n_3$ so that

$$V \sim \sum_{n_1,n_2} V(R_{1n_1} - R_{1n_2}) c^\dagger_{1n_1\uparrow} c^\dagger_{1n_2\downarrow} c_{1n_2\downarrow} c_{1n_1\uparrow}. \tag{2.20}$$

where $V(R)$ is defined by the integral in Eq. (2.19). Using Eq. (2.6). V can be written in terms of Bloch states:

$$V \sim \frac{1}{N^2} \sum_{k_1,k_2,k_3,k_4} c^\dagger_{1k_1\uparrow} c^\dagger_{1k_2\downarrow} c_{1k_3\downarrow} c_{1k_4\uparrow} \sum_{n_1,n_2} V(R_{1n_1} - R_{1n_2}) e^{i(k_4-k_1)\cdot R_{1n_1}} e^{i(k_3-k_2)\cdot R_{1n_2}}. \tag{2.21}$$

If V is a short range potential then the leading order contributions are for $n_2 = n_1$ and $R_{1n_2} = R_{1n_1} + \delta$. where δ is a vector connecting nearest neighbours within the plane. The pairing interaction now simplifies to

$$V \sim \frac{1}{N} \sum_{k_1,k_2,q} c^\dagger_{1k_1+q\uparrow} c^\dagger_{1k_2-q\downarrow} c_{1k_2\downarrow} c_{1k_1\uparrow} \left[V_0 + V_1 \sum_\delta e^{iq\cdot\delta} \right] \tag{2.22}$$

For a square lattice this is

$$V \sim \frac{1}{N} \sum_{k_1,k_2,q} V(q)\, c^\dagger_{1k_1+q\uparrow} c^\dagger_{1k_2-q\downarrow} c_{1k_2\downarrow} c_{1k_1\uparrow}. \tag{2.23}$$

where

$$V(q) = V_0 + 2V_1[\cos(q_x) + \cos(q_y)]. \tag{2.24}$$

There is a simple argument. due to Bardeen. Schrieffer and Cooper. which allows the simplification of V. They demonstrated that the most important contribution to the sum in Eq. (2.23) comes from terms for which $k_2 = -k_1$. For the sake of continuity. the argument and its applicability to this model will not be discussed here. and the interested reader is referred to (Rickayzen 1965). Assuming that the BCS argument holds:

$$V \sim \frac{1}{N} \sum_{k,k'} V(k-k') c^\dagger_{1k\uparrow} c^\dagger_{1-k\downarrow} c_{1-k'\downarrow} c_{1k'\uparrow}. \tag{2.25}$$

In this form. the pairing interaction is still intractable as it is a two body interaction. The simplest approach is to make a *mean field approximation.* In each of the identities

$$c_{1-k\downarrow} c_{1k\uparrow} = \langle c_{1-k\downarrow} c_{1k\uparrow} \rangle + [c_{1-k\downarrow} c_{1k\uparrow} - \langle c_{1-k\downarrow} c_{1k\uparrow} \rangle] \tag{2.26}$$

$$c^\dagger_{1k\uparrow} c^\dagger_{1-k\downarrow} = \langle c^\dagger_{1k\uparrow} c^\dagger_{1-k\downarrow} \rangle + [c^\dagger_{1k\uparrow} c^\dagger_{1-k\downarrow} - \langle c^\dagger_{1k\uparrow} c^\dagger_{1-k\downarrow} \rangle]. \tag{2.27}$$

the operator on the left side of the equation is written as the sum of its mean field value and the fluctuations about that mean field. In mean field theory, the assumption is made that the fluctuations are small. The effects of mean field fluctuations have been examined by Coffey (1990). The mean field form of V is found by inserting Eqs. (2.26) and (2.27) into Eq. (2.25) and dropping the second order term in the fluctuations. Then

$$V \sim \sum_k [c^\dagger_{1k\uparrow} c^\dagger_{1-k\downarrow} \Delta_k + c_{1-k\downarrow} c_{1k\uparrow} \Delta^*_k] + \text{const.}. \tag{2.28}$$

where Δ_k is defined as

$$\Delta_k \equiv \frac{1}{N} \sum_{k'} V(k-k') \langle c_{1-k'\downarrow} c_{1k'\uparrow} \rangle. \tag{2.29}$$

The quantity Δ_k is the *order parameter*. Equation (2.29) is the *BCS equation*, and must be solved self consistently for Δ_k.

The total Hamiltonian in the superconducting state is $H = H_0 + V$. Since the mean field interaction is a one body interaction, the Hamiltonian may be diagonalised. As before, it is easiest to write the Hamiltonian using the Nambu (matrix) notation:

$$H - N\mu = \sum_k C^\dagger(k) Q(k) C(k) + \text{const.}. \tag{2.30}$$

where

$$C(k) = \begin{bmatrix} c_{1k\uparrow} \\ c^\dagger_{1-k\downarrow} \\ c_{2k\uparrow} \\ c^\dagger_{2-k\downarrow} \end{bmatrix} \tag{2.31}$$

and

$$Q = \begin{bmatrix} \xi_1(k) & -\Delta_k & t(k) & 0 \\ -\Delta^*_k & -\xi_1(-k) & 0 & -t^*(-k) \\ t^*(k) & 0 & \xi_2(k) & 0 \\ 0 & -t(-k) & 0 & -\xi_2(-k) \end{bmatrix}. \tag{2.32}$$

Diagonalization of the Hamiltonian leads to four energy bands $E_1 = E_+$, $E_2 = E_-$, $E_3 =$

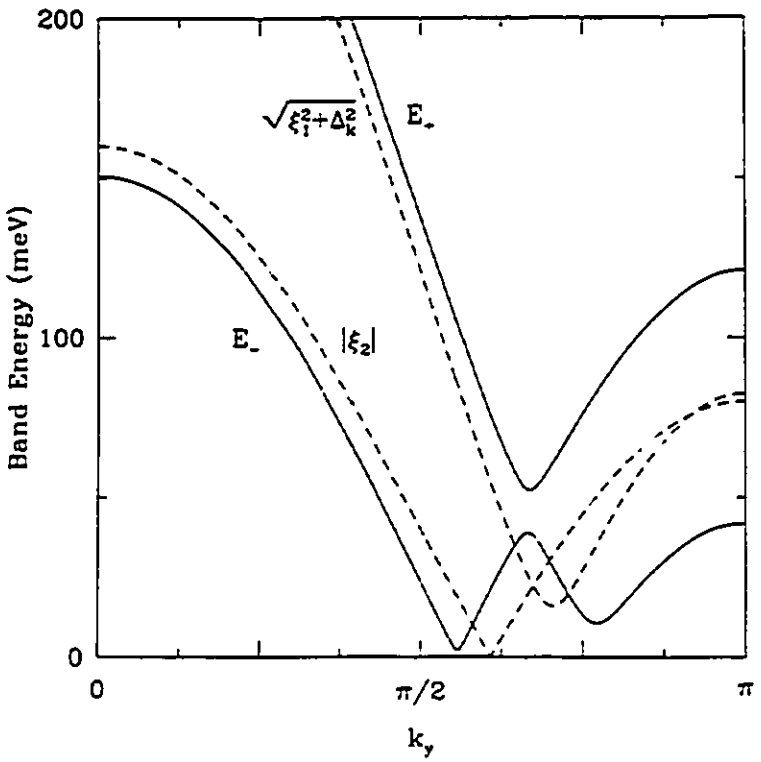

Figure 2.3: Band structure of the model Hamiltonian.
The quasiparticle excitation spectra $E_\pm$ are plotted along the line $k_x = 0$. For these curves, $t_\perp = 20$ meV. The excitation spectra in the decoupled ($t_\perp = 0$) limit are plotted for comparison.

$-E-$. $E_4 = -E+$ with

$$E_\pm^2 = \frac{\xi_1^2+\xi_2^2+\Delta_k^2}{2} + t^2 \pm \sqrt{\left[\frac{\xi_1^2-\xi_2^2+\Delta_k^2}{2}\right]^2 + t^2[(\xi_1+\xi_2)^2+\Delta_k^2]} \tag{2.33}$$

$$= \frac{\xi_1^2+\xi_2^2+\Delta_k^2}{2} + t^2 \pm \sqrt{\left[\frac{\xi_1^2+\xi_2^2+\Delta_k^2}{2}+t^2\right]^2 - (t^2-\xi_1\xi_2)^2 - (\xi_2\Delta_k)^2}. \tag{2.34}$$

Equation (2.33) is useful for discussing the limit of small $t_\perp$, while Eq. (2.34) is useful for finding the nodes of E_-. The quasiparticle spectrum is plotted in Fig. (2.3) along the direction $k_x = k_z = 0$ for a typical set of band parameters.

The annihilation operators for the *band* states are related to the annihilation op-

erators for states in the chain and plane *layers* by

$$\hat{C}_i(k) = \sum_{j=1}^{4} U_{ij}^{\dagger}(k) C_j(k). \tag{2.35}$$

where $U = [U_1\, U_2\, U_3\, U_4]$ with

$$U_j = \frac{1}{\sqrt{C}} \begin{bmatrix} (E_j - \xi_2)A \\ -(E_j + \xi_2)B \\ tA \\ tB \end{bmatrix} \tag{2.36}$$

$$A = t^2 - (\Delta_k + E_j + \xi_1)(E_j + \xi_2)$$

$$B = t^2 - (\Delta_k^* + E_j - \xi_1)(E_j - \xi_2)$$

$$C = A^2[t^2 + (E_j - \xi_2)^2] + B^2[t^2 + (E_j + \xi_2)^2].$$

As before. U diagonalizes Q:

$$\begin{bmatrix} E_+(k) & 0 & 0 & 0 \\ 0 & E_-(k) & 0 & 0 \\ 0 & 0 & -E_-(k) & 0 \\ 0 & 0 & 0 & -E_+(k) \end{bmatrix} = U^{\dagger}(k) Q(k) U(k) \tag{2.37}$$

Now that the Hamiltonian has been diagonalized. it is possible to return to Eq. (2.29) and solve for the order parameter self consistently. Writing

$$\Delta_k = \frac{1}{N} \sum_{k'} V(k - k') \langle c_{1-k'\downarrow} c_{1k'\uparrow} \rangle \tag{2.29}$$

$$= \frac{1}{N} \sum_{k'} V(k - k') \langle C_{2k'}^{\dagger} C_{1k'} \rangle \qquad \text{[from Eq. 2.31]}$$

$$= \frac{1}{N} \sum_{i,j} \sum_{k'} V(k - k') U_{2i}(k') U_{1j}(k') \langle \hat{C}_{ik'}^{\dagger} \hat{C}_{jk'} \rangle$$

$$= \frac{1}{N} \sum_{i} \sum_{k'} V(k - k') U_{1i}(k') U_{2i}(k') f[E_i(k')]. \tag{2.38}$$

Techniques of solving this equation have been developed. based on the method of Fourier transforms. Equation (2.38) has been studied for. among other things. a pairing potential of the form (2.24) in a single layer material (ODonovan and Carbotte 1995). It has been found that this potential leads to a number of different pairing symmetries depending on

the electron density. In most of the interesting cases. it was found that the order parameter had d-wave symmetry. In order to simplify the task of finding the order parameter in this work. we assume a phenomenological form for the pairing interaction which admits *only* the symmetry we wish to study. The pairing interaction is taken to be *separable*:

$$V(k.k') = \tilde{V}\eta_k\eta_{k'} \tag{2.39}$$

with

$$\eta_k = 1$$

for an isotropic s-wave superconductor. and

$$\eta_k = \cos(k_x) - \cos(k_y)$$

for a $d_{x^2-y^2}$-wave superconductor. With this form for $V(k.k')$. it is clear that Δ_k will have the same symmetry as η_k. In particular. it is possible to define Δ_0 such that

$$\Delta_k = \Delta_0\eta_k. \tag{2.40}$$

and where Eq. (2.38) can be solved for Δ_0

$$\Delta_0 = \frac{\tilde{V}}{N}\sum_i\sum_{k'}\eta_{k'}U_{1i}(k')U_{2i}(k')f[E_i(k')]. \tag{2.41}$$

Equation (2.41) is much simpler to solve than Eq. (2.38) because Δ_0 is independent of k. In Fig. 2.4. Δ_0 is plotted as a function of temperature based on the solution of Eq. (2.41).

2.2.3 The Effect of Proximity Coupling

In Fig. 2.5. the critical temperature is plotted against the strength of the plane-chain coupling. As is obvious from the graph. the effect of this coupling is to reduce T_c.

A further effect of the plane-chain coupling is to induce superconductivity on the chains. Although the only order parameter in the problem (Δ_k) is associated with the pairs in the CuO_2 planes. it is possible to introduce the concept of a gap in the chain spectrum. To begin with. it is necessary to distinguish between the terms "gap" and "order parameter". The order parameter is defined by Eq. (2.29). while the gap is the minimum energy of quasiparticle excitation in the superconducting state. In a BCS superconductor.

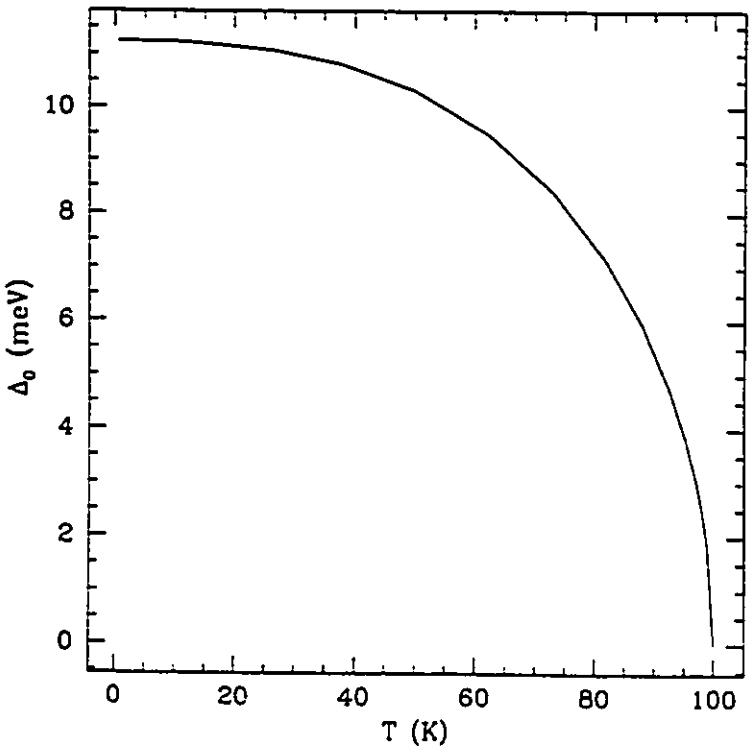

Figure 2.4: Temperature dependence of Δ_0.
The temperature dependence is found by solving Eq. (2.41) self-consistently for a separable d-wave potential.

the quasiparticle spectrum is $E = \sqrt{\epsilon^2 + \Delta^2}$, where ϵ are the free electron energies and Δ is the order parameter. The minimum in the excitation spectrum occurs at the Fermi surface where $\epsilon = 0$. and $E = |\Delta|$. For a BCS superconductor, then, the gap is just the magnitude of the order parameter.

The quasiparticle spectra $E_\pm$ are somewhat more complicated than in the simple BCS model. In fact, the superconductivity is *gapless* since E_- vanishes whenever $t^2 = \xi_1\xi_2$ and $\xi_2 = 0$ or $\Delta_k = 0$ [*cf.* Eq. (2.34)].

Not all gapless superconductors are alike however, since the structure of the low energy excitations plays a role in the low temperature dependence of many properties. For this reason, it is actually useful to redefine the word gap to be the excitation spectrum along the Fermi surface in the superconducting state. The usefulness of this definition is

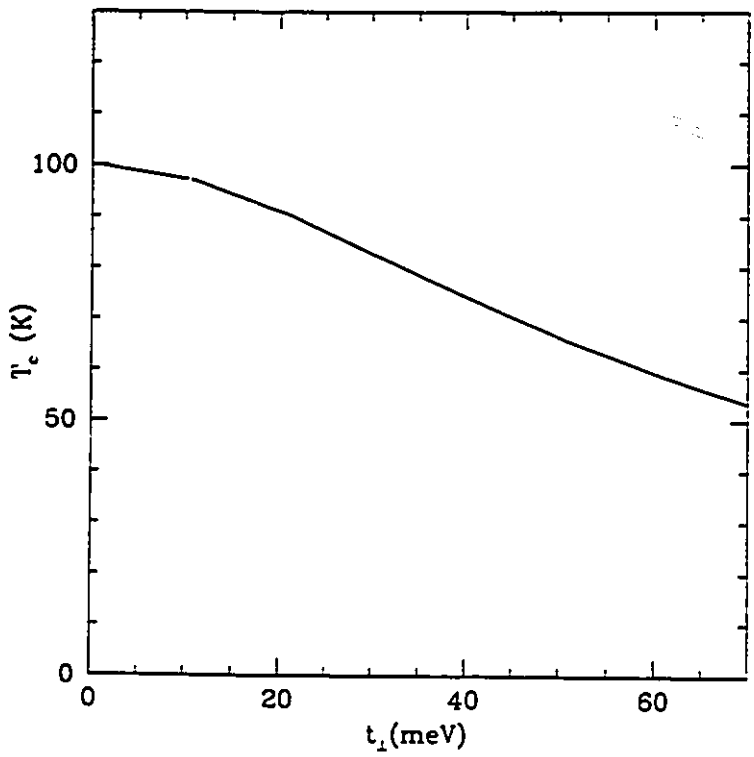

Figure 2.5: T_c as a function of plane-chain coupling.
The critical temperature in the intrinsically superconducting planes is lowered by the proximity of the intrinsically normal chains.

that many physical properties depend only on the structure of the energy spectrum near the Fermi surface. The gap, like the order parameter, is now a function of k although (unlike the order parameter) it is only defined on the Fermi surface.

The gap and the order parameter will, in general have different symmetries. For the separable pairing potential discussed in the previous section, the order parameter will *always* have the symmetry of the potential. On the other hand, the symmetry of the gap will be modified by the band structure. In Fig. 2.6, the gap is shown along the plane and chain Fermi surfaces for both a d wave order parameter. When $t_\perp = 0$, the gap is just the magnitude of the order parameter, but as the chain-plane coupling is increased, the band structure begins to affect the gap.

In order to quantify the notion of a gap, we will return to Eq. (2.34) for E_-. The

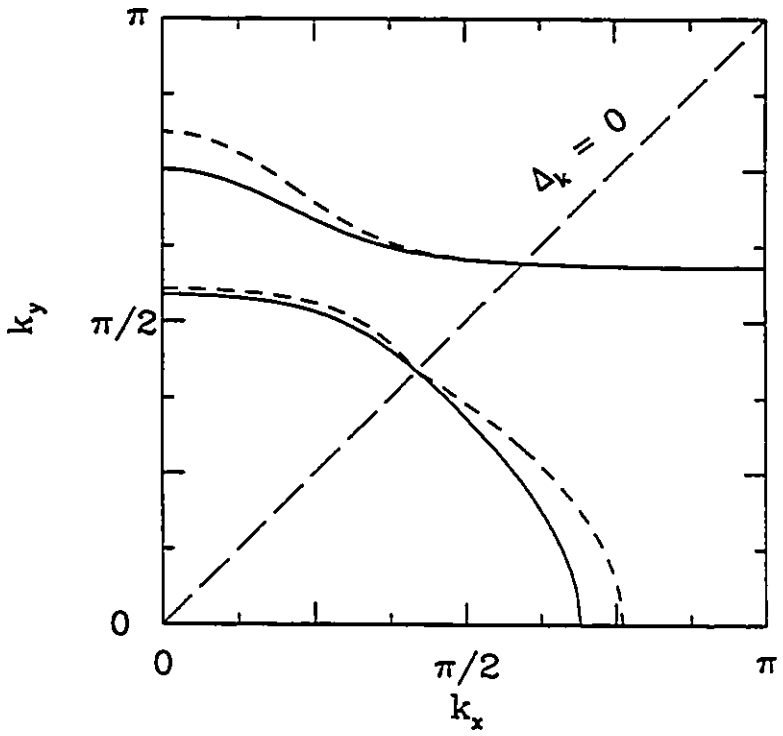

Figure 2.6: Gap in a d wave superconductor.
The value of the lower energy band $E_-(k)$ (dashed line) is plotted along the Fermi surface (solid line) of the chain-plane model for $k_z = 0$. The chain-plane coupling strength is $t_\perp = 25$ meV.

Fermi surfaces for the two normal state bands are given by $\epsilon_\pm = 0$. which (from Eq. (2.16)) occurs when

$$t(k)^2 = \xi_1(k)\xi_2(k). \tag{2.42}$$

The two solutions for this equation are the two Fermi surfaces shown in Fig. 2.2. The quasiparticle excitation energies on these Fermi surfaces are given by

$$E_-^2 = \frac{\xi_1^2 + \xi_2^2 + \Delta_k^2}{2} + t^2 \pm \sqrt{\left[\frac{\xi_1^2 + \xi_2^2 + \Delta_k^2}{2} + t^2\right]^2 - (\xi_2\Delta_k)^2}. \tag{2.43}$$

Except near the avoided crossing (see Fig. 2.2). ξ_1 and ξ_2 will not both be small at the same

time. Further, since we have taken $t_\perp \ll \sigma_1, \sigma_2$, the solutions to Eq. (2.42) will have either $\xi_1 \ll \xi_2$ or $\xi_2 \ll \xi_1$ depending on which section of Fermi surface is being considered. Then

$$E_- \sim |\Delta_k| \times \begin{cases} t^2/\xi_1^2 & \xi_2^2 \ll \xi_1^2 \\ 1 & \xi_1^2 \ll \xi_2^2 \end{cases}. \tag{2.44}$$

The first case above is simply an approximate expression for the induced gap in the chains, while the second case shows that, to lowest order, the gap in the planes is undisturbed by the chain-plane coupling.

Near the avoided crossing, the eigenstates of the Hamiltonian (in the normal state) are mixtures in roughly equal proportions of the chain and plane states so that it is not possible to talk about a gap in the chains or planes based on our definition above.

2.3 Green's Functions

Most of the calculations in this thesis require the use of single particle Green's functions. In this section, the retarded and thermal Green's functions will be introduced, their properties will be discussed and they will be solved for.

The retarded Green's function is defined as

$$\begin{aligned} G^R_{ij}(k,t;k',t') &= -i\langle C_{ik}(t)C^\dagger_{jk'}(t')\rangle\theta(t-t') \\ &= -i\langle C_{ik}(t-t')C^\dagger_{jk}(0)\rangle\delta_{k,k'}\theta(t-t') \\ &= G^R_{ij}(k;t-t'). \end{aligned} \tag{2.45}$$

where the second line holds if the Hamiltonian is time independent and conserves crystal momentum, k (one of the advantages of the mean field pairing Hamiltonian is that k is a good quantum number). The retarded Green's function can be Fourier transformed:

$$G^R_{ij}(k;\omega) = \int_{-\infty}^{\infty} dt\, e^{i(\omega+i0^+)t} G^R(k,t).$$

where the addition of an infinitesimal imaginary part to ω ensures the convergence of the integral.

At finite temperatures, it is much easier to work with the thermal Green's functions

$$G_{ij}(k;\tau) = -\langle T_W C_{ik}(-i\tau)C^\dagger_{jk}(0)\rangle. \tag{2.46}$$

where T_W is the *Wick time ordering operator*. The thermal Green's functions are periodic in τ: $G_{ij}(\tau-\beta) = \mp G_{ij}(\tau)$ where β is the inverse temperature and the sign depends on

whether C is a fermion (-) or boson (+) operator. Because of the periodicity, G_{ij} can be written as a Fourier series

$$G_{ij}(\tau) = \frac{1}{\beta}\sum_l \begin{cases} e^{-i\zeta_l\tau}G_{ij}(i\zeta_l) & \text{(fermions)} \\ e^{-i\omega_l\tau}G_{ij}(i\omega_l) & \text{(bosons)} \end{cases}$$

where $\zeta_l = \pi(2l+1)/\beta$, $\omega_l = 2\pi l/\beta$ and $l = 0, \pm 1, \pm 2\ldots$

Now $G_{ij}(\omega)$ is analytic in the upper half complex plane and it can be shown that $G_{ij}(\omega + i0^+) = G^R(\omega)$ (where ω is real). This property is extremely useful as it means that we can solve for the thermal Green's functions and then analytically continue them to find the retarded Green's functions.

The thermal Green's function satisfies the equation of motion

$$\left[\frac{\partial}{\partial\tau} + Q_{ij}(k)\right] G_{ij}(k;\tau) = -\delta_{ij}. \tag{2.47}$$

where Q is the Hamiltonian matrix given in Eq. (2.32). This equation can be solved by writing G_{ij} in terms of its Fourier series, so that

$$\begin{aligned} G_{ij}(i\zeta_l) &= [i\zeta_l - Q(k)]^{-1}_{ij} \\ &= \left[U(k)U^\dagger(k)(i\zeta_l - Q(k))U(k)U^\dagger(k)\right]^{-1}_{ij} \\ &= \sum_{m,n} U_{im}(k)\left[U^\dagger(k)(i\zeta_l - Q(k))U(k)\right]^{-1}_{mn} U^\dagger_{nj}(k) \\ &= \sum_n \frac{U_{in}(k)U^\dagger_{nj}(k)}{i\zeta_l - E_n}. \end{aligned} \tag{2.48}$$

where U is the 4×4 matrix given in Eq. (2.36). While this form for G_{ij} is useful for numerical work, it is not very transparent. An alternative method for evaluating G_{ij} is to note that given a matrix A,

$$A^{-1} = \frac{1}{\det|A|}(\text{adj}\, A). \tag{2.49}$$

where adj is the classical adjoint of the matrix (*ie.* the transpose of the matrix of cofactors).

As an example, let us consider the gap equation [Eq. (2.29)].

$$\Delta_k \equiv \frac{1}{N}\sum_{k'} V(k-k')\langle c_{1-k'\downarrow}c_{1k'\uparrow}\rangle \tag{2.29}$$

$$= -\frac{1}{N}\sum_{k'} V(k-k')G_{12}(\tau = 0^-). \tag{2.50}$$

From Eq. (2.49), we know that

$$G_{12}(i\zeta_l) = [i\zeta_l - Q]^{-1}_{12}$$
$$= \frac{1}{[(i\zeta_l)^2 - E_+^2][(i\zeta_l)^2 - E_-^2]}\Delta_k[(i\zeta_l)^2 - \xi_2^2]. \tag{2.51}$$

Inserting this into the Fourier series for $G_{12}(\tau = 0^-)$ gives

$$G_{12}(0) = \frac{1}{\beta}\sum_l \frac{\Delta_k[(i\zeta_l)^2 - \xi_2^2]}{[(i\zeta_l)^2 - E_+^2][(i\zeta_l)^2 - E_-^2]}$$
$$= \frac{-\Delta_k}{2(E_+^2 - E_-^2)}\left[\frac{(E_+^2 - \xi_2^2)}{E_+}\tanh(\beta E_+/2) - \frac{(E_-^2 - \xi_2^2)}{E_-}\tanh(\beta E_-/2)\right]. \tag{2.52}$$

so that

$$\Delta_k = \frac{1}{N}\sum_{k'} V(k-k')\frac{\Delta_k}{2(E_+^2 - E_-^2)}\Big[\frac{(E_+^2 - \xi_2^2)}{E_+}\tanh(\beta E_+/2)$$
$$- \frac{(E_-^2 - \xi_2^2)}{E_-}\tanh(\beta E_-/2)\Big]. \tag{2.53}$$

While this form for the gap equation is equivalent to Eq. (2.38), the reduction of (2.38) to this simple analytic form is nontrivial.

Chapter 3

Density of States

The electronic density of states (DOS) is one of the fundamental properties of any quantum system. The usefulness of the DOS comes from the fact that many physical quantities do not depend on the specifics of the band structure, but on the number of available states at any given energy. This is particularly true of thermal properties, such as the specific heat, but is also true of transport properties where the number of carriers is directly related to the DOS.

Density of states measurements hold a special place in the history of superconductivity, as they provided one of the first direct experimental confirmations of the BCS theory of superconductivity. One of the key predictions of BCS theory is that a gap in the DOS opens at the critical temperature. In 1960, Giaever performed tunneling experiments which demonstrated the existence of this gap.

The density of states is also an important quantity for the high T_c superconductors. It seems clear that the superconducting order parameter in these materials is much different from that of the conventional materials. A number of experiments indicate, for example, that the superconductivity is "gapless", in the sense that there is a finite density of states at all energies in the superconducting state. There is still, however, a depletion of states near the Fermi surface which can be directly attributed to the superconductivity. The understanding of the structure of the DOS near the Fermi surface will likely prove crucial to the understanding of high T_c superconductivity.

In this chapter, expressions for the DOS for a layered system will be derived. The results of DOS calculations for the chain-plane model will be discussed, and a number of experiments which depend on the DOS in an important way will be discussed. It is hoped that, with the simple chain-plane model introduced in Chapter 2, it will be possible to draw

some general conclusions about the high T_c materials.

3.1 Theory

3.1.1 General Theory

The DOS is defined as the imaginary part of the single particle Green's function:

$$\rho(\omega) = -\frac{2}{N\pi}\int d^3r \ \mathrm{Im}\, G^R_{\uparrow\uparrow}(r.r.\omega) \tag{3.1}$$

where the factor 2 is because only spin up electrons are counted. and where N is the number of unit cells in the crystal. $G^R_{\sigma\sigma'}$ is the retarded Green's function:

$$G^R_{\sigma\sigma'}(r.r'.\omega) = -i\int_{-\infty}^{\infty} dt\, e^{i(w+i0^+)t}\langle\{\Psi_\sigma(r.t).\Psi^\dagger_{\sigma'}(r'.0)\}\rangle\theta(t) \tag{3.2}$$

where Ψ is the field operator. $\theta(t)$ is the step function and $\{\}$ are anticommutating brackets. This definition is quite formal in appearance and it is not obvious how it is related to the more familiar definition (Ashcroft and Mermin 1976):

$$\rho(\omega) = \sum_k \delta(\xi_k - \omega).$$

where ξ_k is the band energy.

In fact. the familiar form for the DOS shown above applies to the case of a single band system in the normal state. To show this. we expand the field operators in Eq. (3.2) in terms of the Bloch states $\phi_k(r)$.

$$\Psi_\uparrow(r.t) = \sum_k c_{k\uparrow}(t)\phi_k(r). \tag{3.3}$$

so that

$$\rho(\omega) = -\frac{2}{N\pi}\sum_k \mathrm{Im}\ G^R_{\uparrow\uparrow}(k{:}\omega). \tag{3.4}$$

where

$$G^R_{\uparrow\uparrow}(k{:}\omega). = -i\int_{-\infty}^{\infty} dt\, e^{i(w+i0^+)t}\langle\{c_{k\uparrow}(t).c^\dagger_{k\uparrow}(0)\}\rangle\theta(t). \tag{3.5}$$

For a single band material. Eq. (2.48) reduces. after analytic continuation to real frequencies. to

$$G^R_{\uparrow\uparrow}(k{:}\omega) = \frac{1}{\omega + i0^+ - \xi_k} \tag{3.6}$$

so that

$$\mathrm{Im}G^R_{\uparrow\uparrow}(k;\omega) = -\pi\delta(\omega - \xi_k). \tag{3.7}$$

The expected result follows immediately:

$$\rho(\omega) = \frac{2}{N}\sum_k \delta(\omega - \xi_k). \tag{3.8}$$

The factor of 2 in Eq. (3.8) accounts for the two possible electron spins, while the normalisation factor $1/N$ makes ρ the *density of states per unit cell*.

For the chain-plane system (or any other multiband model), there is an additional sum over the layers in the expansion of the the field operators and

$$\Psi_\uparrow(r,t) = \sum_{i,k} c_{ik\uparrow}(t)\phi_{ik}(r).$$

where the subscript i refers to the different layer types. The DOS can therefore be written as the sum of a plane DOS and a chain DOS:

$$\rho(\omega) = \rho_1(\omega) + \rho_2(\omega) \tag{3.9}$$

where

$$\begin{aligned}
\rho_1(\omega) &= -\frac{2}{N\pi}\sum_k G_{11}(k;\omega + i0^+) \\
&= \frac{2}{N}\sum_i \sum_k U_{1i}(k)^2\,\delta(\omega - E_i(k)) \qquad (3.10)\\
\rho_2(\omega) &= -\frac{2}{N\pi}\sum_k G_{33}(k;\omega + i0^+) \\
&= \frac{2}{N}\sum_i \sum_k U_{3i}(k)^2\,\delta(\omega - E_i(k)). \qquad (3.11)
\end{aligned}$$

The Green's functions G_{11} and G_{33} describe spin up electrons in the plane and chain layers respectively [recall Eq. (2.46)]. The spin down electrons (described by G_{22} and G_{44}) are not needed in this calculation as they make an equal contribution to the DOS as the spin up electrons. The densities of states ρ_1 and ρ_2 are the DOS for the plane and chain layers respectively. In Eqs. (3.10) and (3.11) U^2_{1i} and U^2_{3i} can be thought of as projection operators which relate electron states in the various *bands* to electron states in the *layers*.

An alternative (but equivalent) form for ρ_1 and ρ_2 can be found from Eq. (2.49). Noting that

$$G_{11}(\omega) = \frac{(\omega+\xi_1)(\omega^2-\xi_2^2)-t^2(\omega-\xi_2)}{[\omega^2-E_+^2][\omega^2-E_-^2]} \tag{3.12}$$

and

$$G_{33}(\omega) = \frac{(\omega+\xi_2)(\omega^2-\xi_1^2-\Delta_k^2)-t^2(\omega-\xi_1)}{[\omega^2-E_+^2][\omega^2-E_-^2]}. \tag{3.13}$$

we find that

$$\rho_1(\omega) = \frac{1}{N}\sum_k \frac{(\omega+\xi_1)(\omega^2-\xi_2^2)-t^2(\omega-\xi_2)}{E_+E_-(E_+^2-E_-^2)} \times [E_-\delta(\omega-E_+)-E_-\delta(\omega+E_+)-E_+\delta(\omega-E_-)+E_+\delta(\omega+E_-)] \tag{3.14}$$

$$\rho_2(\omega) = \frac{1}{N}\sum_k \frac{(\omega+\xi_2)(\omega^2-\xi_1^2-\Delta_k^2)-t^2(\omega-\xi_1)}{E_+E_-(E_+^2-E_-^2)} \times [E_-\delta(\omega-E_+)-E_-\delta(\omega+E_+)-E_-\delta(\omega-E_-)+E_+\delta(\omega+E_-)]. \tag{3.15}$$

3.1.2 Isolated Planes and Chains, Normal State

The limit of isolated chains and planes can be found by taking $t_\perp \to 0$ in Eqs. (3.14) and (3.15). Furthermore, in the normal state $\Delta_0 = 0$ and

$$\rho_i = \frac{2}{N}\sum_k \delta(\omega-\xi_i).$$

It is worthwhile evaluating this explicitly since the integrals can be done analytically and provide a basis for comparison with later (and more complicated) DOS. Taking ξ_1 and ξ_2 from Eqs. (2.10) and (2.11) we get

$$\rho_2 = \frac{1}{N}\sum_k \delta(\omega+2\sigma_2\cos(k_y)+\mu_2) = \begin{cases} \frac{1}{\pi}\frac{1}{\sqrt{4\sigma_2^2-(\omega+\mu_2)^2}} & \left|\frac{\omega+\mu_2}{2\sigma_2}\right|<1 \\ 0 & \text{otherwise} \end{cases} \tag{3.16}$$

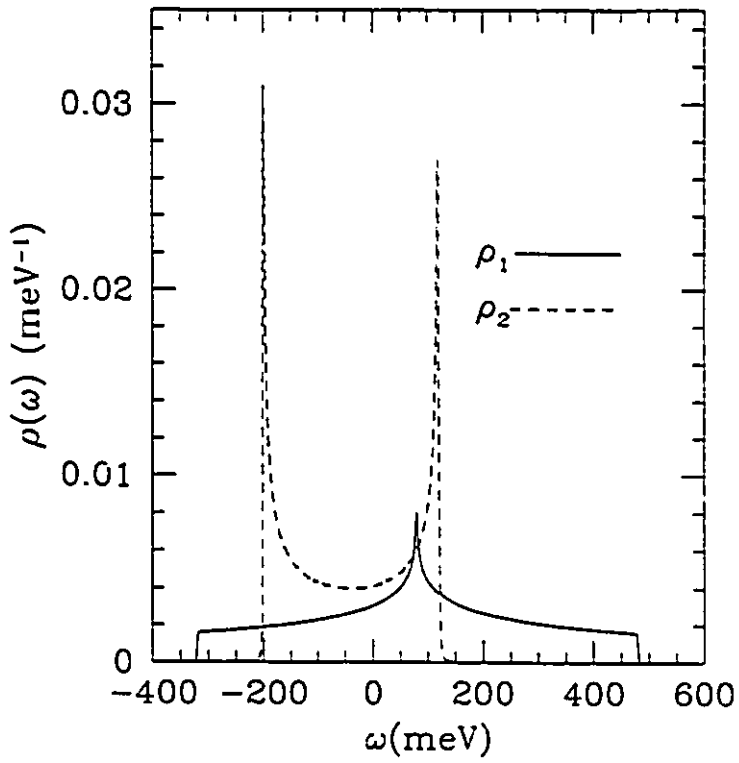

Figure 3.1: Density of states for the decoupled plane-chain system in the normal state. Analytic expressions for these DOS are given in Eqs. (3.16) and (3.17). There is a logarithmic divergence in ρ_1 at $\omega = -\mu_1$ and two square root divergences at the band edges of ρ_2. The band parameters are $\sigma_1 = 100$ meV, $\sigma_2 = 80$ meV, $\mu_1 = -80$ meV, $\mu_2 = 40$ meV.

and

$$\rho_1 = \frac{1}{N}\sum_k \delta\Big(\omega + 2\sigma_1[\cos(k_x) + \cos(k_y)] + \mu_1\Big)$$
$$= \begin{cases} \dfrac{8}{\pi^2}\dfrac{1}{4\sigma_1 + |\omega + \mu_1|} K\left(\left[\dfrac{4\sigma_1 - |\omega + \mu_1|}{4\sigma_1 + |\omega + \mu_1|}\right]^2\right) & \left|\dfrac{\omega + \mu_1}{4\sigma_1}\right| < 1 \\ 0 & \text{otherwise} \end{cases} \tag{3.17}$$

where K is the *complete elliptic integral of the first kind*. The properties of $K(x)$ are described in Abramowitz and Stegun. (Abramowitz and Stegun 1972) The most important things to know are:

1. The domain of $K(x)$ is $0 \leq x < 1$.

2. $K(x)$ increases monotonically with increasing x.

3. $K(0) = \pi/2$

4. $K(x)$ diverges logarithmically as $x \to 1$.

Equations (3.16) and (3.17) are plotted in Fig. 3.1. The divergences in ρ_1 and ρ_2 are due to *van Hove singularities* (vHS) in the energy dispersions ξ_1 and ξ_2. Van Hove singularities occur because

$$\delta(\omega - \xi_i) = \frac{1}{|\nabla_k \xi_i(k_0)|}\delta(k - k_0).$$

where $\xi_i(k_0) = \omega$. When $\nabla_k \xi_i(k_0) = 0$. the integrand in the DOS equation diverges. How this divergence manifests itself in the DOS depends on (1) the nature of the divergence and (2) the dimension of the system. A rule of the thumb is that as the dimension of the system is increased. the effect of the vHS is lessened. The occurence of vHS in tight binding models has been studied by Jelitto (1969) for a number of crystal structures.

Consider a band with dispersion ξ_k. At a band edge. ξ_k is an extremum. Near a minimum. ξ_k can be expanded (in the simplest possible case) as

$$\xi_k = \begin{cases} k_x^2 & \text{1 dimension} \\ k_x^2 + k_y^2 & \text{2 dimensions} \\ k_x^2 + k_y^2 + k_z^2 & \text{3 dimensions.} \end{cases} \tag{3.18}$$

Near the band minimum. then.

$$\begin{aligned} \rho(\omega) &= \frac{2}{N}\sum_k \delta(\omega - \xi_k) \\ &\sim \begin{cases} \theta(\omega)/\sqrt{\omega} & \text{1 dimension} \\ \theta(\omega) & \text{2 dimensions} \\ \sqrt{\omega}\,\theta(\omega) & \text{3 dimensions.} \end{cases} \end{aligned} \tag{3.19}$$

where $\theta(\omega)$ is the step function. In Fig. 3.1. the divergence in ρ_2 at the band edge occurs because the chains are a one dimensional system. Similarly. the discontinuity in ρ_1 at the band edge is a direct result of the two dimensional nature of the planes.

A second type of vHS is the *saddle point singularity*, which can occur in systems of two dimensions or higher. A simple example of a vHS is for a band with the structure

$$\xi_k = \begin{cases} k_x^2 - k_y^2 & \text{2 dimensions} \\ k_x^2 - k_y^2 + t_0 \cos(k_z)^2 & \text{3 dimensions.} \end{cases} \tag{3.20}$$

In the two dimensional case, the vHS is at $k_x = k_y = 0$, where $\xi_k = 0$, and the DOS in the neighbourhood of this point is :

$$\rho(\omega) \sim \ln(\omega) \quad \text{(2 dimensions).} \tag{3.21}$$

For ξ_1 there are saddle point singularities at $k = (0, \pm\pi)$ and $k = (\pm\pi, 0)$, at which points $\xi_1 = -\mu_1$. In Eq. (3.17), the logarithmic divergence is hidden in the elliptic integral, which diverges when its argument is 1 (which in this case means $\omega \to \mu_1$).

The three dimensional case in Eq. (3.20) has been chosen because, as $t_0 \to 0$, it reduces to the two dimensional case. In this way, this example is similar to the chain-plane model. There are two vHS in the three dimensional case. The first is at $k_x = k_y = k_z = 0$ at which $\xi_k = t_0$, and the second is at $k_x = k_y = 0$; $k_z = \pi$ at which $\xi_k = 0$. In the neighbourhood of these points, the dispersion can be written

$$\xi_k \sim \begin{cases} k_x^2 - k_y^2 + t_0(1 - k_z^2) & k_z \sim 0 \\ k_x^2 - k_y^2 + t_0(\pi - k_z)^2 & k_z \sim \pi, \end{cases} \tag{3.22}$$

which leads to the densities of states

$$\rho(\omega) \sim \frac{1}{t_0} \begin{cases} 1 - \theta(-\omega)\sqrt{-\omega} & \omega \sim 0 \\ 1 - \theta(\omega - t_0)\sqrt{\omega - t_0} & \omega \sim t_0. \end{cases} \tag{3.23}$$

For small t_0, the vHS are close together and appear as a peak of width t_0 and height $1/t_0$ in the DOS. The slope of the DOS at $\omega = 0^-$ and $\omega = t_0 + 0^+$ is infinite, while the slope at $\omega = 0^+$ and $\omega = t_0 - 0^+$ is zero. In other words, each of the vHS appears as a sharp corner in the DOS. As $t_0 \to 0$, the two vHS combine to give the logarithmic divergence of the two dimensional case.

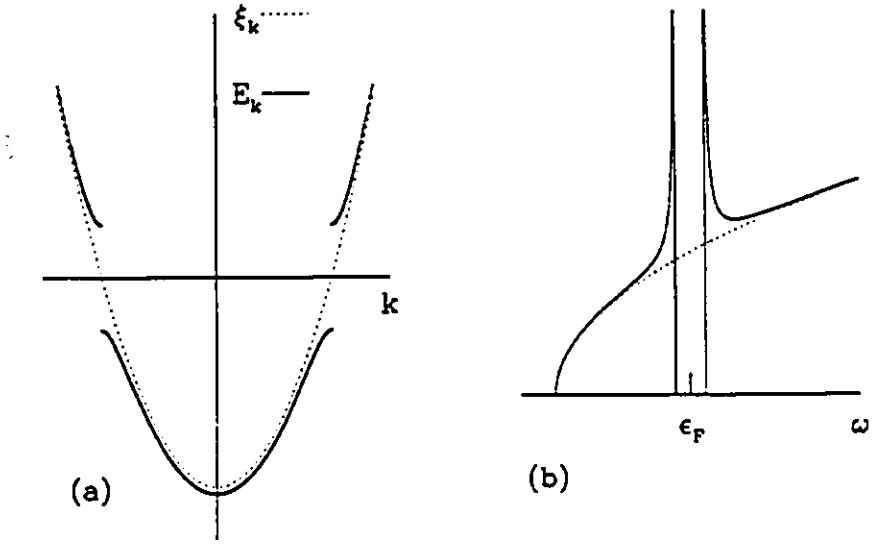

Figure 3.2: Superconductivity in the BCS model.
(a) As T is reduced below T_c, the normal state dispersion (dashed line) develops a gap at the Fermi surface of width 2Δ (solid line). (b) In the superconducting state (solid curve), a gap of width 2Δ opens in the normal state density of states (dotted curve). The size of the gap has been exagerated here and typically, in a BCS superconductor $\Delta/\epsilon_F \sim 10^{-3}$.

3.1.3 Isolated Plane, Superconducting State

The case of an isolated plane in the superconducting state may be studied by letting $t_\perp \to 0$ in Eq. (3.14). Then

$$\rho(\omega) = \frac{1}{N}\sum_k \left(1 + \frac{\xi_k}{E}\right)\delta(\omega - E) + \left(1 - \frac{\xi_k}{E}\right)\delta(\omega + E) \tag{3.24}$$

where ξ is the band energy in the normal state and $E = \sqrt{\xi^2 + \Delta^2}$ is the excitation spectrum of the superconducting state.

For the simple BCS model with a k-independent order parameter Δ, and a free

electron dispersion ξ_k. Eq. (3.24) can be reduced to a one dimensional integral

$$\rho(\omega > 0) = \int_{-\mu}^{\infty} d\xi\, N(\xi) \left(1 + \frac{\xi_1}{E}\right) \delta(\omega - E). \tag{3.25}$$

where $N(\xi)$ is the density of states in the normal state. Clearly, the integral will vanish for $\omega < \Delta$ so that there will be a "gap" in the DOS—that is, $\rho(\omega) = 0$ when $|\omega| < |\Delta|$. The superconducting gap introduces band edges into the dispersion at $\xi = \pm\Delta$ [see Fig. 3.2(a)] and, since the integral in Eq. (3.25) is one dimensional, there is a square root singularity in the dispersion at $\omega = \pm\Delta$ [recall Eq. (3.19)]. The DOS for a BCS superconductor is shown in Fig. 3.2(b).

If, on the other hand, Δ_k is not constant over the Fermi surface, then it is not possible to reduce Eq. (3.24) to a one dimensional integral and the effect of the vHS is weakened. As an example, we will consider a simple two dimensional model in which $\xi = k^2/2 - \mu$ and $\Delta_\phi = \Delta_0 \cos(2\phi)$. The coordinates k and ϕ are radial and angular coordinates in k space so that $k_x = k\cos(\phi)$ and $k_y = k\sin(\phi)$. The quasiparticle spectrum in the superconducting state is

$$E(k, \phi) = \sqrt{\xi_k^2 + \Delta_\phi^2}$$

and there is a saddle point singularity at $\xi = 0$ and $\Delta_\phi = \Delta_0$ (*ie.* at the minimum value of ξ_k^2 and the maximum value of Δ_ϕ^2). There is a corresponding logarithmic divergence in the DOS at $\omega = \pm\Delta_0$ [recall Eq. (3.21)].

This divergence, however, does not correspond to a gap edge since there is a nonzero number of states at energies $E(k, \phi) < \Delta_0$. Strictly speaking then, the energy dispersion is "gapless", although it is common to speak of the "gap structure" anyway and states for which $E(k, \phi) < \Delta_0$ are described as "inside the gap". The usefulness of such language is that the logarithmic divergence occurs at the energy $\omega = \Delta_0$ in the same way that the square root divergence in the BCS case occurs at $\omega = \Delta$. Furthermore, the DOS within the gap is *depleted* in the superconducting state, although it does not vanish completely as in the case of the BCS model.

The density of states within the gap can be described qualitatively near the Fermi surface. $E(k, \phi)$ vanishes at the points $(k_0, \phi_0) = (\sqrt{2\mu}, \pi/4)$. In the neighbourhood of these points

$$E \sim \sqrt{k_0^2(k - k_0)^2 + 4\Delta_0^2(\phi - \phi_0)^2}$$

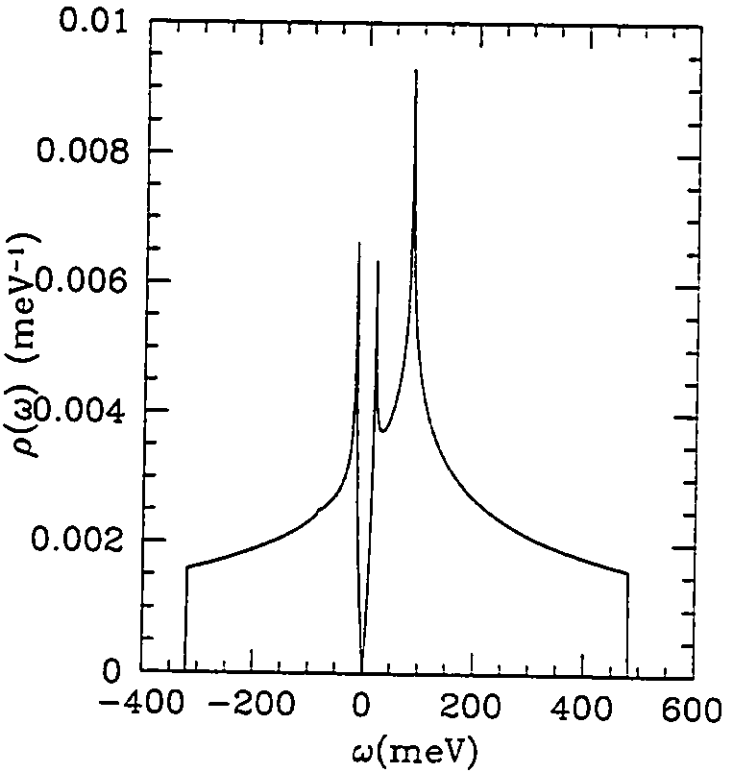

Figure 3.3: Density of states for a single CuO_2 plane in the superconducting state. The order parameter is $\Delta_k = \Delta_0[\cos(k_x) - \cos(k_y)]$.

so that

$$\rho(\omega > 0) \sim \frac{1}{(2\pi)^2} \int_0^\infty k_0 dk \int_0^{2\pi} d\phi \left(1 + \frac{\xi_k}{E}\right) \delta(\omega - E).$$

Writing $k_0(k - k_0) = E\cos(\theta)$ and $2\Delta_0(\phi - \phi_0) = E\sin(\theta)$. the DOS becomes

$$\begin{aligned} \rho(\omega > 0) &\sim \frac{1}{(2\pi)^2} \int_0^\infty \frac{EdE}{2\Delta_0} \int_0^{2\pi} d\theta \, (1 + \cos(\theta)) \, \delta(\omega - E) \\ &= \frac{\omega}{4\pi\Delta_0}. \end{aligned} \tag{3.26}$$

This result is radically different from the BCS result. For the case of an order parameter Δ_k which has *nodes* on the Fermi surface. the DOS varies *linearly* with ω for $\omega \ll \Delta_0$.

In Fig. 3.3. the DOS for a single CuO_2 plane (with dispersion $\xi = -2t[\cos(k_x) + \cos(k_y)] - \mu$) in the superconducting state is shown. The order parameter has a $d_{x^2-y^2}$ symmetry so that there are point nodes on the Fermi surface. This case has been studied

in detail by Zhou and Schultz(1992) who found logarithmic divergences in the DOS at

$$\omega = \frac{\Delta_0(4t - |\mu|)}{\sqrt{4t^2 + \Delta_0^2}}. \tag{3.27}$$

To order $\Delta_0^2/2t$, this is $\omega \sim \Delta_0(2 - |\mu|/2t)$, which is the maximum value of Δ_k on the Fermi surface. Further, the DOS varies linearly with ω when $|\omega| \ll \Delta_0$.

It should be emphasized that the divergences in Fig. 3.3 do not appear at $\omega = \pm\Delta_0$. Many experimental techniques, such as tunneling and Raman spectroscopy, define a gap Δ_{pk} as the energy of the first peak in the superconducting spectrum. This peak corresponds to the peak at the gap edge in the DOS. For a single layer material, Δ_{pk} is the maximum value of Δ_k on the Fermi surface. One immmediate implication of this is that changes in Δ_{pk} with doping might not reflect a change in the superconducting state but may, instead, reflect the changing shape of the Fermi surface. The value of ω found in Eq. (3.27), for example, is simply Δ_{pk} for the single layer $d_{x^2-y^2}$ model, and it varies linearly with the chemical potential μ.

In summary, then, we can say that a two dimensional single band superconductor with an order parameter that has point nodes on the Fermi surface will have

1. a logarithmic divergence in the DOS which can be associated with the maximum value of the order parameter on the Fermi surface and,

2. a linear frequency dependence in the DOS at frequencies much lower than Δ_0.

3.1.4 Chain-Plane Model

We are now in a postion to discuss the effects of chain-plane coupling on the DOS. There have been a number of investigations of the DOS in layered S/N systems (Abrikosov and Klemm 1992; Bulaevskii and Zyskin 1990; Buzdin et al. 1992a; Buzdin et al. 1992b; Tachiki et al. 1990; Atkinson and Carbotte 1995a), but this is the first detailed examination of the DOS in which the one dimensional nature of the chains is properly accounted for, and for which the order parameter is not s wave. All of the articles cited above [with the exception of Tachike *et al.* (1990)] treat the N layer as a two dimensional plane. Although this simplifies the calculations somewhat, it misses one important feature of the chain plane model which we shall discuss shortly.

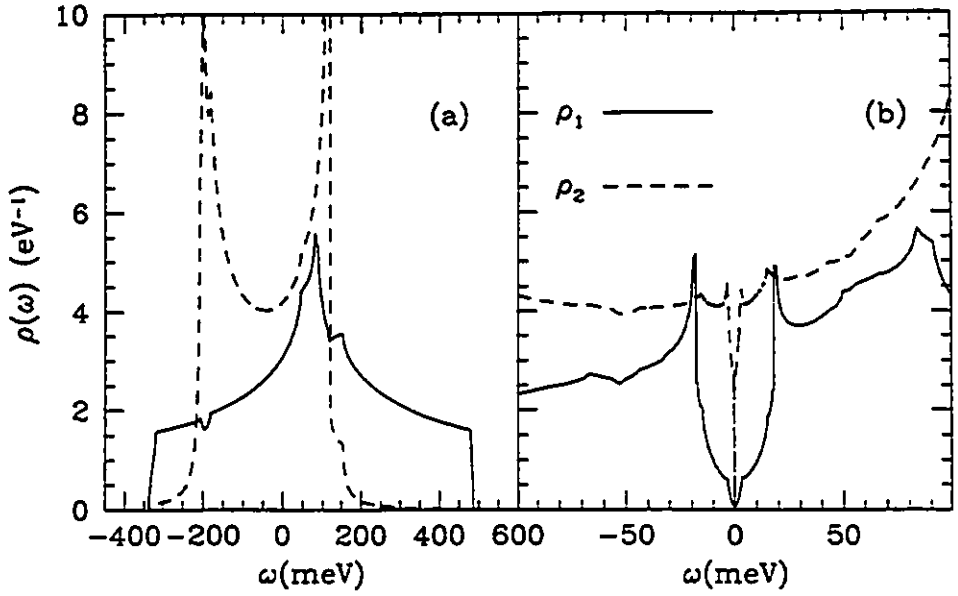

Figure 3.4: Density of states for the coupled chain-plane system.
The density of states is shown in the normal (a) and superconducting (b) states. The strength of the chain-plane coupling is $t_\perp = 25$ meV. All other band parameters are as in Fig. 3.1. In (b), the order parameter has $d_{x^2-y^2}$ symmetry, and $\Delta_0 = 11$ meV when $T_c = 100$ K. The structure near the Fermi surface is quite complicated in the superconducting state: ρ_1 has a nested gap structure where $2\Delta_{pk} \sim 37$ meV for the outer gap and $2\Delta_{pk} \sim 9$ meV for the inner gap. The inner gap is also seen in ρ_2. Finally, ρ_2 has a very small induced gap.

In Fig. 3.4, the DOS for the chain-plane system is shown in the normal and superconducting states. First of all, in the normal state, we can see the effect of the chain-plane coupling by comparing Fig. 3.4(a) with Fig. 3.1. The effects of the coupling are twofold:

1. The system becomes more three dimensional as $t_\perp$ increases, so that the divergences of Fig. 3.1 become finite peaks of width $\propto t_\perp$ and height $\propto 1/t_\perp$ [Eq. 3.23].

2. The chain and plane states are mixed by $t_\perp$, so that features originating in the chains become reflected in the plane DOS ρ_1 and vice versa. One consequence of this is that

ρ_2 becomes finite over the entire width of the plane band.

To estimate the extent of the mixing, we can expand the normal state band energies to first order in $t(k)/|\xi_1(k) - \xi_2(k)|$ [*cf.* Eq. (2.16)].

$$\epsilon_+ \sim \xi_1 + \frac{t^2}{\xi_1 - \xi_2}$$
$$\epsilon_- \sim \xi_2 - \frac{t^2}{\xi_1 - \xi_2}$$

where, for definiteness, we have chosen the case $\xi_1 - \xi_2 > 0$. Evaluating Eq. (3.14) to first order in $t^2/(\xi_1 - \xi_2)^2$ we find that the contribution $\delta\rho_1$ made to the plane DOS by the volume $\delta^3 k$ of the Brillouin zone is

$$\delta\rho_1(\omega) \sim \left\{\left[1 + O\left(\frac{t^2}{(\xi_1 - \xi_2)^2}\right)\right]\delta(\omega - \xi_1) + \frac{2t^2}{(\xi_1 - \xi_2)^2}\delta(\omega - \xi_2)\right\}\delta^3 k. \tag{3.28}$$

An analogous expression holds for $\delta\rho_2$. Equation (3.28) shows that in regions of the Brillouin zone where $t^2 \ll (\xi_1 - \xi_2)^2$, the mixing of ρ_1 and ρ_2 is $O(t^2/(\xi_1 - \xi_2)^2)$. If $t^2 \gg (\xi_1 - \xi_2)^2$, on the other hand, then

$$\epsilon_\pm \sim \frac{\xi_1 + \xi_2}{2} \pm |t| \tag{3.29}$$

and

$$\delta\rho_1 \sim \delta\rho_2. \tag{3.30}$$

In other words, features originating in regions of the Brillouin zone in which $t^2 \gg (\xi_1 - \xi_2)^2$ appear in ρ_1 and ρ_2 with the same weight.

The two different limits contained in Eqs. (3.28) and (3.30) are illustrated quite neatly in Fig. 3.4 (b), where the DOS near the Fermi surface is shown in the superconducting state. To begin with, ρ_1 has a *nested gap structure*, in which the outer gap has $2\Delta_{pk} \sim$ 37 meV and the inner gap has $2\Delta_{pk} \sim 9$ meV. The outer gap is the intrinsic gap in the CuO_2 planes and, although its value is reduced slightly by the chain-plane coupling, we can still use Eq. (3.27) to estimate its value. We find that

$$\Delta_{pk} \sim 1.6\Delta_0$$
$$\sim 18 \text{ meV}.$$

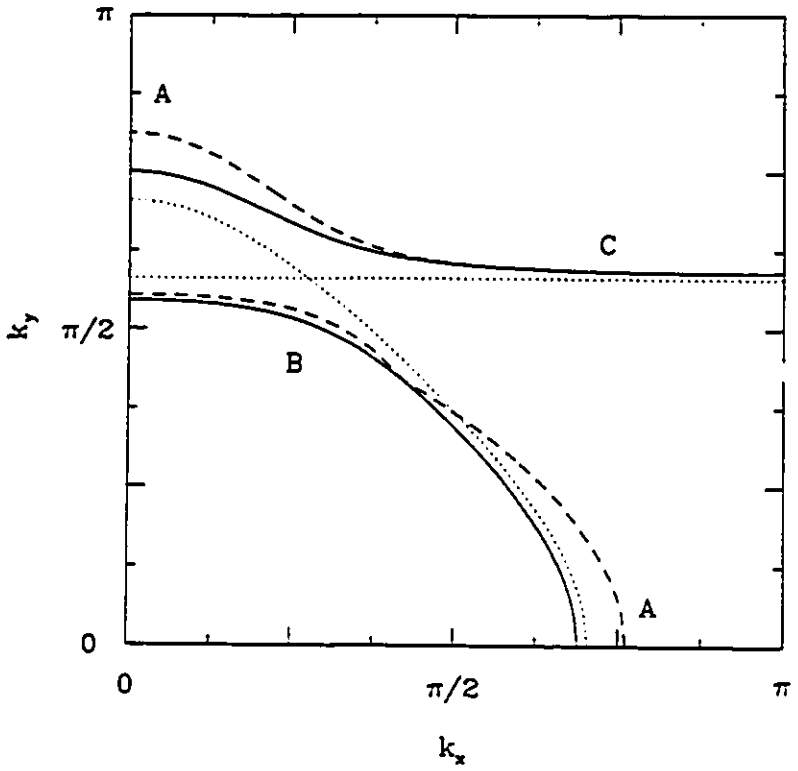

Figure 3.5: Structure of the superconducting gap on the Fermi surface.
The Fermi surfaces of the coupled chain and plane layers is shown (solid line) in comparison to those of the isolated layers (dotted line). The value of E_- is shown along the Fermi surface in the superconducting state (dashed line). In chapter 2. we took this as the definition of the "gap". Local maxima in the gap correspond to van Hove singularities of the saddle point type in E_-. and therefore appear as peaks in the DOS. Three regions which are of interest in the discussion of Fig. 3.4(b) are indicated: the saddle point at A is due to the intrinsic gap in the CuO_2 planes and it appears as the outer gap in Fig. 3.4: the saddle point at B appears as the inner gap in Fig. 3.4: the induced gap in the chains near C is so small that it is nearly invisible in Fig. 3.4. In tunneling experiments done at finite temperature. ρ_2 would have an apparent zero bias anomaly.

in agreement with Fig. 3.4. We can also see that the peak associated with the edge of the intrinsic gap is only weakly reflected in ρ_2. In Fig. 3.5 we show the regions of the Brillouin zone which contribute to the outer peak, and the reader can easily see that $t^2 \ll (\xi_1 - \xi_2)^2$.

The source of the inner gap is also indicated in Fig. 3.5. The inner gap is due to a vHS in the neighbourhood of the avoided Fermi surface crossing, and consequently it appears with roughly equal magnitude in ρ_1 and ρ_2. The width of the inner gap can be estimated as the value of E_- near the avoided crossing. The equation for the Fermi surfaces is $\xi_1\xi_2 = t^2$, and near the avoided crossing $\xi_1 \sim \xi_2 \sim \pm t$. The two choices of sign reflect the two pieces of Fermi surface. In order to choose the Fermi surface indicated in Fig. 3.5, we take $\xi_1 = \xi_2 = -t$. Furthermore, at this point, E_- is a maximum when $t(k_z)$ is a maximum, *ie.* at $k_z = 0$ where $t = 2t_\perp$. At this point $\Delta_k \sim 7$ meV and the inner gap is

$$\begin{aligned}\Delta_{\rm pk} &\sim E_- \\ &\sim \frac{|\Delta_k|}{2} \\ &\sim 3.5 \text{ meV}.\end{aligned}$$

Again, this estimate is in reasonable agreement with Fig. 3.5.

The final feature of note is the very narrow *induced gap* in ρ_2. In Fig. (3.5), we show the section of Fermi surface responsible for the small gap, and we can estimate its size by noting that, whenever $\xi_1^2 + \xi_2^2 \gg t^2$,

$$\begin{aligned}E_- &\sim \Delta_k \frac{t^2}{\xi_1^2 + \xi_2^2} \\ &= O(0.1 \text{ meV}).\end{aligned}$$

Experiments which are performed at temperatures greater than $\sim .1$ meV (~ 1 K) will not see the induced gap, but will instead see a finite density of normal electrons. In other words, it will appear as if there is a finite DOS at the Fermi surface.

This last result is significant and we will summarise it concisely: because the chain and plane Fermi surfaces have very different shapes, there are sections of the chain Fermi surface on which $t^2/(\xi_1 - \xi_2)^2 \ll 1$ and the induced gap is an order of magnitude (or more) smaller than in the planes. This result is independent of the symmetry of the order parameter, and is a feature of the proximity coupling of the chains and planes.

One of the weaknesses of other S/N models is their failure to treat the chains as one dimensional. By taking the N layer to be a two dimensional plane with a similar band

structure to the S layer, it is possible—with an appropriate choice of parameters—to have the S and N Fermi surfaces in sufficient proximity that $t^2/(\xi_1^2+\xi_2^2)$ is never small on the N Fermi surface. These models, therefore, have tended to predict that the gap in the chains can be of the same order as the gap in the planes.

3.2 Experiments

3.2.1 Tunneling experiments

Tunneling experiments provide a direct measurement of the electronic DOS in superconductors. Historically, they are significant for providing early experimental confirmation of BCS theory (Giaever 1960). The basic tunnel junction consists of an SIN multilayer where the S and N layers are superconducting and normal metal electrodes respectively, and the I layer is a thin insulating layer. In the original experiment of Giaever, for example, the current-voltage (I-V) characteristics of a Pb/AlO/Al junction were studied. The insulating AlO layer was 10-20 Å thick, so that a small voltage (millivolts), was sufficient to drive a measurable tunneling current through the junction.

The theory of SIN tunnel junctions can be extremely complicated (Wolf 1985), and we will restrict ourselves to the simplest possible model, in which the junction can be characterised by a single electron tunneling matrix element T_{kq}. A simple application of Fermi's Golden rule gives the current,

$$I=\frac{2\pi}{\hbar}\sum_{k,q}|T_{kq}|^2\Big\{f(E_k)[1-f(\xi_q)]-f(\xi_q)[1-f(E_k)]\Big\}\delta(E_k+eV-\xi_q). \tag{3.31}$$

where it is supposed that the superconducting side of the junction is at a voltage eV relative to the normal side. The labels k and q refer to the superconducting and normal metals respectively, and E_k and ξ_q are their respective energy dispersions. The function $f(x)$ is the Fermi function and the products $f(E_k)[1-f(\xi_q)]$ and $f(\xi_q)[1-f(E_k)]$ describe the availability of initial and final states for the forward (from S into N) and backwards (from N into S) tunneling processes respectively. It is common to make the simplifying assumption that $|T_{kq}|^2$ is independent of k and q, in which case

$$I\propto|T|^2\int d\omega\,\rho_S(\omega+eV)\rho_N(\omega)\left[\tanh\left(\frac{\beta(\omega+eV)}{2}\right)-\tanh\left(\frac{\beta\omega}{2}\right)\right]. \tag{3.32}$$

where ρ_S is the DOS in the superconducting material and ρ_N is the DOS in the normal metal. In the zero temperature limit.

$$I \propto |T|^2 \rho_N(0) \int_0^{eV} d\omega \, \rho_S(\omega). \tag{3.33}$$

where the approximation is made that $\rho_N(\omega)$ is approximately constant over the range $0 < \omega < eV$. The tunneling conductance, $G(V) = \partial I / \partial V$, is therefore

$$G(V) \propto \rho_S(eV). \tag{3.34}$$

At low temperatures, then, the *tunneling conductance* may be compared directly with the electronic DOS.

Despite the long history of the experimental technique, tunneling experiments involving the high T_c materials have provided confusing and contradictory results. Early experiments on SIN junctions were marred by the poor quality of the superconductors. The need for an undamaged surface at the SI interface cannot be overstated for the high T_c cuprates: the coherence length along the c axis in the cuprates is typically of the order $4\AA$, and since this is the characteristic length scale over which Δ may vary spatially, the order parameter at the surface of the superconductor will be determined to a large extent by the crystal structure at the surface. Tunneling experiments probe the DOS at the surface of the crystal, so it is crucial that the surface be free of damage.

In Fig. 3.6, the tunneling conductivity is shown for a YBCO/Pb junction. From the peak to peak distance in the tunneling spectrum, the gap can be estimated as $2\Delta_{pk} \sim$ 40 meV, which is consistent with most of the literature on the subject. It is interesting to note that the DOS agrees quite closely with the total DOS ($\rho_1 + \rho_2$) of Fig. 3.4: The gap appears to have a nested structure, with an inner and outer peak, and there is a significant zero bias anomaly.

The most common criticism of the YBCO/Pb junction experiments is that the quality of the surface adjacent to the junction is unknown. In an effort to preserve the integrity of the surface, *scanning tunneling microscope* (STM) techniques were developped to probe the DOS. The advantage of STM is that there is no contact between the probe and the surface of the superconductor so that the surface is undamaged by the experiment. In STM tunneling experiments, the N electrode is the tip of the STM probe, and the I layer is the small gap between the tip of the probe and the sample surface. The STM probes only a small region of the crystal surface ($\sim$ a few $\AA^2$) and is therefore likely to be able to probe

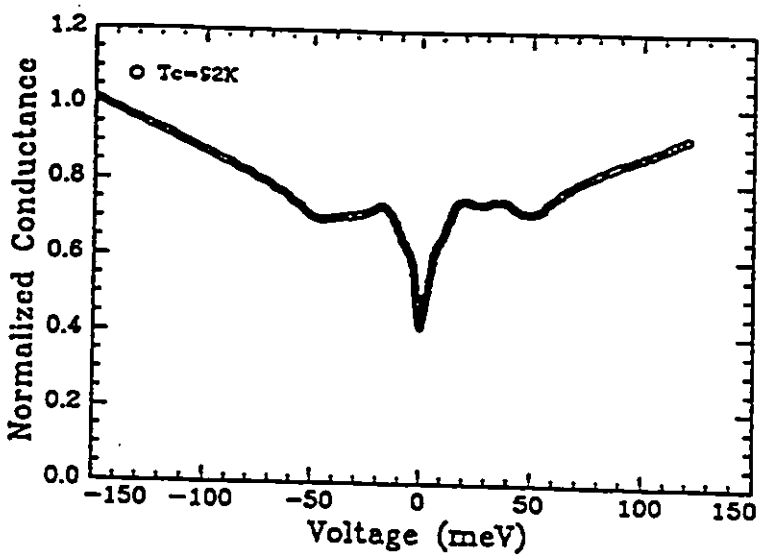

Figure 3.6: Tunneling conductance through a YBCO/Pb junction.
The conductivity is measured through a macroscopic SIN junction (Dynes 1995).

a single layer type. while a macroscopic junction will see an average of all exposed layers. In a recent article. Hasegawa *et al.* (1995) suggest that the structure of the gap seen in Fig. 3.6 is a mix of chain and plane DOS. Using an STM technique. they measure DOS of a single CuO_2 plane and find an *s* wave gap with relatively little structure. When they grow their thin films with a (110) orientation. so that both chain and plane layers are exposed to the surface. they find a DOS which looks much like that of Fig. 3.6. It is interesting to note that they also see a large zero bias anomaly in the chains.

Although Hasegawa *et al.* have consistently reported seeing an *s* wave gap in both YBCO and BSCCO STM experiments for a number of years. there is a reasonable fear that these results are due to Coulombic effects. The capacitance of the STM probe is very small. so that a small buildup of charge on the probe tip can lead to a "Coulomb blockade"—an energy barrier which must be overcome for tunneling to take place. The Coulomb blockade manifests itself as an apparent *s* wave gap in the DOS. In their defense. Hasegawa *et al.* point out that the size of the Coulomb blockade should depend on the distance between the

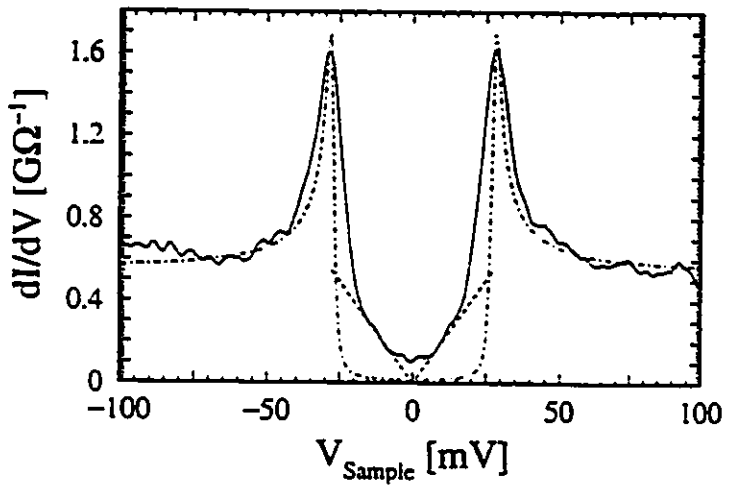

Figure 3.7: Tunneling conductance for BSCCO SIN junction.
The conductance is measured using an STM with a gold tip (Renner and Fischer 1995). The solid curve is the experimental data at 4.8 K. the dot-dashed curve is a BCS fit (s wave gap) with a small pair-breaking contribution. The dashed curve is the asymptotic low-bias behaviour predicted for a d wave symmetry.

tip of the probe and the sample. since that affects the capacitance of the junction. but that they find no change in the gap width with probe/sample distance.

A recent paper by Renner and Fischer(1995). which reports on STM measurements of BSCCO samples. contradicts Hasegawa. In a careful investigation of a single CuO_2 layer. they find a tunneling spectrum which is inconsistent with an s wave gap. Their results are reproduced in Fig. 3.7. and are strongly supportive of a gap with nodes on the Fermi surface.

3.2.2 Low Temperature Heat Capacity

One of the chief advantages of specific heat measurements as a probe of the low energy DOS is that they measure the DOS of the bulk of the sample. and not just of the surface. The relationship between the specific heat C_v at low temperatures and the DOS is

straightforward. The total energy of the crystal is

$$\langle H \rangle = \sum_{i,k} E_{ik} f(E_{ik}) + \text{const.}. \tag{3.35}$$

so that

$$\frac{\partial \langle H \rangle}{\partial T} = -2\beta^2 \sum_k \sum_{\pm} E_{\pm}^2 f'(E_{\pm}). \tag{3.36}$$

where the prime indicates the derivative of f with respect to $\beta E_{\pm}$. Inserting $\int d\omega \delta(\omega - E_{\pm})$ into Eq. (3.36) gives

$$\frac{\partial \langle H \rangle}{\partial T} = -N\beta^2 \int_{-\infty}^{\infty} d\omega \rho(\omega) \omega^2 f'(\omega). \tag{3.37}$$

where $\rho(\omega) = \rho_1(\omega) + \rho_2(\omega)$ and

$$\frac{2}{N} \sum_k \sum_{\pm} \delta(\omega - E_{\pm}) = \rho(\omega) + \rho(-\omega). \quad (\omega > 0).$$

As it is written. Eq. (3.37) is dimensionless. We change the units to J/mol K by letting $N = 6.02 \times 10^{23}$ and multiplying by $k_B = 1.38 \times 10^{-23}$ J/K. The specific heat becomes

$$C_v = 8.31\beta^2 \int_{-\infty}^{\infty} d\omega \rho(\omega) \omega^2 f'(\omega) \quad \frac{\text{J}}{\text{mol K}}. \tag{3.38}$$

where we recall that $\rho(\omega)$ is the DOS *per unit cell.*

At low temperatures. $f'(\omega)$ is strongly peaked about $\omega = 0$. and $\rho(\omega)$ can be expanded in ω. If the DOS near the Fermi surface is of the form

$$\rho(\omega) \sim \rho(0) + \rho'(0)\omega \tag{3.39}$$

then

$$C_v = \gamma_0 T \tag{3.40}$$

where

$$\gamma_0 = 8.31\rho(0) \int_{-\infty}^{\infty} dx\, x^2 \frac{\text{sech}^2(x/2)}{4}. \tag{3.41}$$

and the term proportional to $\rho'(0)$ vanishes. If there is a gap with a nodal structure. however. we have seen that the DOS is actually

$$\rho(\omega) \sim \rho(0) + b|\omega| \tag{3.42}$$

where $b = \rho'(0^+) = |\rho'(0^-)|$. In this case

$$C_v = \gamma_0 T + \alpha T^2. \tag{3.43}$$

where

$$\alpha = 8.31 b \int_{-\infty}^{\infty} dx\, |x|^3 \frac{\mathrm{sech}^2(x/2)}{4}. \tag{3.44}$$

If the DOS at the Fermi surface is nonzero. then $C_v(T)$ will have a *linear* component. If the DOS at the Fermi surface is a local minimum. and rises as $|\omega|$ away from the Fermi surface. then C_v will have a *quadratic* component.

In Fig. 3.8. the heat capacity for the chain-plane model is shown in the normal and superconducting states. In the normal state. C_v is linear. indicating a finite DOS which is constant over the energy interval considered (10 K). In the superconducting state. the linear component in C_v is reduced by an order of magnitude. and is due to the large nonzero DOS in the chains. The quadratic term is due to the lines of nodes in the gap along the plane Fermi surface at $k_x = \pm k_y$. The coefficients of the linear and quadratic terms are $\gamma_0 = 6$ mJ/mol K^2 and $\alpha = 0.4$ mJ/mol K^3. and are comparable to those found in specific heat measurements. Moler *et al.* find. for example. $\gamma_0 = 3.06$ mJ/mol K^2 and $\alpha = 0.11$ mJ/mol K^3 (Moler et al. 1994). Agreement between their value of α and the one found here is fair. Moler *et al.* also make a prediction for α based on a simple d wave model and estimate $\alpha \sim 0.2$—0.3 mJ/mol K^3. which is closer to the value we find here.

The agreement between the value of γ_0 found by Moler *et al.* and the value found here is interesting. Phillips (1994) has commented that no experiment has found a value of γ_0 which is substantially less than 4 mJ/mol K^2. suggesting that it is an intrinsic property of Y-123. As we have indicated above. the linear term is due to a finite density of states at the Fermi surface. Our proximity model suggests that the finite density of states is due to the smallness of the induced gap on certain regions of the chain Fermi surface (marked as "C" in Fig. 3.5). For temperatures which are higher than the energy of the induced gap. these regions of chain will appear to be normal. leading to a linear term in $C_v(T)$.

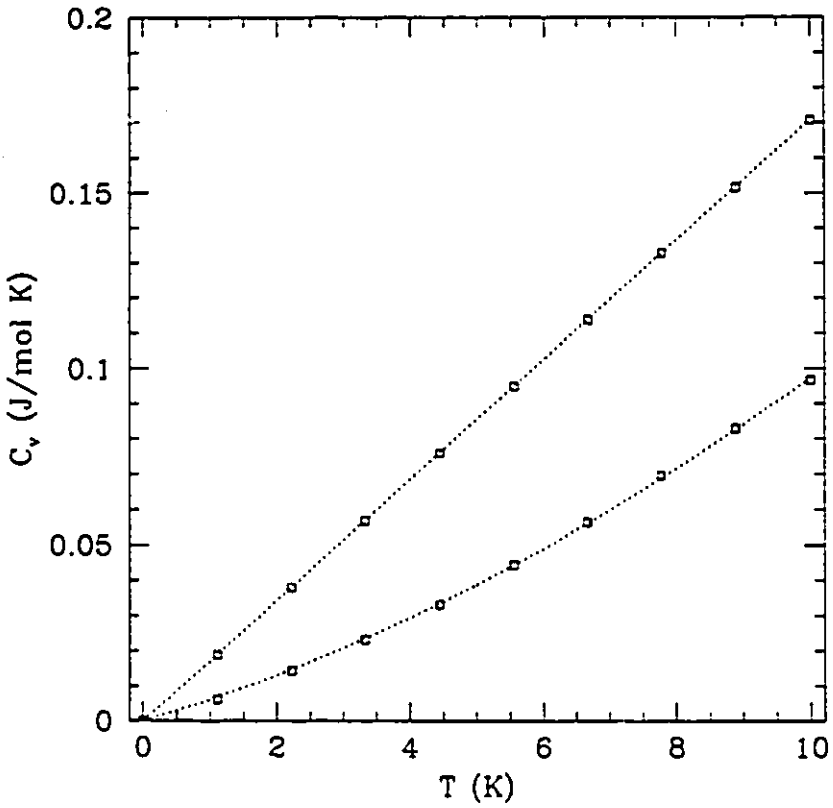

Figure 3.8: Heat capacity of the chain plane model.

The heat capacity is shown for the normal (upper curve) and superconducting (lower curve) states. The points are the results of numerical calculations, while the dotted lines are the results of a least squares fit of $C_v = \gamma_0 T + \alpha T^2$. The fitted parameters in the normal state are $\gamma_0 = 17$ mJ/mol K^2, $\alpha = 5 \times 10^{-4}$ mJ/mol K^3. For the superconducting state they are $\gamma_0 = 6$ mJ/mol K^2, $\alpha = 0.4$ mJ/mol K^3.

3.2.3 Low Temperature Knight Shift

In the presence of a static applied magnetic field $B = B_0\hat{z}$ ($\hat{z}$ is the unit vector in the z direction), an isolated nucleus has an interaction energy U between the field and the nuclear spin (Kittel 1986):

$$U = -g\mu_B B_0 m_z.$$

where g is the Landé g factor, μ_B is the Bohr magneton, and m_z is the quantum number for the z component of the nuclear spin. The nucleus will then absorb an applied r.f. field at a resonant frequency ω_0 which is determined by the energy difference between adjacent quantum levels:

$$\hbar\omega_0 = g\mu_B B_0. \tag{3.45}$$

For a nucleus in the presence of electrons, the resonant frequency is shifted by the hyperfine interaction. This shift is known as the *Knight shift* and is denoted by K. The nucleus can interact with both the electron orbital moments and electron spins. It is the shift K_S due to the electron spins in which we are interested here, and in the experiments with which we shall compare our results, the orbital contribution K_O to the shift is subtracted. As we shall see, a measurement of the the Knight shift due to the electron spins gives a direct measurement of the Pauli susceptibility. The Pauli susceptibility χ_0 of an electron gas is defined as $\partial M/partial B$, where M is the magnetization of the electron gas, and B is the applied magnetic field.

The energy of the nucleus in the presence of conduction electrons is shifted by δU due to the electron spins (Kittel 1986),

$$\delta U = a\langle S_z\rangle m_z. \tag{3.46}$$

where $\langle S_z\rangle$ is the total spin of the electrons and a is a prefactor which is determined by the overlap of the electron wavefunctions with the nucleus. The shift in the resonant frequency is therefore

$$K_S = a\langle S_z\rangle/\hbar. \tag{3.47}$$

Since $\langle S_z\rangle$ is related to the magnetization of the sample, it is possible to determine the Pauli susceptibility from

$$\chi_0 = \frac{\hbar\mu_B}{a}\frac{\partial K}{\partial B_0}. \tag{3.48}$$

In general, a is not known, so that it is only possible to determine relative changes in χ_0 (with temperature, for example).

When there is no external field, $\langle S_z \rangle = 0$. For a finite field, however, the electron energies are shifted by $\pm g\mu_B B_0$, depending on whether the electron spins are aligned with $(-)$ or against $(+)$ B_0. The total spin of the electrons becomes

$$\langle S_z \rangle = \frac{\hbar}{2}(n_\uparrow - n_\downarrow). \tag{3.49}$$

where

$$n_\uparrow = \sum_{i,k} f(E_{ik} - \mu_B B_0) \tag{3.50(a)}$$

$$n_\downarrow = \sum_{i,k} f(E_{ik} + \mu_B B_0). \tag{3.50(b)}$$

$$\tag{3.50}$$

The index i in the sum is the band index, and E_{ik} are the band energies in either the superconducting or normal states. The superconducting condensate is ignored in Eq. (3.50) since, for singlet pairing, $n_\uparrow = n_\downarrow$. As before, we can insert $\int d\omega\, \delta(\omega - E_{ik})$ into Eq. 3.50 to get

$$K_S = \frac{\hbar}{2}\int_{-\infty}^{\infty} d\omega\, \rho(\omega)[f(\omega - \mu_B B_0) - f(\omega + \mu_B B_0)]. \tag{3.51}$$

In the limit of weak magnetic fields ($\mu_B B_0 \ll k_B T$),

$$K_S \propto \frac{B_0}{T}\int_{-\infty}^{\infty} d\omega\, \rho(\omega)\mathrm{sech}^2(\omega/2T). \tag{3.52}$$

so that

$$\chi_0 \propto \frac{1}{T}\int_{-\infty}^{\infty} d\omega\, \rho(\omega)\mathrm{sech}^2(\omega/2T). \tag{3.53}$$

While Eq. (3.53) applies at all temperatures, it must be remembered that $\rho(\omega)$ is a temperature dependent quantity due to the temperature dependence of Δ_0. For low temperatures, Δ_0 is approximately constant, so that we can use our zero temperature density of states to calculate the susceptibility (*cf.* Fig. 2.4). The spin susceptibility, calculated for three different cases is shown in Fig. 3.9. In one case, the susceptibility is calculated for a conventional BCS superconductor with $T_c = 100$ K and $2\Delta/k_B T_c = 3.52$. Because there is a true gap in the DOS at the Fermi surface, the thermal pair breaking—and

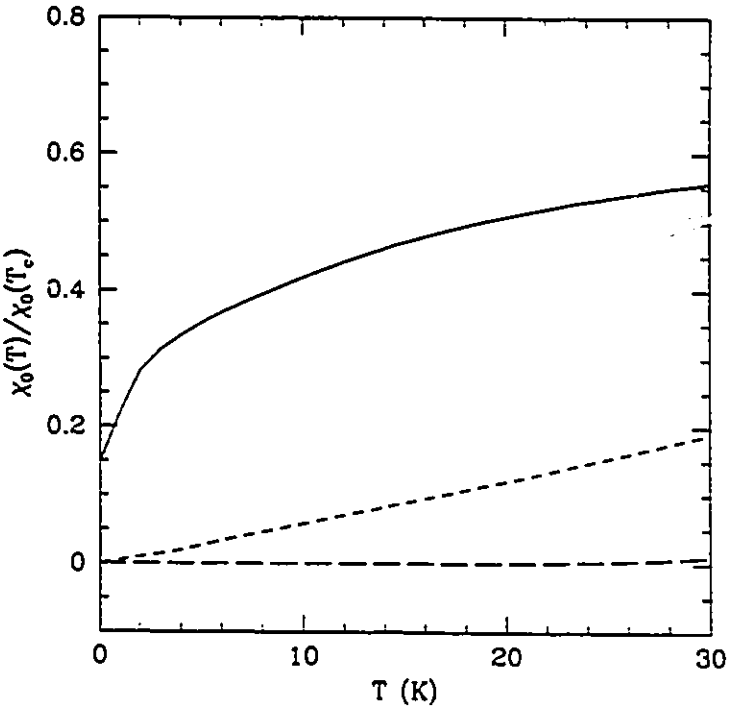

Figure 3.9: Low temperature Pauli susceptibility.
The susceptibility is shown for an s wave model (short dash), a d wave model (long dash) and the chain-plane model (solid). The curves are calculated from Eq. (3.53).

therefore the susceptibility—is exponentially small at low temperatures. In the second case, χ_0 is found for a single d wave layer. Its linear temperature dependence is a direct result of the linear energy dependence of the DOS near the Fermi surface. Finally, χ_0 is shown for the chain-plane model. It rises sharply at low T and then exhibits a linear behaviour similar to that of the d wave case. The rapid rise in χ_0 at low T is due to the small size of the induced gap in the chains. The finite value of χ_0 at $T = 0$ implies that there is a finite DOS at the Fermi surface. While we know that this is not strictly true, it is an indication that there are a significant number of states with an energy less than the thermal energy k_BT at which the lowest point is calculated.

In Fig. 3.10, the Knight shift for a Y-123 powder is shown (Ishida et al. 1993). The data for the clean Y-123 has been fitted phenomenologically to a d wave model in which

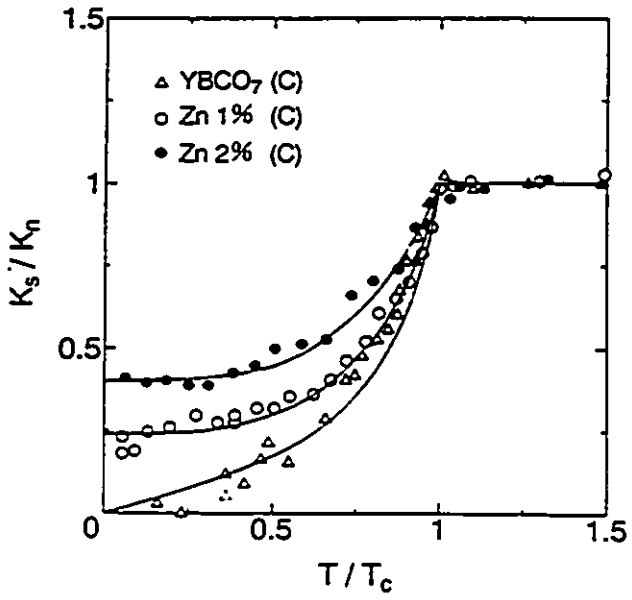

Figure 3.10: Knight shift with orbital contribution subtracted.
The three different data sets show the effect of zinc doping. The optimally doped material (triangles) has a linear low frequency temperature dependence and is fit by a d wave model in which $2\Delta_0/k_bT_c = 8$ (Ishida et al. 1993).

$2\Delta_0/k_BT_c$ is treated *as a free parameter.* The fit is best when $2\Delta_0/k_BT_c = 8$. Although the fit is quite reasonable, it is not the result of self consistent application of d wave theory and should not simply be taken as evidence of d wave symmetry. It should, however, be taken as evidence that the gap has nodes on the Fermi surface. The need to adjust $2\Delta_0/k_BT_c$, reflects the fact that in a simple d wave model $|\nabla_k\Delta_k|$ is too small near the nodes.

One of the most striking differences between Fig. 3.10 and Fig. 3.9 is that experimentally, the spin Knight shift is found to vanish at $T = 0$. This is an artifact of the way in which the data is presented. The Knight shift which is experimentally measured has contributions from both the spin-orbit coupling and from the Pauli susceptibility. In the measurements of the Knight shift, it is assumed (at least for the clean materials) that the spin-orbit contribution is independent of temperature and that the spin contribution vanishes at $T = 0$ (Barrett et al. 1990; Takigawa et al. 1989; Ishida et al. 1993). It is standard practice to take the spin Knight shift to be $K_S(T) = K_{\text{total}}(T) - K_{\text{total}}(0)$. In Fig. 3.10 $K_{\text{total}}(0)$ is of similar magnitude to $K_S(T)$ in the normal state. Knight shift experiments

will not reveal. therefore, whether or not there is a finite spin susceptibility at $T \sim 0$.

There have been at least two attempts to explain the Knight shift data using spin fluctuation models (Monien and Pines 1990: Bulut and Scalapino 1992). In both of these works. the ratio Δ_0/T_c is again treated as an adjustable parameter. Although the fit is quite good in both cases. it is reasonable to question whether this is guaranteed for any model in which there are nodes in the Fermi surface and for which Δ_0/T_c is adjustable. Some of the early data (Takigawa et al. 1989: Barrett et al. 1990) has been successfully fitted to a layered s wave proximity model (Tachiki et al. 1992).

3.3 Summary

In this chapter. we have compared the density of states of the chain-plane model introduced in chapter 2 with tunneling. low T specific heat and Knight shift experiments. We found that both tunneling and specific heat measurements see a finite density of normal carriers at the Fermi surface for the lowest temperatures at which measurements are made ($T \sim 2$ K). We argued that this was consistent with our model. The temperature dependence of the Knight shift. however. does not agree with our model. It should be remembered. though. that Knight shift measurements are problematic because they are unable to clearly distinguish between contributions due to normal electrons at $T = 0$ and contributions due to spin-orbit coupling. Knight shift measurements still disagree with the chain-plane model because they do not see the dramatic change in the slope of $K_S(T)$ below $T = 2$ K which we see in our calculations. For the data presented. 2 K is slightly below the lowest temperature measured.

One should not naïvely expect to find a sudden change in the behaviour of the Knight shift and specific heat measurements below $T \sim 1$ K. however. A point which we have made but not emphasised is that the values of the gap seen by these experiments depends strongly on the band structure. By this. we do not mean that Δ_0 varies strongly with the band structure. but instead that the value of Δ_k near the Fermi surface will change as the Fermi surface shape changes. More importantly. the value of the induced gap in the chains depends dramatically on the relative shapes and locations of the plane and chain Fermi surfaces. While the qualitative structure of the calculations we have presented are independent of the band parameters. the energy scales at which they occur depends on the band structure.

In summary, then, we can say that specific heat measurements suggest that there is a finite fraction of normal electrons at low T ($\sim$ 1 K) in Y-123. The fraction is substantial since, in our calculations, the ratio of the linear terms in the normal and superconducting states is $\gamma_{0sup}/\gamma_{0nor} \sim \rho(0)_{sup}/\rho(0)_{nor} \sim 1/3$, in rough agreement with experiment (Moler et al. 1994). It is unlikely that Knight shift measurements have anything to say on this matter. With our model, we have made a suggestion as to the source of the normal state electrons. These electrons would not be visible in dc measurements (such as the penetration depth, which is calculated in chapter 4) but would be visible in the optical conductivity, which this model would predict to have a Drude peak along the chain direction.

Chapter 4

Penetration Depth

4.1 Introduction

In the following article, we calculate the penetration depth λ for the chain-plane model. The penetration depth is the (microscopic) length scale that an applied magnetic field can penetrate into a superconductor. It is analogous to a skin depth in an ordinary metal, except that (unlike the skin depth) it does not vanish for static fields.

In order to expel an applied magnetic field from its bulk, a superconductor sets up superconducing screening currents. The magnitude of the screening currents (and therefore the penetration depth) depends on two properties of the superconductor. The first is the superfluid density: the higher the density of Cooper pairs, the more an applied field is screened. The second property is the band structure, or rather the Fermi velocities of electrons at the Fermi surface. In penetration depth experiments, both of these properties are probed (Zhang et al. 1994). The temperature dependence of the penetration depth reveals the change in superfluid density with temperature, while the anisotropy of the penetration depth (*ie.* its dependence on the direction of the applied field) is the result of the anisotropy of the Fermi velocity.

At the time that this article was written, interest in the superconducting properties of the CuO chains was beginning to grow. Measurements of transport properties provide an ideal technique for isolating the properties of the chains and planes. Penetration depth experiments at low temperatures effectively measure a density of states which is weighted in favour of electrons with a large Fermi velocity in the direction of the screening current. The penetration depth λ_b (the subscript refers to the direction of the screening currents) therefore contains contributions from both the chains and planes, while λ_a is determined

purely by the planes.

The penetration depth is related to the superfluid density n_s of the single band two fluid model by

$$\lambda_a^{-2} = \frac{n_s e^2}{m_a^* c}$$

where m_a^* is the (diagonal) effective mass tensor. It is not a simple matter of taking the difference between λ_a^{-2} and λ_b^{-2} to find the superfluid density on the chains since the anisotropy of the effective mass tensor is unknown. In fact, in a multiple band model the effects of the band structure can not really be reduced to an effective mass tensor. In order to interpret the penetration depth measurements, therefore, it is necessary to calculate the penetration depth based on a multiple band model of YBCO.

There is a slight change of notation between this paper and the work which has preceeded it. The symbol t_0 is the coefficient of the chain-plane coupling strength. It is defined such that $t_0 \equiv 2t_\perp$.

Effect of proximity coupling of chains and planes on the penetration-depth anisotropy in $YBa_2Cu_3O_7$

W. A. Atkinson and J. P. Carbotte
Department of Physics and Astronomy, McMaster University, Hamilton, Ontario, Canada L8S 4M1
(Received 12 May 1995)

We calculate the penetration depth λ in the a, b, and c directions for a simple model of $YBa_2Cu_3O_7$. In this model there are two layers—representing a CuO_2 plane and a CuO chain—per unit cell. There is a BCS-like pairing (both s-wave and d-wave are considered) interaction localized in the CuO_2 planes. The CuO chains become superconducting at temperatures lower than T_c because of their proximity to the planes and there is an induced gap in the chains. Since the temperature dependence of the penetration depth in the b direction (along the chains) is sensitive to the size of the induced gap, the difference between the shapes of the penetration depth curves in the a and b directions reveals a great deal about the nature of the condensate in the chains. We find that in our proximity model there are always regions of the chain Fermi surface on which the induced gap is much smaller than T_c, so that the temperature dependence of λ_b is always different than that of λ_a. Experimental observations of the of the ab anisotropy show nearly identical temperature dependences. The main result of our paper, then, is that a simple proximity model in which the pairing interaction is localized to the planes, and the planes are coherently coupled to the chains cannot account for the superfluid on the chains.

I. INTRODUCTION

It is widely believed that the source of the pairing interaction which is responsible for the superconducting transition in the high-T_c cuprates lies in the CuO_2 planes, which are common to all of the cuprates. Many models which attempt to explain high-T_c superconductivity are two dimensional, which is a reflection of the assumption that the only active pieces of the crystal are the CuO_2 planes and that the remaining ions act as placeholders or as charge reservoirs. In some materials, however, there are additional layers whose behavior is not clear. In $Bi_2Sr_2CaCu_2O_8$, for example, it has been suggested that the BiO layer plays the role of a normal metal in close proximity to a superconducting material.[1]

The only materials in which there is clear evidence that the CuO_2 planes are not the only active portion of the unit cell are $YBa_2Cu_3O_7$ (Y-123), $YBa_2Cu_4O_8$ (Y-124) and their close relatives. In these materials there are quasi-one-dimensional CuO chain structures. Experiments measuring the dc resistivity,[2,3] the infrared and optical conductivity,[4] and the penetration depth in untwinned crystals[5] and ceramics[6] have found large anisotropies between the a direction (in-plane, perpendicular to the chains) and the b direction (in-plane, parallel to the chains) which suggest that substantial currents are carried along the chains in both the normal and superconducting state.

In the superconducting state, the source of the condensate on the chains in unclear. One possibility is that the pairing interaction is localized to the CuO_2 planes, but that the chains become superconducting by a proximity effect. In the proximity effect, an intrinsically normal metal which is in close contact with a superconductor becomes superconducting near the junction as a result of pair tunneling through the junction. The size of the induced gap in the normal metal depends on the strength of the coupling across the junction. Y-123 and Y-124 are good candidates for proximity effect models because they have the least anisotropy between the in-plane and c axis transport properties of the cuprate superconductors, and should therefore have a relatively large coupling between the chains and planes.

Proximity effect models have been studied in the context of high-T_c materials for a number of years. The most common point of view is that the unusual properties of the cuprates can be explained by an isotropic BCS pairing interaction which is contained in one of the planes.[1,7–12] The idea behind most of the work is that although the pairing interaction may be inherently isotropic, the strongly anisotropic band structure leads to a gap structure which may account for the unusual superconducting properties of the cuprates. The current authors have taken a different point of view in recent work on proximity effect models.[13–15] We have assumed that the pairing interaction in the planes is intrinsically d-wave and then attempted to assess the influence of coupling to the chains. Closely related to the proximity models are the S/S' multilayer models in which there are two (or more) different superconducting layers in the unit cell. There have been detailed examinations of the roles played by interplane and intraplane pairing[16–18] and a few quantitative calculations of physical properties,[8,16,17] but these models have been less thoroughly explored than the proximity model because of their relative complexity.

In this work we address the issue of whether a proximity model can account for the condensate on the chains in the YBaCuO compounds. We do this by calculating

Reprinted from Phys. Rev. B 52, pp. 10601–10609 (1995).

the penetration depth λ for a simple s or d wave model in the a, b, and c directions. In particular, we are interested in comparing the temperature dependences of λ_a and λ_b with experiment.[5] In our model, the unit cell consists of a CuO_2 plane layer and a CuO chain layer. The CuO_2 planes contain the pairing interaction and are coupled to the CuO chains through coherent single-electron tunneling so that there is an induced gap in the chains. Calculations of the penetration depth in a similar model have been made before,[11,14] although the intrinsically normal layers were planes and not chains, and the emphasis was on the anisotropy between λ_{ab} and λ_c.

In Sec. II we introduce our model Hamiltonian and find the single-particle Green's functions which we will need for the penetration depth. In Sec. III we derive an expression for the penetration depth which is suitable for a two-band, tight binding model. The calculation differs slightly from one we made previously.[14] In Sec. IV we discuss the results of numerical calculations of the penetration depth, and in Sec. V we broaden the scope to a discussion of the nature of the condensate on the chains.

II. HAMILTONIAN

The goal of this section is to introduce our model for YBCO, and to find the single-particle Green's functions necessary for the calculation of the penetration depth in Sec. III. We begin with a Hamiltonian which describes a system with two layers per unit cell. Adjacent layers are separated by a distance $d/2$. The first layer represents a CuO_2 plane and it contains a BCS-like pairing interaction. The second layer represents a CuO chain. It has a one-dimensional dispersion and is intrinsically normal. The chains are superconducting, however, because of their coupling to the planes through single-electron tunneling. The Hamiltonian, expressed in the Nambu formalism, is

$$\mathbf{H} - \mathbf{N}\mu = \sum_{\mathbf{k}} \mathbf{C}^\dagger(\mathbf{k}) Q(\mathbf{k}) \mathbf{C}(\mathbf{k}) + \text{const}, \tag{1}$$

where

$$\mathbf{C}(\mathbf{k}) = \begin{bmatrix} c_{1\mathbf{k}\uparrow} \\ c^\dagger_{1-\mathbf{k}\downarrow} \\ c_{2\mathbf{k}\uparrow} \\ c^\dagger_{2-\mathbf{k}\downarrow} \end{bmatrix} \tag{2}$$

and

$$Q = \begin{bmatrix} \xi_1(\mathbf{k}) & -\Delta_{\mathbf{k}} & t(\mathbf{k}) & 0 \\ -\Delta^*_{\mathbf{k}} & -\xi_1(-\mathbf{k}) & 0 & -t^*(-\mathbf{k}) \\ t^*(\mathbf{k}) & 0 & \xi_2(\mathbf{k}) & 0 \\ 0 & -t(-\mathbf{k}) & 0 & -\xi_2(-\mathbf{k}) \end{bmatrix}. \tag{3}$$

This Hamiltonian has been discussed at length elsewhere[1,13,15] and we only describe it briefly here. The dispersions ξ_1 and ξ_2 are for the plane and chain layers, respectively. We assume tight binding dispersions so that $\xi_1 = -2\sigma_1[\cos(k_x a) + \cos(k_y b)] - \mu_1$ and $\xi_2 = -2\sigma_2 \cos(k_y b) - \mu_2$, where a and b are the lattice constants in the planes. In optimally doped Y-123 crystals, a and b differ by $\sim 1\%$. For the numerical calculations done in this work, we take $a = b$. We take $\sigma_1 = 100$ meV so that the full bandwidth of the CuO_2 plane is 0.8 eV. For the chain layer we take $\sigma_2 = 80$ meV so that $\lambda_a^2(T=0)/\lambda_b^2(T=0) \sim 2.5$, as seen experimentally by Basov *et al.*[4] The chemical potentials are $\mu_1 = -80$ meV and $\mu_2 = 40$ meV, which yields a Fermi surface that is in qualitative agreement with band structure calculations.[33,34] We have absorbed an arbitrary band offset into the chemical potentials so that $\mu_1 \neq \mu_2$. The chains and planes are coupled by the matrix element $t(k_z) = -t_0 \cos(k_z d/2)$, where $d/2$ is the distance between the chains and planes. The chain-plane coupling affects the penetration depth in two ways. First, $t(k_z)$ determines the c-axis transport properties. In a previous paper[14] we have shown that the ratio $\lambda_c(T=0)/\lambda_{ab}(T=0)$ varies inversely with t_0. Second, $t(k_z)$ determines the size of the superconducting gap induced on the chains, which is reflected in the temperature dependence of λ_b. In this work we choose $t_0 = 50$ meV which yields $\lambda_c^2(T=0)/\lambda_a^2(T=0) \sim 100$, which is in rough agreement with experimental observations.[19–22]

The final feature of our Hamiltonian is that there is a pairing interaction in the plane which drives the superconducting transition. As we have mentioned above, the chains also become superconducting at T_c through their coupling to the planes. The pairing interaction in the planes has the form $V_{\mathbf{k}\mathbf{k}'} = V\eta_{\mathbf{k}}\eta_{\mathbf{k}'}$ with $\eta_{\mathbf{k}} = 1$ for an s-wave superconductor and $\eta_{\mathbf{k}} = \cos(k_x) - \cos(k_y)$ for a $d_{x^2-y^2}$ superconductor. Since the pairing interaction is separable, the order parameter

$$\Delta_{\mathbf{k}} \equiv \frac{1}{\Omega} \sum_{\mathbf{k}'} V_{\mathbf{k}\mathbf{k}'} \langle c_{1-\mathbf{k}'\downarrow} c_{1\mathbf{k}'\uparrow} \rangle \tag{4}$$

(where Ω is the volume of the crystal) can be written $\Delta_{\mathbf{k}} = \Delta_0 \eta_{\mathbf{k}}$.

Diagonalization of the Hamiltonian leads to four energy bands $E_1 = E_+$, $E_2 = E_-$, $E_3 = -E-$, $E_4 = -E+$ with

$$E_\pm^2 = \frac{\xi_1^2 + \xi_2^2 + \Delta_{\mathbf{k}}^2}{2} + t^2 \pm \sqrt{\left[\frac{\xi_1^2 - \xi_2^2 + \Delta_{\mathbf{k}}^2}{2}\right]^2 + t^2[(\xi_1 + \xi_2)^2 + \Delta_{\mathbf{k}}^2]}. \tag{5}$$

In Fig. 1 we show the Fermi surface for a range of k_z values between 0 and π/d. The Fermi surface consists of two surfaces on which E_- vanishes in the normal state. The two surfaces are given by the two solutions to $\xi_1(\mathbf{k})\xi_2(\mathbf{k}) = t(k_z)^2$. When $k_z = \pi/d$, $t(k_z) = 0$ and the two pieces of Fermi surface are those of the isolated chain and plane subsystems. When $t(k_z) \neq 0$, the chain and plane states form hybrid bands whose energies are given by

$$\epsilon_\pm = \frac{\xi_1 + \xi_2}{2} \pm \sqrt{\left(\frac{\xi_1 - \xi_2}{2}\right)^2 + t^2},$$

in the normal state. The shift in the band energy due the

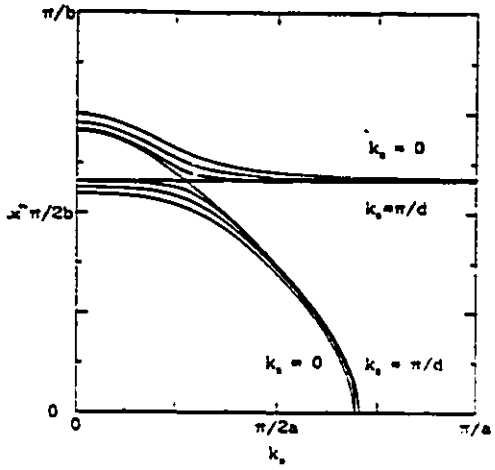

FIG. 1. The Fermi surface for the model Hamiltonian is shown for a range of k_z between $k_z = 0$ and $k_z = \pi/d$. When $k_z = \pi/d$, the chain-plane coupling vanishes and the two pieces of Fermi surface are those of the isolated chains and planes. As the chain-plane coupling increases, the Fermi surfaces hybridize and are pushed apart. The effect of the chain-plane coupling is largest where the two Fermi surfaces are closest together. There is an induced gap on the chains whose size is greatest where there is the most chain-plane mixing.

chain-plane coupling is clearly dependent on the relative sizes of t^2 and $(\xi_1 - \xi_2)^2$. The effect of the chain-plane coupling on the Fermi surfaces shown in Fig. 1 is largest in the neighborhood of the Fermi surface crossing at $\xi_1 = \xi_2 = 0$.

The quasiparticle operators in the diagonalized representation are

$$\tilde{\mathbf{C}}_i(\mathbf{k}) = \sum_{j=1}^{4} U_{ij}^{\dagger}(\mathbf{k})\mathbf{C}_j(\mathbf{k}), \tag{6}$$

where $U(\mathbf{k})$ is the 4×4 matrix which diagonalizes Q: $U = [U_1 U_2 U_3 U_4]$ with

$$U_j = \frac{1}{\sqrt{C}} \begin{bmatrix} (E_j - \xi_2)A \\ -(E_j + \xi_2)B \\ tA \\ tB \end{bmatrix}, \tag{7}$$

$$A = t^2 - (\Delta_{\mathbf{k}} + E_j + \xi_1)(E_j + \xi_2),$$

$$B = t^2 - (\Delta_{\mathbf{k}}^{*} + E_j - \xi_1)(E_j - \xi_2),$$

$$C = A^2[t^2 + (E_j - \xi_2)^2] + B^2[t^2 + (E_j + \xi_2)^2].$$

Now that we have diagonalized the Hamiltonian, we can find the single-particle Green's functions which we will require in the following section. Defining the temperature Green's function $G(\mathbf{k};\tau)_{ij} = -(1/\hbar)\langle \mathbf{T}\mathbf{C}_i(\mathbf{k};-i\tau)\mathbf{C}_j^{\dagger}(\mathbf{k};0)\rangle$, where T is the fermion time-ordered product, we have

$$G(\mathbf{k};i\zeta_l)_{ij} = \sum_{m=1}^{4} \frac{U_{im}(\mathbf{k})U_{mj}^{\dagger}(\mathbf{k})}{i\hbar\zeta_l - E_m(\mathbf{k})}, \tag{8}$$

where

$$G(\mathbf{k};i\zeta_l)_{ij} = \int_0^{\hbar\beta} d\tau\, e^{i\zeta_l\tau} G(\mathbf{k};\tau)_{ij},$$

$\zeta_l = (2l+1)\pi/\hbar\beta$ are the fermion Matsubara frequencies and $\beta = 1/k_B T$, where k_B is the Boltzmann constant and T is temperature. In our calculation of the penetration depth we will need

$$G(\mathbf{k};\tau = 0^{-})_{ij} = \frac{1}{\hbar}\sum_{l=1}^{4} U_{il}(\mathbf{k}) f[E_l(\mathbf{k})] U_{lj}^{\dagger}(\mathbf{k}), \tag{9}$$

where $f(x) = 1/[1 + \exp(\beta x)]$.

We finish this section with a brief discussion of our usage of the word "gap." In the model presented above, there is only one order parameter, $\Delta_{\mathbf{k}}$, and it describes the condensate in the CuO_2 planes. For a separable potential, $\Delta_{\mathbf{k}}$ has the symmetry of the pairing interaction. In a multiband material, however, $\Delta_{\mathbf{k}}$ is not simply related to the pair wave function. For example, the anomalous Green's function (which is essentially the pair wave function) in the CuO_2 plane is

$$G(\mathbf{k};\omega)_{12} = -\frac{\Delta_{\mathbf{k}}(\omega^2 - \xi_2^2)}{(\omega^2 - E_+^2)(\omega^2 - E_-^2)}.$$

Notice that the symmetry of G_{12} is *not* the same as the symmetry of $\Delta_{\mathbf{k}}$. For this reason, the term "gap" is kept distinct from the term "order parameter," which refers to $\Delta_{\mathbf{k}}$. Perhaps the most useful working definition of "gap" is that it is the value of E_- on the Fermi surface. Clearly, by this definition, the gap is k dependent. In regions of the Brillouin zone where a section of Fermi surface has predominantly chain (or plane) character, the gap can be associated with the chains (or planes). It is wrong to think of the pairs being localized to the chains or planes. however; the pairing amplitude between an electron in the chains and an electron in the planes (measured by G_{14} and G_{23}) is nonzero. In fact the picture of a gap belonging to a plane or a chain breaks down in regions of the Brillouin zone where the Fermi surface is a strong hybridization of the chain and plane bands.

III. PENETRATION DEPTH

The penetration depth is found using an approach which is suitable for the tight binding limit. This approach is slightly different than that of our previous work,[14] although it yields quantitative results which are

nearly identical. As we shall see, however, the current method, which is based on one used by Hirsch and Marsiglio for a one band tight binding model,[23] is more satisfying from a physical point of view.

We begin by writing out the current operator $\mathbf{j_0}$ in the absence of a magnetic field:[24]

$$\mathbf{j_0}(\mathbf{q}=0) \equiv \int d^3r\, \mathbf{j}(\mathbf{r}) = \frac{ie}{\hbar}[\mathbf{H_0^n}, \mathbf{P}], \tag{10}$$

where

$$\mathbf{P} \sim \sum_{i,\mathbf{R}_i} \mathbf{R}_i c_i^\dagger(\mathbf{R}_i) c_i(\mathbf{R}_i) \tag{11}$$

is the polarization vector and $\mathbf{H^n}$ is the Hamiltonian in the normal state. The operator $c_i^\dagger(\mathbf{R}_i)$ creates an electron in the Wannier state located at the sublattice point $\mathbf{R}_i$. The set of points $\{\mathbf{R}_1\}$ refers to the plane sublattice while $\{\mathbf{R}_2\}$ refers to the chain sublattice. The Wannier representation is connected to the k-space representation by

$$c_i(\mathbf{R}_i) = \frac{1}{\sqrt{N}} \sum_{\mathbf{k}} e^{i\mathbf{k}\cdot\mathbf{R}_i} c_i(\mathbf{k}), \tag{12}$$

where N is the number of lattice sites.

In the normal state the Hamiltonian, Eq. (1), can be written in the Wannier representation as

$$\begin{aligned}\mathbf{H_0^n} = &-\sum_{i=1}^{2} \sum_{\mathbf{R}_i,\mathbf{r}_1} \sigma_i c_i^\dagger(\mathbf{R}_i + \mathbf{r}_1) c_i(\mathbf{R}_i) \\ &-\frac{t_0}{2} \sum_{\mathbf{R}_1,\mathbf{R}_2} \{c_1^\dagger(\mathbf{R}_1) c_2(\mathbf{R}_2)[\delta_{\mathbf{R}_1+\hat{z}d/2,\mathbf{R}_2} \\ &+ \delta_{\mathbf{R}_1-\hat{z}d/2,\mathbf{R}_2}] + \text{H.c.}\}. \end{aligned} \tag{13}$$

The vector $\mathbf{r}_1$ is the displacement to the nearest neighbors of $\mathbf{R}_1$ within the plane, $\hat{z}$ is the unit vector in the z direction, and H.c. indicates the Hermitian conjugate. This Hamiltonian describes nearest neighbor hopping both within and between the chains and planes. Substituting Eqs. (11) and (13) into Eq. (10) we get

$$\begin{aligned}\mathbf{j_0} = &\frac{ie}{\hbar} \sum_{i,\mathbf{R}_i,\mathbf{r}_1} \sigma_i \mathbf{r}_1 c_i^\dagger(\mathbf{R}_i + \mathbf{r}_1) c_i(\mathbf{R}_i) \\ &-\frac{iet_0 d}{4\hbar} \sum_{\mathbf{R}_1} \hat{z} \left[c_1^\dagger(\mathbf{R}_1) c_2(\mathbf{R}_1 + \hat{z}d/2)\right. \\ &\left. - c_1^\dagger(\mathbf{R}_1) c_2(\mathbf{R}_1 - \hat{z}d/2) - \text{H.c.}\right]. \end{aligned} \tag{14}$$

In the presence of a finite magnetic vector potential $\mathbf{A}(\mathbf{r})$, the tight binding Wannier states are modified by a phase so that

$$c_i(\mathbf{R}_i) \to c_i(\mathbf{R}_i) \exp\left[-\frac{ie}{\hbar c}\mathbf{R}_i \cdot \mathbf{A}(\mathbf{R}_i)\right], \tag{15}$$

where c is the speed of light. The assumption is made that the vector potential is slowly varying over the length scale of the crystal lattice, and we will make use of the fact that $\mathbf{A}(\mathbf{q})$ is strongly peaked about $\mathbf{q}=0$ throughout this section. To linear order in $\mathbf{A}$, then, Eq. (13) becomes

$$\mathbf{H^n} = \mathbf{H_0^n} - \frac{1}{c\Omega}\mathbf{j_0} \cdot \mathbf{A}(\mathbf{q}=0) \tag{16}$$

and Eq. (14) becomes

$$\begin{aligned}\mathbf{j} = \mathbf{j_0} &- \frac{e^2}{\hbar^2 c} \sum_{i,\mathbf{R}_i,\mathbf{r}_1} \sigma_i \mathbf{r}_1[\mathbf{r}_1 \cdot \mathbf{A}(\mathbf{R}_i)] c_i^\dagger(\mathbf{R}_i + \mathbf{r}_1) c_i(\mathbf{R}_i) \\ &-\frac{e^2 t_0 d^2}{8\hbar^2 c} \sum_{\mathbf{R}_1} \hat{z}[\hat{z} \cdot \mathbf{A}(\mathbf{R}_1)] \left[c_1^\dagger(\mathbf{R}_1) c_2(\mathbf{R}_1 + \hat{z}d/2)\right. \\ &\left. + c_1^\dagger(\mathbf{R}_1) c_2(\mathbf{R}_1 - \hat{z}d/2) + \text{H.c.}\right]. \end{aligned} \tag{17}$$

In the presence of a magnetic field, the observable current is given by $\langle \mathbf{j} \rangle$, and not $\langle \mathbf{j_0} \rangle$. We can rewrite Eq. (17) in a k space representation using Eq. (12):

$$\begin{aligned}\mathbf{j}(\mathbf{q}=0) = \frac{e}{\hbar} \sum_{\mathbf{k}} &\left[\mathbf{C}^\dagger(\mathbf{k}) \vec{\gamma}_{\mathbf{k}} \mathbf{C}(\mathbf{k})\right. \\ &\left. - \frac{e}{\hbar c\Omega} \mathbf{C}^\dagger(\mathbf{k}) [\vec{\vec{\gamma}}'_{\mathbf{k}} \cdot \mathbf{A}(\mathbf{q}=0)]\, \mathbf{C}(\mathbf{k})\right]. \end{aligned} \tag{18}$$

The vector $\vec{\gamma}_{\mathbf{k}}$ is a 4×4 matrix with three spatial components. It is essentially the Fermi velocity

$$\vec{\gamma}_{\mathbf{k}ij} = (-1)^{i-1} \frac{\partial Q_{ij}}{\partial \mathbf{k}},$$

where Q_{ij} is the Hamiltonian matrix of Eq. (3) and the factor $(-1)^{i-1}$ comes from the fact that C_i annihilates electron states for $i = 1,3$ and hole states for $i = 2,4$. The dyadic $\vec{\vec{\gamma}}'_{\mathbf{k}}$ is also a 4×4 matrix and it is essentially the effective mass tensor

$$\vec{\vec{\gamma}}'_{\mathbf{k}ij} = \frac{\partial^2 Q_{ij}}{\partial \mathbf{k} \partial \mathbf{k}}.$$

The first term in Eq. (18) is $\mathbf{j_0}(\mathbf{q}=0)$ while the second term contains the remaining two terms in Eq. (17).

The current $\langle \mathbf{j} \rangle$ which is generated by the applied magnetic field is given, to linear order in $\mathbf{A}$, by the Kubo formula[25]

$$\langle \mathbf{j}(t) \rangle = \langle \mathbf{j}(t) \rangle_0 + \frac{i}{\hbar} \int_{-\infty}^{t} dt' \left\langle \left[-\frac{1}{c}\mathbf{j_0}(t') \cdot \mathbf{A}(t'), \mathbf{j_0}(t)\right] \right\rangle_0.$$

In the London limit, for the case of a static applied field, this gives

$$\langle \mathbf{j}(\mathbf{r}) \rangle = \langle \mathbf{j}(\mathbf{r}) \rangle_0 - \frac{1}{c\Omega} \sum_{\nu} G^j_{\mu\nu}(0,0;0) \mathbf{A}_\nu(\mathbf{r}), \tag{19}$$

where

$$\begin{aligned}G^j_{\mu\nu}(\mathbf{q},\mathbf{q}',i\omega_l) = &-\frac{1}{\hbar\Omega} \int_0^{\hbar\beta} d\tau\, e^{i\omega_l \tau} \\ &\times \langle \mathbf{T} \mathbf{j_0}_\mu(\mathbf{q},-i\tau) \mathbf{j_0}_\nu(\mathbf{q}',0) \rangle_0. \end{aligned}$$

G^j is the current-current correlation function, T is the

boson time-ordered product, $\omega_l = 2l\pi/\hbar\beta$ are the boson Matsubara frequencies, and μ and ν refer to the spatial components of j_0. The expectation values $\langle\rangle_0$ are taken with respect to the zero-field wave function. It is straightforward to evaluate G^2 in terms of the single-particle Green's functions:

$$G^2_{\mu\nu}(0,0;i\omega_l) = \lim_{q\to 0} \frac{e^2}{\beta\hbar^2\Omega} \sum_{n,k} \mathrm{Tr}\left[G(k;i\zeta_n - i\omega_l)\tilde{\gamma}_{k\mu} \times G(k+q;i\zeta_n)\tilde{\gamma}_{k\nu}\right]. \quad (20)$$

The first term in Eq. (19) is the diamagnetic contribution to the screening current. Using Eqs. (9) and (18) we may evaluate this explicitly:

$$\begin{aligned}\langle j(r)\rangle_{dia} &= \frac{1}{\Omega}\sum_q \langle j(q)\rangle_{dia} e^{iq\cdot r} \\ &= \frac{e^2}{\Omega\hbar c}\sum_k \mathrm{Tr}\left[G(k;\tau=0^-)\tilde{\gamma}'_k\right]\cdot A(r) \\ &= \frac{e^2}{\Omega\hbar^2 c}\sum_k \sum_{i=1}^{4} f[E_i(k)]\hat{\gamma}'_{kii}\cdot A(r). \quad (21a)\end{aligned}$$

where Tr is a trace over the components of the 4×4 matrix contained in the square brackets, and $\hat{\gamma}'_k = U^\dagger(k)\tilde{\gamma}'_k U(k)$. In order to derive Eq. (21a), we have used the fact that $\langle j_0\rangle_0 = 0$ and that $A(q)$ is peaked about $q = 0$. The second term in Eq. (19) is the paramagnetic contribution to the screening current. Evaluating Eq. (20) explicitly we have

$$\begin{aligned}\langle j\rangle_{para} = -\frac{e^2}{\Omega\hbar^2 c}\sum_{i,j=1}^{4}\sum_k \hat{\gamma}_{kij}[\hat{\gamma}_{kji}\cdot A(r)] \\ \times\left[\delta_{i,j}\frac{\partial f(E_i)}{\partial E_i} \right. \\ \left. +[1-\delta_{i,j}]\frac{f(E_i)-f(E_j)}{E_i-E_j}\right], \quad (21b)\end{aligned}$$

where $\hat{\gamma}_k = U^\dagger(k)\tilde{\gamma}_k U(k)$. This expression for the paramagnetic current is the same as in Ref. 14 where it was discussed at length. We will only repeat the points which are directly relevant to the current work, and the interested reader is referred to our earlier work. The total current produced by the magnetic field is

$$\begin{aligned}\langle j\rangle &= \langle j\rangle_{dia} + \langle j\rangle_{para} \\ &= -K\cdot A. \quad (22)\end{aligned}$$

It is straightforward to show that $K_{\mu\nu} = 0$ if $\mu \neq \nu$ (recall that μ and ν refer to spatial directions) so that the penetration depth is given by

$$\frac{1}{\lambda^2_\mu} = K_{\mu\mu}. \quad (23)$$

This is the main result for this section. In order to plot λ_μ^{-2} as a function of temperature in Sec. IV, we must evaluate the integrals in Eqs. (21a) and (21b) numerically.

We will finish this section with a few comments about Eqs. (21a) and (21b). In the usual treatment of the penetration depth the diamagnetic contribution to the screening current is $j_{dia} = -ne^2A/mc$, which is independent of temperature. The temperature dependence of the penetration depth, then, comes from the paramagnetic contribution to the screening currents which, for a one-band free electron metal with an isotropic gap, is

$$j_{para} = -\frac{ne^2}{2\mu\hbar c}\int_{-\mu}^{\infty} d\epsilon\,[v^f]^2\frac{\partial f(E)}{\partial E}, \quad (24)$$

where $E = [\epsilon^2+\Delta^2]^{1/2}$, v^f is the Fermi velocity, and μ is the chemical potential. The paramagnetic term counts the number of thermal excitations (broken Cooper pairs) which degrade the screening current. At $T = 0$ the paramagnetic term vanishes, so that $j = -ne^2A/mc$. When $\Delta = 0$ the paramagnetic term cancels the diamagnetic term exactly so that $j = 0$. For systems which are more complicated than the free electon gas, it is common to make the approximation $j_{dia} = -j_{para}|_{\Delta=0}$. The approximation is exact at $T = T_c$ and, provided the temperature dependence of the diamagnetic term is weak, the approximation is a good one. This is the approximation we made in our previous discussion of the two-layer model.[14] In the current work, however, we have treated j_{dia} in a fashion which is more consistent with the tight binding model, so that while Eq. (21b) is the same as we found previously, Eq. (21a) is different. There is little quantitative difference between the two approaches, however, since both expressions for the diamagnetic current are weakly temperature dependent and both cancel the paramagnetic current above T_c.

The most significant difference between Eq. (21a) and the usual expression for the penetration depth is the interband term, which is proportional to $[f(E_i) - f(E_j)]/[E_i - E_j]$. While the intraband term [which is proportional to $\partial f(E_i)/\partial E_i$] counts the number of thermally broken pairs, the interband term describes the degradation of the screening currents by interband transitions. The interband term does not vanish at $T = 0$ so that, unlike the single band case, there is a finite paramagnetic contribution to the screening current.

IV. RESULTS

The question we are attempting to address in this work is whether a proximity effect model can account for the experimentally observed anisotropy in the temperature dependence of the penetration depth in Y-123. In this section we will present the results of numerical calculations of the penetration depth for the model Hamiltonian introduced in Sec. II. We will compare these results to experiments and to related calculations made with a two-plane proximity model (in which the intrinsically normal layer is a two-dimensional plane). One of the main goals of this section is to emphasize the difference between two-plane proximity models and chain-plane models of the

type studied here.

To begin with, we will discuss calculations of the penetration depth in the two-plane proximity models.[11,14] One of the important features of the proximity model is that it introduces low energy excitations into the superconducting spectrum. The reason for this is that the induced gap in the intrinsically normal plane is proportional to the strength of the chain-plane coupling $t(k_z)$ (which vanishes at $k_z = \pi/d$) so that the gap will have a nodal structure even if the pairing interaction has isotropic s-wave symmetry. The need for a gap structure with nodes has been suggested, for example, by measurements[28] of λ_{ab} (the in-plane penetration depth) in twinned single crystals of Y-123. The linear dependence of $\lambda_{ab}(T)$ on T at low temperatures is easily explained by any gap structure with nodes.[29] While these measurements are commonly taken as support for d-wave models,[28] it has also been shown[11,14] that two-plane proximity models also result in linear low T behavior. Since a central theme in much of the work on proximity models[1,7–10,12,16] is that the pairing interaction in the intrinsically superconducting plane is s-wave, the low energy excitations in the induced gap are an essential feature of the proximity models.

In Fig. 2(a) we plot the penetration depth for our plane-chain proximity model for the case of an s-wave gap. We find that, unlike the case of the two-plane model, the temperature dependences of λ_a and λ_b are dramatically different. The most important difference is that the temperature dependence of λ_a is nearly identical to that of a single-layer s-wave material with no chains, while λ_b has a linear low T behavior similar to that found in the two-plane proximity models.[14] The factor of 2 difference between $\lambda_a(0)^{-2}$ and $\lambda_b(0)^{-2}$ comes from the screening currents carried in the b direction by the chains, and the linear T dependence in λ_b^{-2} at low temperatures comes from the node in the induced gap at $k_z = \pi/d$. The fact that the low T behavior of λ_a^{-2} is exponential and not linear indicates that pairs associated with a axis screening currents have a finite gap for all values of k_z. We can understand this in more concrete terms as follows: In Sec. III we showed that the screening current has two parts—a diamagnetic part which is roughly independent of T and a paramagnetic part which accounts for processes (such as thermal pair breaking) which degrade the screening currents. The temperature dependence of the penetration depth comes from the paramagnetic screening current, given in Eq. (21a). Despite its complicated appearance, Eq. (21b) has a simple physical interpretation. The factors $\hat{\gamma}_k$ are electron Fermi velocity *vectors*, while the two terms involving Fermi functions count the number of thermally excited quasiparticles which participate in intraband ($i = j$) or interband ($i \neq j$) paramagnetic processes. When we calculate the screening current in the a direction, then, the integrand in Eq. (21b) is weighted by the square of the Fermi velocity in the a direction. In Fig. 1, we can see that this is small both on segments of the Fermi surface associated with the chains and on segments of the plane Fermi surface which are distorted by the chains. The most obvious consequence of this is that the chains do not participate significantly in carrying currents in the a direction. A more subtle result is that, even though there is a node in the induced gap in the chains, it is not seen by electrons traveling in the a direction so that Cooper pairs which are part of the a axis screening current have a finite gap. The onset of thermal pair breaking, then, occurs at a much lower temperature in the b axis supercurrent than in the a axis supercurrent.

In Fig. 2(b) we plot the penetration depth for a d-wave order parameter and find results which are similar to the s-wave case: $\lambda_a(T)$ is essentially the same as found in single-layer d-wave models and $\lambda_b(T)$ resembles $\lambda_{ab}(T)$ found in the two-plane proximity models. As for the

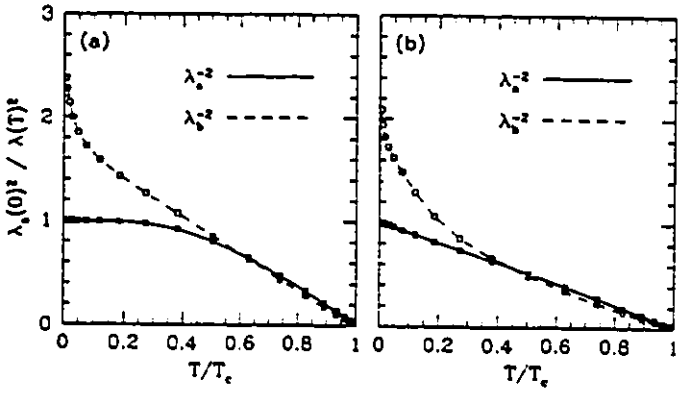

FIG. 2. (a) In-plane penetration depth for an s-wave order parameter. The penetration depth in the a direction (perpendicular to the chains) is nearly that of a pure s-wave superconductor in the absence of chains. The penetration depth in the b direction has a very different temperature dependence from that in the a direction because the size of the induced gap in the chains is much different from the size of the gap in the planes. The relative bandwidths of the chains and planes were determined by setting $\lambda_a^2(0)/\lambda_b^2(0) \sim 2.5$, in accordance with experiment. (b) In-plane penetration depth for a d-wave order parameter. Again, $\lambda_a(T)$ is essentially the same as for a single-layer d-wave superconductor, while the shape of $\lambda_b(T)$ reflects the structure of the induced gap in the chains as well as the planes.

case of an s-wave gap, the reason is that there are a larger number of low energy excitations in the chains than in the planes. The d-wave gap in the planes has nodes along $k_x = \pm k_y$, while the induced gap has nodes along $k_x = \pm k_y$ and $k_z = \pi/d$.

The large temperature dependence of the ab anisotropy seen in Figs. 2(a) and 2(b) is difficult to reconcile with measurements of $\lambda_a(T)$ and $\lambda_b(T)$ in untwinned crystals. In these experiments[5] λ_a and λ_b have a nearly identical temperature dependence, although their absolute magnitude differs by a factor of 1.5 at $T = 0$. In our model, the temperature dependence of the anisotropy is a result of the fact that Cooper pairs in the chains are more easily broken than Cooper pairs in the planes. Clearly, then, in a realistic model, the density of low energy excitations in the chains must be similar to that in the planes. This is not a trivial requirement. It implies that both the nodal structure and the magnitude of the gaps in the chains and planes be similar. It is possible to eliminate the nodes in the induced gap at $k_z = \pi/d$ by, for example, making the ansatz that $t(k_z) = t_0$ (this would describe a single bilayer). However, this is not sufficient to eliminate the temperature dependence of the anisotropy. For regions of the chain Fermi surface where $|\xi_1| \gg |t(k_z)|$, the induced gap is of the order[14] $\Delta_k t(k_z)^2/\xi_1^2$. In Fig. 1, the smallest induced gap occurs at the intersection of the chain Fermi surface with the Brillouin zone boundary (at $k_x = \pi/a$) at which $t_0^2/\xi_1(k)^2 \sim 0.023$. The onset of thermal pair breaking in the chains, therefore, will occur at a much lower temperature than in the planes.

The penetration depth in the c direction as a function of temperature is shown in Fig. 3. The shapes of the curves are similar to what we found in previous work[14] in which we examined a model with two planes per unit cell. Experimental observations of λ_c in Y-123 (Refs. 20, 22, and 29 and Y-124[19] are contradictory. All of the experiments find that at low temperatures $\lambda_c^{-2}(T)$ can be fitted by a linear T dependence, $\lambda_c(0)^2/\lambda_c(T)^2 \sim 1 - \alpha T/T_c$, but the slope of the fit varies dramatically. Two of the infrared experiments[19,22] find that $\alpha \ll 1$, while the third[29] finds that $\alpha \sim 1$ and the microwave experiment[20] finds that $\alpha \gg 1$. Until some sort of consensus is achieved, it will be difficult to say anything about our model.

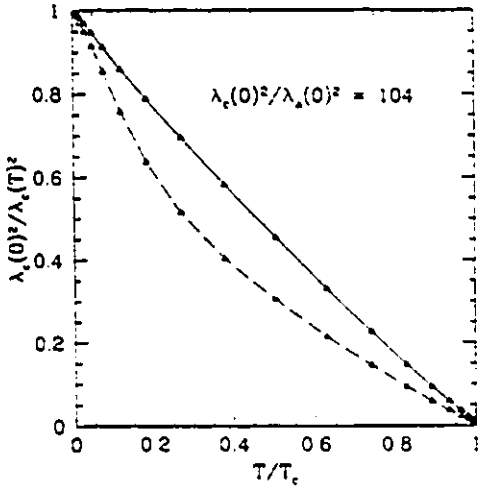

FIG. 3. Penetration depth in the c direction for both an s-wave (solid line) and a d-wave (dashed line) order parameter. The strength of the chain-plane coupling is chosen to be $t_0 = 50$ meV so that $\lambda_c^2(0)/\lambda_a^2(0) \sim 100$, as observed experimentally.

V. CONCLUSIONS

It is clear that our proximity effect model cannot describe the temperature dependence of the ab anisotropy of the penetration depth which has been observed experimentally by Zhang *et al.*[5] Essentially, the problem with our proximity model is that, unlike the case of the two-plane model, there are always regions of the chain Fermi surface on which the gap is small, so that the temperature scale over which the penetration depth parallel to the chains varies is much lower than the scale perpendicular to the chains. The question that needs to be answered, then, is to what extent is our model representative of proximity models in general.

The common feature of proximity models is that the chains are intrinsically normal but driven superconducting by their coupling to the planes. Where proximity models differ is in the nature of the chain-plane coupling. In our model we have made the assumption that the chain-plane coupling is coherent, so that chain states are coupled to plane states with the same value of k. The amount of mixing between the two states depends on the difference in energy between them so that, for example, in Fig. 1 the chain and plane Fermi surfaces are most strongly mixed in the neighborhood of their crossing. In a similar fashion, the induced gap on the chain is small (of the order of a few percent of the intrinsic gap in the plane) wherever the chain and plane Fermi surfaces are far apart. This is the reason for the large difference in the temperature dependence of λ_a and λ_b.

One solution to this is to couple the chains and planes incoherently, so that every state k on the planes is coupled equally to every state k′ on the chains. There is some evidence that there is incoherence along the c axis: Kleiner and Müller[30] have found an intrinsic Josephson effect in $Bi_2Sr_2CaCu_2O_8$ and, more recently, in underdoped Y-123. The dc resistivity of Y-123 in the normal state[3] shows semiconducting behavior in underdoped samples, and the optical conductivity along the c axis (see, e.g., Ref. 22, and references contained therein) has a nonmetallic response. For an incoherent model of the type described above, the induced gap on the chains is proportional to the average over the Fermi surface of the gap on the planes. The difficulty with this model is that, for a d-wave order parameter, the induced gap in the chains will vanish. It is, in fact, a general feature of d-wave order parameters that they do not contribute to incoherent processes (see, for example, Refs. 31 and 15). If on the other hand, we assume that the order parameter in the planes has an isotropic s-wave symmetry, then the induced gap on the chains will not vanish. The problem

now, however, is that incoherent coupling does not introduce a nodal structure into the gap the way coherent coupling does so that it is difficult to reconcile such a model with a linear low temperature penetration depth. For a model with incoherent chain-plane coupling to successfully describe the low temperature penetration depth, it would have to have an order parameter with nodes on the Fermi surface but whose Fermi surface average was nonzero, and the induced gap in the chains would have to be of the order of T_c so that the temperature dependence of λ_a and λ_b would be similar.

Leaving, for a moment, the discussion of the nature of the chain-plane coupling, we will now turn to a more conceptual problem–that of the size of the chain-plane coupling. The coupling strength t_0 is chosen to account both for the fact that $\lambda_c(T=0)/\lambda_a(T=0) \sim 10$ (Refs. 19–22) and for the size of the induced gap in the chains. As is well known, the chain-plane coupling can degrade T_c substantially. We find that for $t_0 = 50$ meV, T_c is only 65% of its value at $t_0 = 0$. It is also difficult to reconcile the picture of weakly coupled two-dimensional planes with such large values of the chain-plane coupling. In our model the ratio of the electron hopping strengths along the c and in-plane directions is $t_0/2\sigma_1 = 0.25$, so that it is difficult to imagine that the c axis coupling is a weak perturbation in an otherwise two-dimensional system. The challenge, therefore, for theories which begin with models of a single CuO_2 plane is to explain the large anisotropy between the a and b supercurrents in YBCO without invoking a large chain-plane coupling.

Kresin and Wolf[12] have suggested that proximity effect models require an inelastic channel for the chain-plane coupling. In their two-plane model, electrons can hop between the planes through coherent tunneling or through scattering from a phonon. Their model is more three-dimensional than the ones discussed above since the inelastic interplane coupling acts as a pairing process which leads to an increase in T_c. It is possible that in a chain-plane model, some kind of inelastic transport mechanism along the c axis might lead to a sufficiently large gap in the chains that λ_a and λ_b would have similar T dependences. The idea of a mixture of pairing interactions has recently been proposed by Song and Annett,[32] although they have limited their discussion to mixing phonons and Coulomb interactions within a single plane.

There is also the issue of whether a simple two-band model can be representative of Y-123. More careful band structure calculations[33,34] find that the Fermi surface has four pieces instead of two. The two additional pieces of Fermi surface come from the internal structure of the CuO_2 bilayer (which we have treated as a single-layer) and from the internal structure of the CuO chains. The inclusion of these two pieces of Fermi surface is not likely to affect the important results contained within this paper however: the additional piece of Fermi surface due to the CuO_2 bilayer has a nearly tetragonal symmetry (and will therefore not contribute to the anisotropy in the penetration depth) and the piece due to the CuO chains is small and will only make a small change to the screening currents.

Our final conclusion, then, is as follows: A proximity model for Y-123 in which the superconducting pairing interaction is localized to the planes and the chain-plane coupling is coherent will not account for the temperature dependence of the anisotropy of the penetration depth seen in experiments. It is possible that other models for the chain-plane coupling will be able to adequately describe the ab anisotropy. The single largest problem faced by proximity models is that penetration depth experiments[5] seem to indicate that the gap in the chains is of the same order as the gap in the planes.

ACKNOWLEDGMENTS

This work was supported by a Natural Sciences and Engineering Research (NSERC) grant, and by the Canadian Institute for Advanced Research (CIAR). The authors would like to thank D. N. Basov and J. S. Preston for helpful discussions.

[1] A. A. Abrikosov, Physica C **182**, 191 (1991); A. A. Abrikosov and R. A. Klemm, *ibid.* **191**, 224 (1992).
[2] T. A. Friedmann *et al.*, Phys. Rev. B **42**, 6217 (1990).
[3] R. Gagnon, C. Lupien, and L. Taillefer, Phys. Rev. B **50**, 3458 (1994).
[4] D. N. Basov *et al.*, Phys. Rev. Lett. **74**, 598 (1995).
[5] K. Zhang *et al.*, Phys. Rev. Lett. **73**, 2484 (1994).
[6] J. L. Tallon *et al.*, Phys. Rev. Lett. **74**, 1008 (1995).
[7] M. Tachiki, S. Takahashi, F. Steglich, and H. Adrian, Z. Phys. B **80**, 161 (1990); M. Tachiki, T. Koyama, and S. Takahashi, Prog. Theor. Phys. Suppl. **108**, 297 (1992); S. Takahashi and M. Tachiki, Physica C **170**, 505 (1990).
[8] A. I. Buzdin, V. P. Damjanović, and A. Yu. Simonov, Phys. Rev. B **45**, 7499 (1992); Physica C **194**, 109 (1992).
[9] L. N. Bulaevskii and M. V. Zyskin, Phys. Rev. B **42**, 10230 (1990).
[10] A. Yu. Simonov, Physica C **211**, 455 (1993).
[11] R. A. Klemm and S. H. Liu, Phys. Rev. Lett. **74**, 2343 (1995).
[12] V. Z. Kresin, H. Morawitz, and S. A. Wolf, *Mechanisms of Conventional and High T_c Superconductivity* (Oxford University Press, Oxford, 1993); V. Z. Kresin and S. A. Wolf, Phys. Rev. B **51**, 1229 (1995).
[13] W. A. Atkinson and J. P. Carbotte, Phys. Rev. B **52**, 1161 (1995)
[14] W. A. Atkinson and J. P. Carbotte, Phys. Rev. B **51**, 16371 (1995).
[15] W. A. Atkinson and J. P. Carbotte, Phys. Rev. B **52**, 6894 (1995).
[16] S. H. Liu and R. A. Klemm, Phys. Rev. B **45**, 415 (1992); R. A. Klemm and S. H. Liu, Physica C **191**, 383 (1992); **216**, 293 (1993).
[17] T. Schneider, H. De Raedt, and M. Frick, Z. Phys. B **76**, 3 (1989).
[18] S. Kettemann and K. B. Efetov, Phys. Rev. B **48**, 8515 (1992).
[19] D. N. Basov, T. Timusk, B. Dabrowski, and J. D. Jorgensen, Phys. Rev. B **49**, 3511 (1994).
[20] J. Mao, D. H. Wu, J. L. Peng, R. L. Greene, and S. M. Anlage, Phys. Rev. B **51**, 3316 (1995).

[21] J. Schützmann, S. Tajima, S. Miyamoto, and S. Tanaka, Phys. Rev. Lett. 73, 174 (1994).
[22] C. C. Homes, T. Timusk, D. A. Bonn, R. Liang, and W. N. Hardy (unpublished).
[23] J. E. Hirsch and F. Marsiglio, Phys. Rev. B 45, 4807 (1992).
[24] G. D. Mahan, *Many-Particle Physics* (Plenum Press, New York, 1986), p. 30.
[25] G. Rickayzen, *Green's Functions and Condensed Matter* (Academic Press, San Diego, 1980), p. 8.
[26] W. N. Hardy *et al.*, Phys. Rev. Lett. 70, 3999 (1993).
[27] J. Annett, N. Goldenfeld, and S. R. Renn, Phys. Rev. B 43, 2778 (1991).
[28] M. Prohammer and J. P. Carbotte, Phys. Rev. B 43, 5370 (1991).
[29] J. Münzel *et al.*, Physica C 235-240, 1087 (1994).
[30] R. Kleiner and P. Müller, Phys. Rev. B 49, 1327 (1994); P. Müller, Bull. Am. Phys. Soc. 40, 376 (1995).
[31] R. J. Radtke, C. N. Lau, and K. Levin (unpublished).
[32] J. Song and J. F. Annett, Phys. Rev. B 51, 3840 (1995).
[33] W. E. Pickett, H. Krakauer, R. E. Cohen, and D. J. Singh, Science 255, 46 (1992); W. E. Pickett, R. E. Cohen, and H. Krakauer, Phys. Rev. B 42, 8764 (1990).
[34] J. Yu, S. Massida, A. J. Freeman, and D. D. Koelling, Phys. Lett. A 122, 203 (1987).

4.3 Comment

In the time which has passed since the writing of this article, we have been able to extend our understanding of the implications of the penetration depth anisotropy. We will now share this improved understanding with the reader.

As we have pointed out in the article, the different temperature dependences of λ_a and λ_b are the result of the differences in the structure of the low energy excitations on different sections of the Fermi surface. In chapter 3, three energy scales in the superconducting density of states were identified. The lowest energy scale was that of the induced gap in the chains (*cf.* Fig. 3.5) which was of the order of 1 K. At the temperatures at which the penetration depth is measured, there is a large normal fluid component in the chains. In Fig. 2 of this section, the condensation of this fluid can only be seen for the lowest few temperatures. Since normal electrons do not contribute to the screening currents (their contributions to $\langle \mathbf{j} \rangle_{dia}$ and $\langle \mathbf{j} \rangle_{para}$ cancel), penetration depth experiments are not sensitive to a normal fluid. The experiments of (Zhang et al. 1994) will not see a small induced gap in the chains.

In chapter 3 we also identified an intermediate energy ($\sim$ 50 K) gap structure which we associated with the intersection of the chain and plane Fermi surfaces. It is *this* gap structure which results in the significant differences between $\lambda_a(T)$ and $\lambda_b(T)$. As we pointed out earlier, the penetration depth in a direction α is sensitive to low energy excitations which have a large component of Fermi velocity in the direction α. In the neighbourhood of the avoided Fermi surface crossing, the Fermi velocity is predominantly in the b direction (again recall Fig. 3.5), so that the intermediate energy gap only determines the structure of λ_b.

In summary then, we can say that the penetration depth experiments are not sensitive to regions of the chain Fermi surface on which there is a small induced gap. The essential problem with the chain-plane model is that the gap in the neighbourhood of the chain-plane crossing is much lower than the intrinsic gap in the planes.

Chapter 5

Josephson Effect

5.1 Introduction

The most innovative and powerful experimental techniques to have been developed recently have been Josephson junction techniques which are used to probe the symmetry of the order parameter (*cf.* Sec. 1.3.4). They rely on the fact that the current through a superconducting-insulating-superconducting (SIS) junction is driven by the phase difference accross the junction and—unlike most experiments—are sensitive to both the magnitude and phase of the order parameter.

In this chapter, we include an article which is concerned with one such experiment(Sun et al. 1994). The experiment was designed to measure the average of the gap in a CuO_2 plane over the entire Brillouin zone. The predictions were simple: if the average gap were not zero, then YBCO could not have a *d* wave gap. When Sun *et al.* measured a small, but finite, average gap, their experiments were criticized on technical grounds. It was suggested that the junction quality was poor, or that the Y-123 was susceptible to forming surface states.

We took the point of view, however, that the results are correct. The gist of our article is that the chains provide a sufficient orthorhombic distortion of the system to produce Josephson currents of the magnitude seen experimentally.

There is a slight change of notation between this paper and the work contained in Chapters 1, 2 and 3. The symbol t_0 is the coefficient of the chain-plane coupling strength. It is defined such that $t_0 \equiv 2t_\perp$.

Critical Josephson current in a model Pb/$YBa_2Cu_3O_{7-\delta}$ junction

W. A. Atkinson and J. P. Carbotte
Department of Physics and Astronomy, McMaster University, Hamilton, Ontario, Canada L8S 4M1
(Received 20 March 1995)

We consider a simple model for a c-axis Pb/$YBa_2Cu_3O_{7-\delta}$ Josephson junction. The observation of a nonzero current in such a junction by Sun *et al.* [Phys. Rev. Lett. 72, 2267 (1994)] has been taken as evidence against *d*-wave superconductivity in $YBa_2Cu_3O_{7-\delta}$. We suggest, however, that the pairing interaction in the CuO_2 planes may well be *d* wave but that the CuO chains destroy the tetragonal symmetry of the system. We examine two ways in which this happens. In a simple model of an incoherent junction, the chains distort the superconducting condensate away from $d_{x^2-y^2}$ symmetry. In a specular junction the chains destroy the tetragonal symmetry of the tunneling matrix element. In either case, the loss of tetragonal symmetry results in a finite Josephson current. Our calculated values of the critical current for specular junctions are in good agreement with the results of Sun and co-workers.

I. INTRODUCTION

The debate over the symmetry of the order parameter in the high-T_c copper-oxide superconductors has intensified over the last few years because of a number of suggestive experimental findings.[1] The discovery of linear low-temperature behavior in the penetration depths of single crystals of $YBa_2Cu_3O_{7-\delta}$ (Refs. 2 and 3) (YBCO) and $Tl_2CaBa_2Cu_2O_{8-\delta}$ (Ref. 4) has been taken as support for *d*-wave superconductivity,[5] although such experiments have been unable to exclude anisotropic *s*-wave models.[6–8] NMR relaxation rates[9,10] have been interpreted in terms of a *d*-wave order parameter.[11,12] More recently, angle-resolved photoemission experiments[13–15] have been able to map out the Fermi surface in the normal and superconducting states for $Bi_2Sr_2CaCu_2O_{8+\delta}$ and have found an anisotropic gap with nodes (or at least minima smaller than the resolution of the experiment) located approximately along the diagonals of the Brillouin zone. This is strongly suggestive of a *d*-wave gap although the experiments have been criticized because they sample only the surface states of the crystals.

A recent generation of experiments has attempted to resolve the issue of order-parameter symmetry by measuring its relative *phase* between different regions of the Brillouin zone. These experiments are all based on the fact that the current through a Josephson junction depends on the phase difference between the condensates on either side. Some of the experiments which have been performed[16–18] have attempted to measure the phase difference between electrons tunneling through different faces of a single crystal of YBCO. In a *d*-wave material, these electrons will have a phase of π relative to each other. Two of the experiments[16,17] suggest that YBCO has a *d*-wave order parameter, while the third[18] suggests an *s*-wave order parameter. More recently, there have been experiments which attempt to detect phase shifts of π across YBCO/YBCO junctions[19,20] in which the crystals are misaligned. These phase shifts, which are a signature of *d*-wave symmetry, have been found in both of the cited experiments.

The experiment in which we are interested in this article is that of Sun *et al.*[21] It is slightly different than the others: it relies on the fact that in a c-axis Pb/YBCO junction (in which the junction face is perpendicular to the YBCO *c* axis) the Josephson current will vanish if YBCO has a *d*-wave gap. Since the experiment finds a small, but finite Josephson current ($J_cR_n \approx 0.3$–0.9 mV, where R_n is the normal-state resistance of the junction and J_c is the critical Josephson current) the authors conclude that the order parameter cannot be purely *d* wave. On the other hand, their results are also inconsistent with simple *s*-wave theory since the measured critical voltages J_cR_n are an order of magnitude lower than expected. Following Ambegaokar and Baratoff,[22] and assuming that the gaps in YBCO and Pb are $\Delta_Y \sim 14$ meV and $\Delta_P \sim 1.4$ meV, respectively, they find

$$J_cR_n = \frac{2}{e}\frac{\Delta_Y\Delta_P}{\Delta_Y+\Delta_P}K\left(\frac{|\Delta_Y-\Delta_P|}{\Delta_Y+\Delta_P}\right) \sim 8\ \text{mV},$$

where K is the complete elliptic integral of the first kind.

In fact, the experiment of Sun *et al.*[21] does not immediately rule out YBCO having a $d_{x^2-y^2}$ order parameter. Tanaka[23] has shown, that while the usual treatment of the barrier as a second-order perturbation does lead to a vanishing Josephson current, higher-order terms in the perturbation series will not vanish. Unfortunately, attempts by one of the current authors[24] to fit the experimental results with a fourth-order calculation have been unsuccessful. On the other hand, it may be reasonable to expect that YBCO does not have a gap structure with a full $d_{x^2-y^2}$ symmetry since (optimally doped) YBCO is not tetragonal. Band-structure calculations[25,26] show that the CuO chains both contribute a piece of Fermi surface with orthorhombic symmetry and distort the band structure in the CuO_2 planes. O'Donovan *et al.*[27] have a

simple model of this: they consider a single CuO_2 plane in which the Fermi surface is distorted slightly away from tetragonal symmetry. They find that the reduced symmetry is strongly reflected in the gap, which picks up a small extended s-wave component while retaining its nodal structure. Another point of view is that of Xu *et al.*,[28] who treat YBCO as having tetragonal symmetry but take the gap to be $s+id$. Despite the very different starting points, both of these articles reach the conclusion that a gap which is roughly 10% s wave will explain the results of Sun *et al.*

In this article, we suggest that the nonzero critical current seen in Pb/YBCO c-axis Josephson junctions may be due to the CuO chains. We consider a phenomenological model for YBCO in which the unit cell contains a CuO_2 plane and a CuO chain and calculate the tunneling current for a Pb/YBCO junction as a function of the chain-plane coupling strength. In Sec. II, we introduce our model for YBCO. In Sec. III we derive an expression for the critical Josephson current. In Sec. IV we discuss the results of numerical calculations. We finish with a brief conclusion in Sec. V.

II. MODEL

We wish to consider a simple model for a Pb/YBCO Josephson junction. For the sake of clarity, we will take Pb (YBCO) to be on the left (right) side of the junction. We treat Pb as an ordinary free-electron metal with an isotropic BCS gap. YBCO is treated with a simplified model in which there are alternating layers of chains and planes. The planes and chains are weakly coupled by coherent electron hopping and the planes contain a BCS-like pairing interaction with a $d_{x^2-y^2}$ symmetry. The chains are driven superconducting by a proximity effect. This model is related to models studied elsewhere[29–35] in which both layers are treated as planes and (with the exception of Ref. 35 where it is d wave) the order parameter is s wave. It should be emphasized that this model is only suitable for weak chain-plane coupling. As the coupling is increased, the pairing potential begins to affect electrons in the chains directly. The problem becomes more complicated in this case and has only been examined in various special limits.[30,33,36–38]

The experiment we wish to describe is one in which the c axis of YBCO is normal to the junction.[21] Furthermore, we assume that the tunneling junction is adjacent to a CuO_2 plane.[39] Then our Hamiltonian can be written

$$\mathrm{H} = \mathrm{H_0}^l + \mathrm{H_0}^r + \mathrm{T}, \tag{1}$$

where $\mathrm{H_0}^l$ and $\mathrm{H_0}^r$ describe the uncoupled Pb and YBCO subsystems and T describes the coupling through the junction. We define $c_{k\sigma}$, $a_{1k\sigma}$, and $a_{2k\sigma}$, to be the electron annihilation operators with wavevector k and spin σ, in the Pb, YBCO planes and YBCO chains, respectively. We can write

$$\mathrm{H_0}^l - \mathrm{N}^l\mu = \sum_{k,\sigma} \epsilon(k) c^\dagger_{k\sigma} c_{k\sigma} - \sum_k \left[\Delta^l c^\dagger_{k\uparrow} c^\dagger_{-k\downarrow} + \Delta^{l*} c_{-k\downarrow} c_{k\uparrow}\right], \tag{2a}$$

$$\mathrm{H_0}^r - \mathrm{N}^r\mu = \sum_{k,\sigma} \left[a^\dagger_{1k\sigma} a_{1k\sigma} \xi_1(k) + a^\dagger_{2k\sigma} a_{2k\sigma} \xi_2(k)\right] + \sum_{k,\sigma} \left[t(k) a^\dagger_{1k\sigma} a_{2k\sigma} + t^*(k) a^\dagger_{2k\sigma} a_{1k\sigma}\right] - \sum_k \left[\Delta^r_k a^\dagger_{1k\uparrow} a^\dagger_{1-k\downarrow} + \Delta^{r*}_k a_{1-k\downarrow} a_{1k\uparrow}\right], \tag{2b}$$

$$\mathrm{T} = \sum_{k,q} T_{kq} c^\dagger_{k\sigma} a_{1q\sigma} + T^*_{kq} a^\dagger_{1q\sigma} c_{k\sigma}. \tag{2c}$$

The normal-state dispersion in Pb is $\epsilon = \hbar^2k^2/2m^* - \mu$, and the mean-field order parameter Δ^l is isotropic. The dispersions ξ_1 and ξ_2 are the normal-state dispersions of the YBCO planes and chains in the limit of no chain-plane coupling:

$$\xi_1 = -2\sigma_1[\cos(k_x) + \cos(k_y)] - \mu_1, \tag{3a}$$

$$\xi_2 = -2\sigma_2 \cos(k_y) - \mu_2 \tag{3b}$$

with $-\pi < k_x, k_y < \pi$ and where μ_1 and μ_2 include information about both the chemical potential and the offset of the bands from one another. The strength of the plane-chain coupling is given by $t(\mathbf{k})$ which, in the tight binding limit, depends[35] only on k_z. To simplify matters further, we take the chain-plane distances to be the same on either side of a chain, so that

$$t(k_z) = t_0 \cos(k_z/2), \tag{4}$$

with $-\pi < k_z < \pi$. The mean-field order parameter in YBCO, Δ^r_k, is a thermal average of electron pairs in the CuO_2 planes *only*. This is because we make the ansatz that the pairing is localized to the planes:

$$\Delta^r_k = \sum_{k'} V_{kk'} \langle a_{1-k'\downarrow} a_{1k'\uparrow} \rangle, \tag{5}$$

where $V_{kk'}$ is the BCS-like pairing interaction in the planes. If, for simplicity, we assume that the pairing interaction is separable, so that $V_{kk'} = V\eta_k\eta_{k'}$, with $\eta_k = \cos(k_x) - \cos(k_y)$ for a d-wave interaction, then we may write $\Delta^r_k = \Delta^r_0 \eta_k$.

We will find it convenient to work within the Nambu formalism, in which we define

$$\mathrm{C}(k) = \begin{bmatrix} c_{k\uparrow} \\ c^\dagger_{-k\downarrow} \end{bmatrix} \tag{6a}$$

and

$$\mathbf{A}(\mathbf{k}) = \begin{bmatrix} a_{1\mathbf{k}\uparrow} \\ a^{\dagger}_{1-\mathbf{k}\downarrow} \\ a_{2\mathbf{k}\uparrow} \\ a^{\dagger}_{2-\mathbf{k}\downarrow} \end{bmatrix}, \tag{6b}$$

so that the uncoupled Hamiltonians may be written,

$$\mathbf{H}^0 = \sum_{\mathbf{k}} \mathbf{C}^{\dagger}(\mathbf{k})\mathcal{H}_0^l(\mathbf{k})\mathbf{C}(\mathbf{k}) + \sum_{\mathbf{k}} \mathbf{A}^{\dagger}(\mathbf{k})\mathcal{H}_0^r(\mathbf{k})\mathbf{A}(\mathbf{k}) \tag{7a}$$

with

$$\mathcal{H}_0^l(\mathbf{k}) = \begin{bmatrix} \epsilon(\mathbf{k}) & -\Delta^l \\ -\Delta^{l*} & \epsilon(-\mathbf{k}) \end{bmatrix} \tag{7b}$$

and

$$\mathcal{H}_0^r = \begin{bmatrix} \xi_1(\mathbf{k}) & -\Delta_{\mathbf{k}}^r & t(\mathbf{k}) & 0 \\ -\Delta_{\mathbf{k}}^{r*} & -\xi_1(-\mathbf{k}) & 0 & -t^*(-\mathbf{k}) \\ t^*(\mathbf{k}) & 0 & \xi_2(\mathbf{k}) & 0 \\ 0 & -t(-\mathbf{k}) & 0 & -\xi_2(-\mathbf{k}) \end{bmatrix}. \tag{7c}$$

The eigenvalues of the Hamiltonian matrices are $E_i^{l/r}(\mathbf{k})$ with $E_i^l = (E^l, -E^l)$,

$$E^l = \sqrt{\epsilon^2 + \Delta^{l2}}, \tag{8a}$$

and $E_i^r = (E_+^r, E_-^r, -E_-^r, -E_+^r)$,

$$E_{\pm}^{r2} = \frac{\xi_1^2 + \xi_2^2 + \Delta_{\mathbf{k}}^{r2}}{2} + t^2 \pm \sqrt{\left[\frac{\xi_1^2 - \xi_2^2 + \Delta_{\mathbf{k}}^{r2}}{2}\right]^2 + t^2[(\xi_1 + \xi_2)^2 + \Delta_{\mathbf{k}}^{r2}]} \tag{8b}$$

and the unitary transformations which diagonalize the Hamiltonian are

$$\mathcal{U}^l(\mathbf{k}) = \frac{1}{\sqrt{2E^l}} \begin{bmatrix} \frac{\Delta^l}{\sqrt{E^l - \epsilon}} & \frac{\Delta^l}{\sqrt{E^l + \epsilon}} \\ \frac{\epsilon - E^l}{\sqrt{E^l - \epsilon}} & \frac{\epsilon + E^l}{\sqrt{E^l + \epsilon}} \end{bmatrix} \tag{9a}$$

and $\mathcal{U}_{ij}^r = \mathcal{U}_i^r(E_j)$,

$$\mathcal{U}_i^r(E_j^r) = \frac{1}{\sqrt{C}} \begin{bmatrix} (E_j^r - \xi_2)A \\ -(E_j^r + \xi_2)B \\ tA \\ tB \end{bmatrix}, \tag{9b}$$

$$A = t^2 - (\Delta_{\mathbf{k}}^r + E_j^r + \xi_1)(E_j^r + \xi_2),$$

$$B = t^2 - (\Delta_{\mathbf{k}}^{r*} + E_j^r - \xi_1)(E_j^r - \xi_2),$$

$$C = A^2[t^2 + (E_j^r - \xi_2)^2] + B^2[t^2 + (E_j^r + \xi_2)^2]. \tag{9c}$$

The Hamiltonian may, therefore, be written

$$\mathbf{H}_0 - \mathbf{N}\mu = \sum_{\mathbf{k}} \sum_{i=1}^{2} \tilde{\mathbf{C}}_i^{\dagger}(\mathbf{k})\tilde{\mathbf{C}}_i(\mathbf{k})E_i^l(\mathbf{k}) + \sum_{\mathbf{k}} \sum_{i=1}^{4} \tilde{\mathbf{A}}_i^{\dagger}(\mathbf{k})\tilde{\mathbf{A}}_i(\mathbf{k})E_i^r(\mathbf{k}), \tag{10}$$

where, for example, $\tilde{\mathbf{C}}_i(\mathbf{k}) = \sum_j \mathcal{U}_{ij}^{l\dagger}(\mathbf{k})\mathbf{C}_j(\mathbf{k})$.

In the normal state, the YBCO band energies are

$$\epsilon_{\pm} = \frac{\xi_1 + \xi_2}{2} \pm \sqrt{\frac{(\xi_1 - \xi_2)^2}{4} + t^2}. \tag{11}$$

and their Fermi surfaces are given by $t^2 = \xi_1\xi_2$. In Fig. 1(a) we plot the Fermi surfaces in the $k_x k_y$ plane for a range of t. When $t = 0$, the two pieces of Fermi surface are just the Fermi surfaces of the isolated planes and chains, given by $\xi_1 = 0$ and $\xi_2 = 0$, respectively. There is a Fermi surface crossing at $\xi_1 = \xi_2 = 0$. As t is increased, the Fermi surfaces are pushed apart, and the crossing becomes an avoided crossing. Far away from the avoided crossing, each piece of Fermi surface is predominantly chain or plane in character. However, near the avoided crossing, the two bands are hybridizations of the chain and plane states. In the superconducting state this has the important effect of distorting the gap away from the $d_{x^2-y^2}$ symmetry of the pairing interaction. In Figs. 1(b) and 1(c), we show the quasiparticle band structure [given by Eq. (8b)] in the superconducting state along the two paths $k_y = 0$ and $k_y = 2k_x/3$ (with $k_z = 0$ in both cases). For comparison purposes, we show the same spectra in the $t = 0$ limit. Along $k_y = 0$, the two pieces of Fermi surface are far enough apart that one piece is predominantly chainlike, while the second is predominantly planelike. If we take the term "gap" to mean a local minimum in E_- along paths of the type $k_y = \alpha k_x$ then we can see that there is a double gap structure along the $k_y = 0$ direction. The larger of the two gaps can be identified with the CuO_2 plane and is perturbed from $|\Delta_{\mathbf{k}}|$ by a term of order $|\Delta_{\mathbf{k}}|t^2/(\xi_1^2 - \xi_2^2)$. The second gap is the induced gap in the chains, and it is of order $|\Delta_{\mathbf{k}}|t^2/(\xi_1^2 - \xi_2^2)$. The second path, $k_y = 8k_x/3$, passes through the avoided crossing. In Fig. 1(c), the band structure near the Fermi surface has little in common with the band structure in the $t = 0$ limit, and the two gaps are nearly equal to each other, but very different from $\Delta_{\mathbf{k}}$. It is the effect of the chain-plane coupling in this region of the Brillouin zone which produces the finite c-axis Josephson current.

The shape of the Fermi surfaces in Fig. 1(a) was chosen to qualitatively resemble the results of first-principles band-structure calculations.[25,26] Such calculations find a Fermi surface that has four pieces, two of which are similar to the ones shown in Fig. 1(a). The remaining two pieces of Fermi surface have a (nearly) tetragonal symmetry. These have not been accounted for here since the goal is to describe the effects of orthorhombic distortion with a simple model.

III. JOSEPHSON CURRENT

The current generated by T is $e\dot{\mathbf{N}}^l$, where $\mathbf{N}^l = \sum_{k,\sigma} c_{k\sigma}^{\dagger} c_{k\sigma}$ is the number of electrons in Pb and $\dot{\mathbf{N}}^l = -i/\hbar[\mathbf{N}^l, \mathbf{T}]$ so that

$$\langle \dot{\mathbf{N}}^l \rangle = 2\,\mathrm{Im} \sum_{k,q,\sigma} T_{kq} \langle c_{k\sigma}^{\dagger} a_{1q\sigma} \rangle. \tag{12}$$

Taking T as a perturbation we find that, to lowest order, the Josephson current is[40]

$$I = \frac{-2e}{\hbar^2}\mathrm{Re}\sum_{k,q,\sigma} T_{kq}\int_{-\infty}^{t} dt'\, e^{\eta t'}\langle[c^\dagger_{k\sigma}(t)a_{1q\sigma}(t), T(t')]\rangle, \tag{13}$$

where η is positive and vanishingly small, and the expectation value is now taken with respect to the uncoupled system. Equation (13) has both a supercurrent contribution, which depends on the expectation values $\langle c^\dagger_{k\uparrow}(t)c^\dagger_{-k\downarrow}(t')\rangle$ and $\langle a_{1-k\downarrow}(t')a_{1k\uparrow}(t)\rangle$, and a quasiparticle contribution, which depends on $\langle c^\dagger_{k\sigma}(t)c_{k\sigma}(t')\rangle$ and $\langle a^\dagger_{1k\sigma}(t)a_{1k\sigma}(t')\rangle$. In our case, the voltage across the

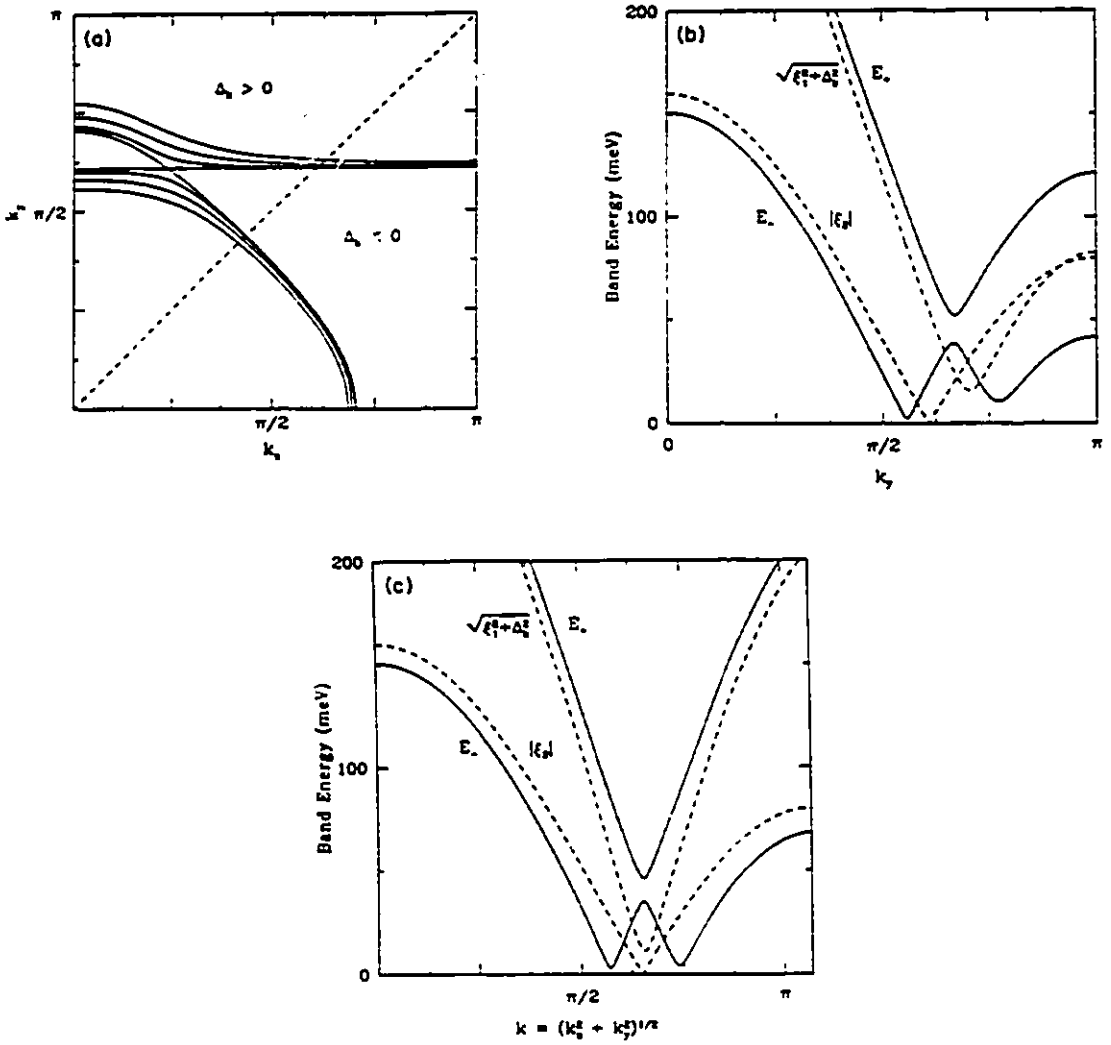

FIG. 1. Band structure of YBCO. In (a) we show the normal-state Fermi surface for the dispersion given in Eq. (11). The Fermi surface has two different pieces since the unit cell consists of a chain and a plane. The Fermi surfaces are shown for a range of chain-plane coupling values ($0 < t < 50$ meV). In the absence of chain-plane coupling ($t = 0$), the Fermi surfaces cross. As t is increased, the Fermi surfaces are pushed apart. The dashed line is the line along which Δ_k vanishes. In (b) and (c) we plot the quasiparticle excitation energies $E_\pm$ [Eq. (8b)] along $k_y = 0$ and $k_y = 8k_x/3$, respectively. We have taken $t = 40$ meV for these curves and have plotted $t = 0$ limits of $E_\pm$ $[(\xi_1^2 + \Delta_k^2)^{1/2}$ and $|\xi_2|]$ for comparison. At temperatures lower than the T_c of Pb, thermal excitation of quasiparticles in the YBCO is limited to the nodes of E_-. All results presented in this paper are for $\sigma_1 = 100$ meV, $\sigma_2 = 60$ meV, $\mu_1 = -80$ meV, $\mu_2 = 40$ meV.

junction is zero and the quasiparticle part vanishes. The supercurrent can be evaluated by rewriting the electron creation and annihilation operators in terms of the superconducting quasiparticle operators and noting that, for example,

$$\tilde{C}_m(\mathbf{k},t) = e^{-iE_m^l(\mathbf{k})t/\hbar}\tilde{C}_m(\mathbf{k},0). \tag{14}$$

It follows directly that

$$J = \frac{4e}{\hbar}\mathrm{Im}\sum_{i,j,\mathbf{k},\mathbf{q}} T_{\mathbf{kq}}T_{-\mathbf{k}-\mathbf{q}}\mathcal{U}_{1i}^{l*}(\mathbf{k})\mathcal{U}_{2i}^{l}(\mathbf{k})\mathcal{U}_{1j}^{r}(\mathbf{q})\mathcal{U}_{2j}^{r*}(\mathbf{q}) \times\frac{f(E_i^l(\mathbf{k})) - f(E_j^r(\mathbf{q}))}{E_i^l(\mathbf{k}) - E_j^r(\mathbf{q})}. \tag{15}$$

This is the basic equation for the Josephson current in the absence of an external voltage. For our particular model, this expression becomes

$$J(\phi) = \frac{4e}{\hbar}\sum_{\mathbf{k},\mathbf{q}}|T_{\mathbf{kq}}|^2\frac{\mathrm{Im}[\Delta^{l*}\Delta_{\mathbf{q}}^r]}{2E^l[E_+^{r2} - E_-^{r2}]}\left\{\frac{E_+^{r2} - \xi_2^2}{E_+^r}\left[\frac{1}{E^l + E_+^r} + 2\frac{E_+^r f(E^l) - E^l f(E_+^r)}{E^{l2} - E_+^{r2}}\right] - \frac{E_-^{r2} - \xi_2^2}{E_-^r}\left[\frac{1}{E^l + E_-^r} + 2\frac{E_-^r f(E^l) - E^l f(E_-^r)}{E^{l2} - E_-^{r2}}\right]\right\}. \tag{16}$$

In this equation $\mathbf{k}$ is the variable of integration for all terms associated with Pb (i.e., all variables with superscript l) and $\mathbf{q}$ is the variable of integration for all terms associated with YBCO. We have also used $T_{\mathbf{kq}} = T_{-\mathbf{k}-\mathbf{q}}^*$, which follows from time-reversal symmetry. The phase ϕ is the complex phase of $\Delta^{l*}\Delta_{\mathbf{q}}^r$. Equation (16) can be written $J(\phi) = J_c\sin(\phi)$, which defines the critical current J_c.

Although Eq. (16) is complicated in appearance, its behavior can actually be understood fairly easily. First of all, since $E_+ > |\xi_2|$ everywhere (see, e.g., Fig. 1) the sign of the coefficient of the first term is the same as the sign of $\Delta_{\mathbf{q}}$. Furthermore, the term inside the square brackets can easily be seen to be positive and decreasing with increasing T. A similar argument holds for the second term in Eq. (16), except that $E_-^2 - \xi_2^2$ changes sign between different regions of the Brillouin zone. In Fig. 1, however, we can see that $E_-^2 - \xi_2^2 < 0$ near the Fermi surface, so that at low enough temperatures (recall that T is less than one tenth of the T_c of YBCO here) the sign of the temperature dependent part of the second term is also determined by $\Delta_{\mathbf{q}}$. Whether J_c is an increasing or decreasing function of T, then, depends on the strength with which the integrand contributes to the integral in different regions of the Brillouin zone.

It is simple to show that, in the limit $t_0 \to 0$, Eq. (16) becomes the well-known equation of Ambegaokar and Baratoff[22]

$$J = \frac{2e}{\hbar}\sum_{\mathbf{kq}}|T_{\mathbf{kq}}|^2\frac{\mathrm{Im}[\Delta^{l*}\Delta_{\mathbf{q}}^r]}{E^lE^r} \times\left\{\frac{f(E^l) - f(E^r)}{E^l - E^r} - \frac{f(E^l) - f(-E^r)}{E^l + E^r}\right\}, \tag{17}$$

with $E^r = [\xi_1^2 + \Delta_{\mathbf{q}}^{r2}]^{1/2}$. Provided that $|T_{\mathbf{kq}}|$ is invariant under $\pi/2$ rotations in the q_xq_y plane, the Josephson current will vanish for a d-wave order parameter.

In order to proceed with Eq. (16) it is necessary to choose a form for the tunneling matrix element. The two common choices are

$$|T_{\mathbf{kq}}|^2 = |T|^2, \tag{18a}$$

(which describes an incoherent tunneling process) and

$$|T_{\mathbf{kq}}|^2 = \frac{P}{L^lL^r}|v_x^l(\mathbf{k})v_x^r(\mathbf{q})|\,\delta_{k_y,q_y} \tag{18b}$$

(which describes a specular tunneling process[41]). In Eq. (18b), P is the probability of transmission through the barrier for a single electron, L^l and L^r are the thicknesses of Pb and YBCO perpendicular to the junction and v^l and v^r are the semiclassical electron velocities in the x direction: $v_x^l = \partial\epsilon/\partial k_x$ and

$$|v_x^r| = \left|\frac{\partial\epsilon_\pm}{\partial q_x}\right| = |t_0\sin(q_x/2)|\frac{|t(q_x)|}{\sqrt{(\xi_1 - \xi_2)^2 + 4t(q_x)^2}}. \tag{19}$$

The δ function in Eq. (18b) conserves the momentum parallel to the junction face.

In the case of specular tunneling, the choice of v_x^r plays an important role in determining the magnitude of the Josephson current. For a single-band material, in which there are only CuO_2 planes, $v_x = t_0\sin(q_x)$ so that the entire Fermi surface contributes to the tunneling process, and the Josephson current vanishes because of the antisymmetry of the d-wave order parameter. In Eq. (19), however, there is a weighting factor which is only appreciable in regions where $|\xi_1 - \xi_2| < 2|t|$. Physically, this means that currents can only flow along the z axis in regions of the Brillouin zone near to where the Fermi surfaces cross: electrons traveling in the x direction must hop between the chains and planes and, since the chain-plane coupling is coherent (conserves $\mathbf{q}$), hopping can only take place in regions where the chain and plane Fermi surfaces are close together. In the $\mathbf{q}$-space integral in Eq. (16), v_x^r has the effect of restricting the integral

to one small region of the Brillouin zone over which the order parameter is roughly constant. Because of this Eq. (16) is not able to distinguish whether YBCO is s-wave or d wave for small t_0.

Another useful way of looking at v_z^r is that it destroys the antisymmetry of the integrand under rotations of $\pi/2$. For small t_0, the Josephson current is approximately given by Eq. (17). The integral is nonvanishing, however, because of $|T_{kq}|$'s lack of symmetry.

We will finish this section with a brief derivation of the normal-state junction reistance R_n, which is necessary to determine the critical voltage, J_cR_n. The calculation is similar to the one performed above for the supercurrent and, as before, we begin with Eq. (13). In this case, however, we are finding the quasiparticle current, J_n, driven through the junction in the normal state by a voltage V, and the supercurrent contribution to the integral vanishes. The voltage is taken into account by shifting the operators $c_{k\sigma}$ by a phase $\exp(ieVt/\hbar)$. Performing the integration over t' in Eq. (13), we find that, for small V and $T = 0$, we regain Ohm's law: $J_n = R_n^{-1}V$. For incoherent tunneling

$$R_n^{-1} = \frac{8\pi e^2|T|^2N^l(0)}{\hbar}\sum_q\sum_{+/-}\frac{t^2}{t^2+\xi_1^2}\delta(\epsilon_\pm), \quad (20a)$$

while for specular tunneling,

$$R_n^{-1} = \frac{8e^2P}{\hbar L^r}\sum_q|v^r(q)|\sum_{+/-}\frac{t^2}{t^2+\xi_1^2}\delta(\epsilon_\pm). \quad (20b)$$

The advantage of reporting J_cR_n instead of J_c is that J_cR_n is independent of the strength of the tunneling matrix element.

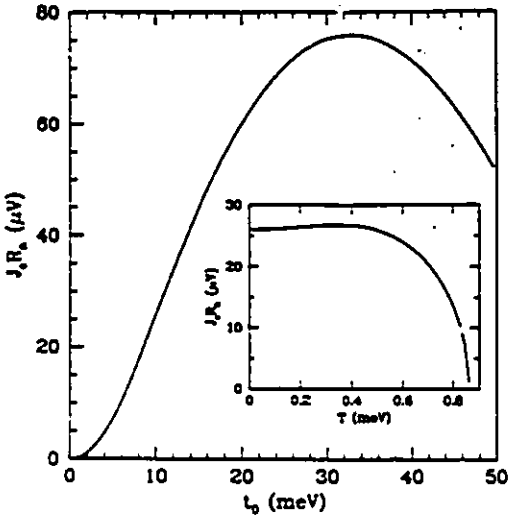

FIG. 2. Critical voltage, J_cR_n, for an incoherent junction. We show the dependence of $J_cR_n(T = 0)$ on the chain-plane coupling parameter t_0. For small t_0 we find the expected quadratic increase in the critical voltage as the coupling distorts the gap away from $d_{x^2-y^2}$. At larger t_0, the coupling to the chains weakens the condensate, as well as distorting its structure, leading to a maximum in the curve. This curve shows that, for the simple model of incoherent tunneling, distortion of the condensate by the chains cannot account for the experimentally measured values of $J_cR_n \sim O(0.5$ mV). The inset shows the temperature dependence of the critical voltage for $t_0 = 10$ meV. The curve increases slightly at low T. This stems from the multiband nature of the YBCO and the antisymmetry of the order parameter.

IV. RESULTS AND DISCUSSION

In this section we present the results of numerical calculations of the Josephson current through a c-axis junction. In Fig. 2 the dependence of the critical voltage at $T = 0$ on the chain-plane coupling is shown for an incoherent junction [Eq. (18a)]. The voltage scale of J_cR_n is tens of μV, which is two orders of magnitude lower than the value found from the Ambegaokar–Baratoff formula[22] (assuming both materials to be s wave), and a full order of magnitude lower than found in the experiments of Sun *et al.*[21] For small t_0 we have a quadratic increase in J_cR_n with t_0 which is due to the distortion of the gap away from $d_{x^2-y^2}$ symmetry by the chain-plane coupling. Increasing the coupling further, however, does not increase J_cR_n indefinitely. The maximum in the critical voltage is due to the fact that chain-plane coupling, as well as breaking the symmetry, reduces the gap in the CuO_2 planes. This is a feature which is particular to proximity-effect models. In the inset figure we plot the temperature dependence of J_cR_n for a relatively weak ($t_0 = 10$ meV) chain-plane coupling. The shape of the curve differs slightly from single-band models by the fact that the maximum value of J_cR_n ($J_cR_n \sim 0.026$ mV) does not occur at $T = 0$, but at $T \sim 0.4$ meV. This happens at temperatures which are low enough that $f(E^l) \sim 0$. As we have mentioned in the discussion following Eq. (16), whether J_c is an increasing or decreasing function of T depends on the sign of the order parameter in the regions of the Brillouin zone which contribute most to the integral. Since the induced gap in the chain is smaller than the gap in Pb in the region of the Brillouin zone where the chain and plane Fermi surfaces are far apart, the temperature dependence of J_cR_n at low T is determined by the induced gap. In Fig. 1 we can see that $\Delta_q < 0$ in the region where the induced gap is small so that J_cR_n is an increasing function of T. At larger values of T, thermal excitation of quasiparticles in Pb determines the temperature dependence of the critical voltage. It is clear from this discussion that $J_cR_n(T)$ will not have this kind of nonmonotonic behavior for an s-wave gap.

In our discussion of the current through an incoherent junction, we have used the word "gap" in a loose sense to describe the state of the condensate. The fact that the structure of the gap can be distorted by the chains highlights the fundamental difference between the gap and the order parameter, which is defined in Eq. (5). From the definition, it is clear that the order parameter has the

$d_{x^2-y^2}$ symmetry of the pairing interaction *regardless* of the strength of the chain-plane coupling. In fact, our intuitive definition of the "gap" is more closely related to the anomalous Green's function, F, which describes both the density and phase of the superconducting condensate. We can rewrite Eq. (15) for the Josephson current in terms of F:

$$J = \frac{4e}{\beta}\mathrm{Im}\sum_{\mathbf{kq}}\sum_{l} T_{\mathbf{kq}}T_{-\mathbf{k}-\mathbf{q}}F^{\mathrm{pl}}(\mathbf{k};i\zeta_l)F^{\mathrm{ch}}_{11}(\mathbf{q};i\zeta_l), \quad (21)$$

where F^{pl} is the anomalous Green's function in Pb, $F^{\mathrm{ch}}_{11} \equiv -\langle T a_{1-k_\uparrow}(-i\tau)a_{1k_\downarrow}(0)\rangle$ is the anomalous Green's function in the CuO_2 plane, β is the inverse temperature, $\zeta_l = (2l+1)\pi/\beta$ are the fermion Matsubara frequencies and β is the inverse temperature. Equation (21) makes it clear that Josephson junctions are sensitive to the structure of the *condensate* and not the pairing interaction. In a single-band material

$$F(\mathbf{k};\omega) = -\frac{\Delta_{\mathbf{k}}}{\omega^2 - E^2}, \quad (22)$$

where E is the quasiparticle energy. In our multiband model,

$$F^{\mathrm{ch}}_{11}(\mathbf{k};\omega) = -\frac{\Delta_{\mathbf{k}}(\omega^2 - \xi_z^2)}{(\omega^2 - E_+^2)(\omega^2 - E_-^2)}. \quad (23)$$

By comparing Eqs. (23) and (22) we can see how the chains affect the symmetry of the condensate, and that F_{11} does not share the symmetry of $\Delta_{\mathbf{k}}$. The point we would like to emphasize with this discussion, then, is that a finite current through an incoherent c-axis junction does seem to suggest that the condensate is not d wave, but does not not rule out the possibility that the *pairing interaction* is d wave.

In Figs. 3(a) and 3(b) we plot J_cR_n for a specular junction, in which the tunneling matrix element is given by Eq. (18b). For an isotropic Fermi surface and gap, the specular and incoherent cases yield identical results. As we can see in Fig. 3(a), however, the critical voltage is a full order of magnitude larger for a specular junction than for an incoherent junction. Furthermore, J_cR_n is a monotonically decreasing function of T. In Fig. 3(b), the dependence of both J_c and J_cR_n on t_0 is shown. As expected, J_c vanishes as $t_0 \to 0$, although here the reason is that the Fermi velocity of electrons in the z direction, v_z^r, vanishes. From Eq. (20b), it is clear that R_n^{-1} also vanishes as $v_z^r \to 0$, so that the product J_cR_n is nonvanishing. This is very different from the case of incoherent tunneling where R_n is largely independent of t_0. It seems, then, that our model for specular tunneling is in good agreement with the observations of Sun *et al.*[21] From Fig. 3(c) we can see that for $t_0 = 40$ meV, the critical voltage is around 1 mV, while Sun and his coworkers find critical voltages of 0.3–0.9 mV. This value of t_0 is also consistent with the observed anisotropy of the penetration depth, λ_c/λ_{ab}, as we have shown using a closely related model.[8]

The large difference between the results of the specular

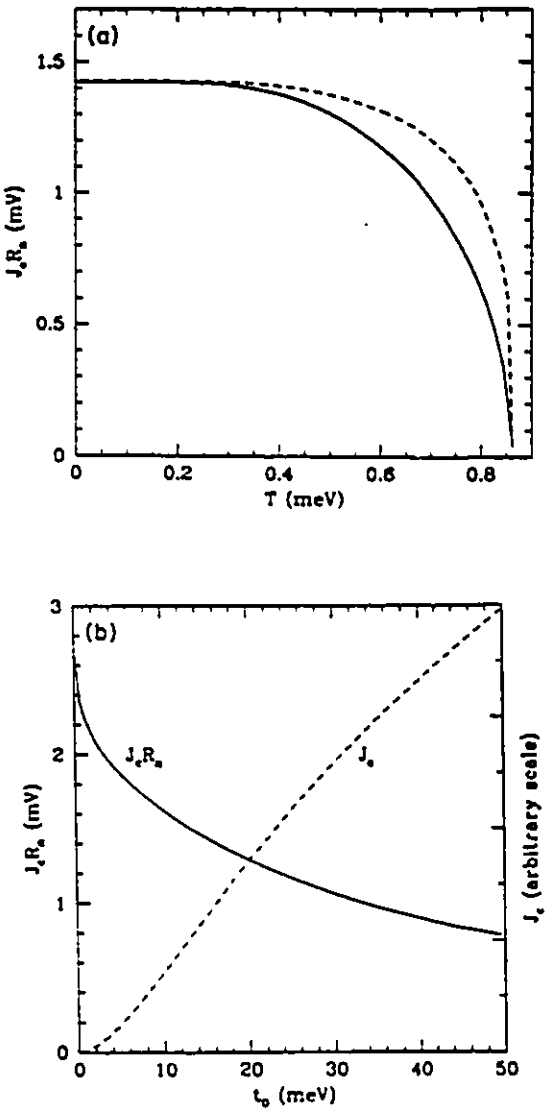

FIG. 3. Critical voltage, J_cR_n, for specular tunneling. Here the tunneling matrix element is chosen to conserve the component of the wave vector parallel to the junction. Furthermore, the tunneling matrix element is weighted in favor of particles with a large perpendicular velocity [Eq. (18b)]. In (a), we show the temperature dependence of J_cR_n for our multiband d-wave model (solid line), and for the simple s-wave model of Ambegaokar and Baratoff (Ref. 22) (dashed line). In order to make the $T = 0$ values of J_cR_n agree, we have taken $2\Delta/T_c \sim 0.12$ in the s-wave model. The most important difference between this figure and Fig. 2 is that critical current is a full order of magnitude larger here. In (b), both $J_cR_n(T = 0)$ and $J_c(T = 0)$ are plotted as functions of t_0. The magnitude of $J_c(T = 0)$ is arbitrary since the tunneling probability, P, has not been specified. The critical voltage is nonvanishing as $t_0 \to 0$ because R_n diverges.

and incoherent tunneling is a reflection of the important difference between the roles of the chains in the two types of tunneling. As we discussed earlier, an incoherent junction is sensitive to the symmetry of the condensate over the entire Brillouin zone. For a specular junction, on the other hand, the most important effect of the chains is to change the component of the Fermi velocity perpendicular to the junction. In Sec. III we showed that the tunneling is strongly weighted in favor of electrons with a large perpendicular component so that only one small region of the Brillouin zone, near where the chain and plane Fermi surfaces cross, contributes to the total tunneling current. The symmetry of the order parameter is largely irrelevant in this case. In the case of specular tunneling, then, the c-axis tunneling current is less a probe of the symmetry of the condensate than it is of the normal-state band structure.

We would like to finish this section with a brief discussion of an unresolved issue which is relevant to this work. Experiments on c-axis Josephson junctions have been performed with both twinned and untwinned crystals, and find similar values for the critical currents. Dynes[39] has suggested that the total critical current through a junction, in which one of the materials is heavily twinned and has a gap which changes sign under rotations of $\pi/2$, should vanish. This is because the phase locking of the condensate at twin boundaries causes overall phase shifts of π between adjacent regions. Adjacent regions should therefore have Josephson currents in opposite directions, and the total current should vanish. This argument is problematic for the work presented in this article. The argument is uncertain, however, because the behavior of the order parameter at twin boundaries is not well understood.

V. CONCLUSION

In this article we have calculated the Josephson current in a model c-axis YBCO/Pb junction. We have assumed that YBCO is made up of alternating layers of CuO_2 planes and CuO chains, stacked in the z direction, and that the layer adjacent to the junction is a CuO_2 plane. We take the pairing interaction in the YBCO to have $d_{x^2-y^2}$ symmetry. For an incoherent junction the tunneling current is sensitive to the symmetry of the superconducting condensate (although not of the pairing interaction), and we find that distortions of the condensate due to the chains are sufficient to yield nonzero Josephson currents. The currents are an order of magnitude smaller than observed experimentally. For a specular junction, the Josephson current is insensitive to the symmetry of the condensate because the tunneling matrix element is strongly influenced by the normal-state band structure. In our model, the Josephson current is due to one small region of the Brillouin zone over which the gap is roughly constant. The calculated currents for a specular junction are of the same order of magnitude as those found experimentally by Sun *et al.*[21]

[1] A review of the status of the debate as of early 1993 is contained in B. G. Levi, Phys. Today 46(5), 17 (1993).
[2] W. N. Hardy, D. A. Bonn, D. C. Morgan, R. Liang, and K. Zhang, Phys. Rev. Lett. 70, 3999 (1993); K. Zhang *et al.*, Phys. Rev. Lett. 73, 2484 (1994).
[3] J. E. Sonier *et al.*, Phys. Rev. Lett. 72, 744 (1994).
[4] H. Ning, H. Duan, P. D. Kirven, A. M. Hermann, and T. Datta, J. Supercond. 5, 503 (1993).
[5] M. Prohammer and J. P. Carbotte, Phys. Rev. B 43, 5370 (1991).
[6] J. Annett, N. Goldenfeld, and S. R. Renn, Phys. Rev. B 43, 2778 (1991).
[7] R. A. Klemm and S. H. Liu, Phys. Rev. Lett. 74, 2343 (1995).
[8] W. A. Atkinson and J. P. Carbotte, Phys. Rev. B 51, 16 371 (1995).
[9] J. A. Martindale *et al.*, Phys. Rev. B 47, 9155 (1993); C. P. Slichter *et al.*, J. Phys. Chem. Solids 54, 1439 (1993); S. E. Barrett *et al.*, Phys. Rev. B 41, 6283 (1990).
[10] Y. Kitaoka, K. Ishida, G. Q. Zheng, S. Oshugi, and K. Asayama, J. Phys. Chem. Solids 54, 1385 (1993).
[11] N. Bulut and D. J. Scalapino, Phys. Rev. B 45, 2371 (1992); Phys. Rev. Lett. 68, 706 (1992).
[12] D. Thelen, D. Pines, and J. P. Lu, Phys. Rev. B 47, 915 (1993).
[13] Z.-X. Shen *et al.*, Phys. Rev. Lett. 70, 1553 (1993); Z. X. Shen, D. S. Desseau, B. O. Wells and D. M. King, J. Phys. Chem. Solids 54, 1169 (1993); B. O. Wells *et al.*, Phys. Rev. B 46, 11 830 (1992).
[14] Y. Hwu *et al.*, Phys. Rev. Lett. 67, 2573 (1991).
[15] R. J. Kelley, J. Ma, B. Margaritondo, and M. Onellion, Phys. Rev. Lett. 71, 4051 (1993).
[16] D. A. Wollman, D. J. Van Harlingen, J. Giapintzakis, and D. M. Ginsberg, Phys. Rev. Lett. 74, 797 (1995); D. A. Wollman, D. J. Van Harlingen, W. C. Lee, D. M. Ginsberg, and A. J. Leggett, *ibid.* 71, 2134 (1993).
[17] D. A. Brawner and H. R. Ott, Phys. Rev. B 50, 6530 (1994).
[18] Pl Chaudhari and S.-Y. Lin, Phys. Rev. Lett. 72, 1084 (1994).
[19] C. C. Tsuei *et al.*, Phys. Rev. Lett. 73, 593 (1994).
[20] J. H. Miller, Jr., *et al.*, Phys. Rev. Lett. 74, 2347 (1995).
[21] A. G. Sun, D. A. Gajewski, M. B. Maple, and R. C. Dynes, Phys. Rev. Lett. 72, 2267 (1994).
[22] V. Ambegaokar and A. Baratoff, Phys. Rev. Lett. 10, 486 (1963); 11, 104 (1963).
[23] Y. Tanaka, Phys. Rev. Lett. 72, 3871 (1994).
[24] W. A. Atkinson (unpublished).
[25] W. E. Pickett, H. Krakauer, R. E. Cohen, and D. J. Singh, Science 255, 46 (1992); W. E. Pickett, R. E. Cohen, and H. Krakauer, Phys. Rev. B 42, 8764 (1990).
[26] J. Yu, S. Massida, A. J. Freeman, and D. D. Koelling, Phys. Lett. A 122, 203 (1987).
[27] C. O'Donovan, D. Branch, J. P. Carbotte, and J. S. Preston, Phys. Rev. B 51, 6588 (1995).
[28] J. H. Xu, J. L. Shen, J. H. Miller, and C. S. Ting, Phys.

Rev. Lett. 73, 2492 (1994).
[30] A. A. Abrikosov, Physica C 182, 191 (1991); A. A. Abrikosov and R. A. Klemm, *ibid.* 191, 224 (1992).
[31] L. N. Bulaevskii and M. V. Zyskin, Phys. Rev. B 42, 10230 (1990).
[32] M. Tachiki, S. Takahashi, F. Steglich, and H. Adrian, Z. Phys. B 80, 161 (1990); S. Takahashi and M. Tachiki, Physica C 170, 505 (1990); M. Tachiki, T. Kogama, and S. Takahashi, Prog. Theor. Phys. Suppl. 108, 297 (1992).
[33] A. L. Bundin, V. P. Damjanović, and A. Yu. Simonov, Phys. Rev. B 45, 7499 (1992); Physica C 194, 109 (1992).
[34] V. Z. Kresin, H. Morawitz, and S. A. Wolf, *Mechanisms of Conventional and High-T_c Superconductivity* (Oxford University Press, Oxford, 1993); V. Z. Kresin and S. A. Wolf, J. Supercond. 7, 865 (1994).
[34] A. Yu. Simonov, Physica C 211, 455 (1993).
[35] W. A. Atkinson and J. P. Carbotte, Phys. Rev. B 51, 1161 (1995).
[36] T. Schneider, H. De Raedt, and M. Frick, Z. Phys. B 76, 3 (1989).
[37] R. A. Klemm and S. H. Liu, Phys. Rev. B 44, 7526 (1991); S. H. Liu and R. A. Klemm, Physica C 216, 293 (1993); Phys. Rev. B 48, 4080 (1993).
[38] A. Bussmann-Holder, L. Genzel, A. Simon, and A. R. Bishop, Z. Phys. B 92, 149 (1993).
[39] R. C. Dynes (private communication).
[40] A. Barone and G. Patterno, *Physics and Applications of the Josephson Effect* (Wiley, New York, 1982).
[41] W. A. Harrison, *Solid State Theory* (McGraw-Hill, New York, 1970), pp. 264–270.

5.3 Comment

The abilibity of the chain-plane model to predict a critical Josephson current of the correct order of magnitude is very satisfying. One might question. however. the validity of this calculation given the failure of the model to correctly determine the penetration depth.

In answer to this. we simply point out that the penetration depth and the Josephson current calculations rely on two different properties of the chain-plane model. As we discussed at length in chapter 4. the penetration depth probes the low energy structure of the superconducting state. In marked contrast. the finite Josephson current for specular junction results from the normal state band structure. Since the Fermi surface of the chain-plane model does not have tetragonal symmetry. the tunneling matrix element through the junction also does not have tetragonal symmetry (Eq. (18b) of this chapter). The structure of the gap. therefore. plays almost no role in determining the current through a c axis Josephson junction in the chain-plane model.

This discussion would also hold for a realistic model of an incoherent junction. Although. in our treatment. the tunneling matrix element is tetragonally symmetric (Eq. (18a) of this chapter). a more realistic matrix element would not be. For a realistic model of an incoherent tunneling junction. we should probably have

$$|T_{\mathbf{k},\mathbf{q}}|^2 = \frac{P}{L^l L^r} |v_z^l(\mathbf{k}) v_z^r(\mathbf{q})|.$$

[compare with Eq. (18a)]. For this model of the junction. the results will be nearly the same as for the specular junction.

Chapter 6

Conclusions

To a large extent, the work in this thesis has been concerned with the spectrum of low energy excitations in $YBa_2Cu_3O_7$. The chain-plane model introduced in Chapter 2 provides a specific mechanism for calculating these excitations. We found that the low lying excitations fall into three energy scales: very low energy excitations (< 1 K) on the chains, intermediate energy excitations (< 50 K) near the intersection of the chain and plane Fermi surfaces and higher energy excitations (< 150 K) associated with the intrinsic gap in the planes. The gap in the chain-plane model has a great deal of structure.

In our comparisons of the chain-plane model with experiment we have not found much evidence for a complicated gap structure. In fact, it is tempting to conclude that, beyond its d wave structure, the gap is relatively featureless. Most of the modifications to the model which were suggested in Chapter 4 amount to attempting to reduce variations of the gap, both in k space and in real space (*ie.* between the chains and planes). The spatial variation of the gap lies at the heart of many of the problems we are having reconciling the model with experiment. It is interesting that it is the short coherence length along the c axis which allows the gap to vary so much between the chains and the planes. Perhaps the interpretation of the penetration depth measurements should be that the coherence length along the c axis is sufficiently large to suppress spatial variation of the order parameter.

We should stress that our calculations of the Josephson current through a Pb/$YBa_2Cu_3O_7$ junction do not depend on the structure of the gap. The success of our calculations in predicting the critical current are entirely the result of the band structure breaking the tetragonal symmetry of the tunneling matrix element. The chain-plane model would predict a finite current for nearly any gap structure provided that the normal state band structure did not have tetragonal symmetry. It is tempting to suggest that the success of

the model in predicting the Josephson current implies that the essential features of the band structure have been captured. This would probably be optimistic though.

Nonetheless, it might be fruitful to retain the simple model of the band structure but change the pairing interaction to increase the density of superfluid on the chains. In Chapter 4, many possible approaches to this were discussed.

There are several interesting experiments which were not discussed in much detail in the thesis which could provide insight into how to formulate the next generation of the model. The relatively short c axis scattering length found in Chapter 2 should probably be incorporated. Studies of the c axis optical conductivity can be interpreted in terms of a very broad Drude peak which is consistent with this (Homes et al. 1995a). The inclusion of incoherence along the c axis provides an additional twist since incoherent scattering is known to suppress d wave superconductivity (Radtke et al. 1993). We should point out that incoherence in the c axis transport does not necessarily mean that the chains and planes are coupled incoherently. One perfectly reasonable model of YBCO would have the chains and planes strongly (and coherently) coupled, with the weak link occurring at the Yttrium ion.

There is also mounting evidence of strong electron-phonon coupling for certain phonon modes (Homes et al. 1995b; Bussmann-Holder and Bishop 1995; Reedyk et al. 1994). One of the phonons which has been studied involves oscillations of the O(4) ion, which lies between the chains and planes. It would be interesting to pursue the possibility of phonon assisted hopping between the chains and planes [this possibility has been proposed (Kresin et al. 1993), although it has not been explored in detail].

There have been a few attempts to connect the c axis transport properties to the in-plane transport properties (Graf et al. 1993; Zha et al. 1995), but for the most part the scattering mechanisms in the two directions have been treated as separate entities. Any theory which includes the relatively large scattering necessary to explain the broad c axis optical response must also predict the correct in-plane optical response.

In summary, we can point to two deficiencies of the chain-plane model used in this thesis. The easiest of the failings to rectify is the lack of incoherence in the c axis transport. The more serious problem is the inability for this model to correctly account for the superfluid in the CuO chains.

Bibliography

Abramowitz. M. and I. Stegun (Eds.) (1972). *Handbook of Mathematical Functions*. New York: Dover.

Abrikosov. A. A. (1991). *Physica C 182*. 191.

Abrikosov. A. A. and R. A. Klemm (1992). *Physica C 191*. 224.

Aebi. P. et al. (1994). *Phys. Rev. Lett. 72*. 2757.

Anderson. P. W. (1992). *Science 256*. 1526.

Annett. J.. N. Goldenfeld. and S. R. Renn (1991). *Phys. Rev. B 43*. 2778.

Ashcroft. N. W. and N. D. Mermin (1976). *Solid State Physics*. Philadelphia: Saunders College.

Atkinson. W. A. and J. P. Carbotte (1995a). *Phys. Rev. B 51*. 1161.

Atkinson. W. A. and J. P. Carbotte (1995b). *Phys. Rev. B 51*. 16371.

Bardeen. J.. L. N. Cooper. and J. R. Schrieffer (1957). *Phys. Rev. 108*. 1175.

Barrett. S. E. et al. (1990). *Phys. Rev. B 41*. 6283.

Basov. D. N. et al. (1995). *Phys. Rev. Lett. 74*. 598.

Bednorz. J. G. and K. A. Müller (1986). *Z. Phys. B 64*. 189.

Brawner. D. A. and H. R. Ott (1994). *Phys. Rev. B 50*. 6530.

Bulaevskii. L. N. and Zyskin (1990). *Phys. Rev. B 42*. 10230.

Bulut. N. and D. J. Scalapino (1992). *Phys. Rev. B 45*. 2371.

Bussmann-Holder. A. and A. R. Bishop (1995). *Phys. Rev. B 51*. 3246.

Buzdin. A. I.. V. P. Damjanović. and A. Y. Simonov (1992a). *Phys. Rev. B 45*. 7499.

Buzdin. A. I.. V. P. Damjanović. and A. Y. Simonov (1992b). *Physica C 194*. 109.

Carbotte. J. P. (1990). *Rev. Mod. Phys. 62*. 1027.

Chaudhari. P. and S. Y. Lin (1994). *Phys. Rev. Lett. 72.* 1084.

Coffey. D. (1990). *Phys. Rev. B 42.* 6040.

Cooper. S. L. and K. E. Gray (1994). In D. M. Ginsberg (Ed.). *Physical Properties of High Temperature Superconductors IV.* pp. 61. New Jersey: World Scientific.

Dagotto. E. (1994). *Rev. Mod. Phys. 66.* 763.

de Wette. F. W.. J. Prade. A. D. Kulkarni. and U. Schröder (1988). *Phys. Rev. B 38.* 6583.

deGennes. P. G. (1966). *Superconductivity of Metals and Alloys.* New York: W. A. Benjamin. Inc.

Dynes. R. C. (1995). *J. Supercond. 8.* 345.

Fedro. A. J. and D. D. Koelling (1993). *Phys. Rev. B 47.* 14342.

Franck. J. P. (1994). In D. M. Ginsberg (Ed.). *Physical Properties of High Temperature Superconductors IV.* pp. 189. New Jersey: World Scientific.

Friedmann. T. A. et al. (1990). *Phys. Rev. B 42.* 6217.

Gagnon. R.. C. Lupien. and L. Taillefer (1994). *Phys. Rev. B 50.* 3458.

Giaever. I. (1960). *Phys. Rev. Lett. 5.* 147.

Graf. M. J.. D. Rainer. and J. A. Sauls (1993). *Phys. Rev. B 47.* 12089.

Haghighi. H. et al. (1991). *Phys. Rev. Lett. 67.* 383.

Hardy. W. N. et al. (1993). *Phys. Rev. Lett. 70.* 3999.

Hasegawa. T. et al. (1995). *J. Supercond. 8.* 467.

Hasegawa. T. and K. Kitazawa (1990). *Jpn. J. Appl. Phys. 29.* L434.

Hazen. R. M. (1990). In D. M. Ginsberg (Ed.). *Physical Properties of High Temperature Superconductors II.* pp. 121. New Jersey: World Scientific.

Homes. C.. T. Timusk. D. A. Bonn. R. Liang. and W. N. Hardy (1995a. Oct.). To Be Published in Physica C.

Homes. C.. T. Timusk. D. A. Bonn. R. Liang. and W. N. Hardy (1995b). To Be Published Can. J. Phys.

Hwu. Y. et al. (1991). *Phys. Rev. Lett. 67.* 2573.

Ishida. K. et al. (1993). *J. Phys. Soc. Jap. 62.* 2803.

Iye. Y. (1992). In D. M. Ginsberg (Ed.). *Physical Properties of High Temperature Superconductors III.* pp. 285. New Jersey: World Scientific.

Jelitto. R. J. (1969). *J. Phys. Chem. Solids 30.* 609.

Jiang. C. and J. P. Carbotte (1993). *Phys. Rev. B 48.* 4231.

Jorgensen. J. D. et al. (1990). *Phys. Rev. B 41.* 1863.

Josephson. B. D. (1962). *Phys. Lett. 1.* 251.

Kelley. R. J.. J. Ma. B. Margaritondo. and M. Onellion (1993). *Phys. Rev. Lett. 71.* 4051.

Kettemann. S. and K. B. Efetov (1992). *Phys. Rev. B 46.* 8515.

Kittel. C. (1986). *Introduction to Solid State Physics.* Toronto: Wiley.

Kleiner. R. and P. Müller (1994). *Phys. Rev. B 49.* 1327.

Klemm. R. A. and S. H. Liu (1995). *Phys. Rev. Lett. 74.* 2343.

Kotliar. G. (1988). *Phys. Rev. B 37.* 3664.

Kresin. V. Z.. H. Morawitz. and S. A. Wolf (1993). *Mechanisms of Conventional and High Tc Superconductivity.* Oxford: Oxford University Press.

Kresin. V. Z. and S. A. Wolf (1994). *Phys. Rev. B 49.* 3652.

Kuboki. K. and P. A. Lee (1995). cond-mat/9501030.

Lee. P. A. and N. Nagaosa (1992). *Phys. Rev. B 46.* 5621.

Leggett. A. J. (1992). *Braz. J. Phys. 22.* 129.

Ling. D. C.. G. Yong. J. T. Chen. and L. E. Wenger (1995). *Phys. Rev. Lett. 75.* 2011.

Liu. D. Z.. K. Levin. and J. Maly (1995). *Phys. Rev. B 51.* 1995.

Liu. R. et al. (1992). *Phys. Rev. B 45.* 5614.

Liu. S. H. and R. A. Klemm (1992). *Phys. Rev. B 45.* 415.

Liu. S. H. and R. A. Klemm (1993). *Physica C 216.* 293.

Manuel. A. A. et al. (1993). *J. Phys. Chem. Solids 54.* 1993.

Mathai. A. et al. (1995). *J. Supercond 8.* 491.

McMillan. W. L. (1968). *Phys. Rev. 175.* 537.

Miller. J. H.. Jr.. et al. (1995). *Phys. Rev. Lett. 74*. 2347.

Moler. K. A. et al. (1994). *Phys. Rev. Lett. 73*. 2744.

Monien. H. and D. Pines (1990). *Phys. Rev. B 41*. 6297.

Monthoux. P. and D. Pines (1993). *Phys. Rev. B 47*. 6069.

Nazarenko. A. and E. Dagotto. cond-mat/9510030.

ODonovan. C. and J. P. Carbotte (1995. Oct.). To Be Published in Physica C.

Pankaluoto. R.. A. Bansil. L. C. Smedskjaer. and P. E. Mignarends (1994). *Phys. Rev. B 50*. 6408.

Parks. R. D. (Ed.) (1969). *Superconductivity*. Volume I & II. New York: Dekker.

Phillips. N. E. et al. (1994). *J. Supercond. 7*. 251.

Pickett. W. E.. R. E. Cohen. and H. Krakauer (1990). *Phys. Rev. B 42*. 8764.

Pickett. W. E.. H. Krakauer. R. E. Cohen. and D. J. Singh (1992). *Science 255*. 46.

Plakida. N. M. (1995). *High Temperature Superconductivity*. New York: Springer.

Radtke. R. J.. K. Levin. H.-B. Schüttler. and M. R. Norman (1993). *Phys. Rev. B 48*. 653.

Reedyk. M.. T. Timusk. J. S. Xue. and J. E. Greedan (1994). *Phys. Rev. B 49*. 15984.

Renner. C. and O. Fischer (1995). *Phys. Rev. B 51*. 9208.

Rickayzen. G. (1965). *Theory of Superconductivity*. New York: Wiley-Interscience.

Schneider. T.. H. DeRaedt. and M. Frick (1989). *Z. Phys. B 76*. 3.

Shen. Z. X. et al. (1993a). *J. Phys. Chem. Solids 54*. 1169.

Shen. Z. X. et al. (1993b). *Phys. Rev. Lett. 70*. 1553.

Simonov. A. Y. (1993). *Physica C 211*. 455.

Song. J. and J. F. Annett (1995). *Phys. Rev. B 51*. 3840. Erratum: *Phys. Rev. B 52*. 6930 (1995).

Sun. A. G.. D. A. Gajewski. M. B. Maple. and R. C. Dynes (1994). *Phys. Rev. Lett. 72*. 2267.

Tachiki. M.. T. Koyama. and S. Takahashi (1992). *Prog. Theor. Phys. Suppl 108*. 297.

Tachiki. M.. S. Takahashi. F. Steglich. and H. Adrian (1990). *Z. Phys. B 80.* 161.

Takahashi. S. and M. Tachiki (1990). *Physica C 170.* 505.

Takigawa. M.. P. C. Hammel. R. H. Heffner. and Z. Fisk (1989). *Phys. Rev. B 39.* 7371.

Tikofsky. A. M. (1995). cond-mat/9501088.

Tobin. J. G. et al. (1992). *Phys. Rev. B 45.* 5563.

Tsuei. C. C. et al. (1994). *Phys. Rev. Lett. 73.* 593.

van Dover. R. B.. R. J. Cava. B. Batlogg. and E. A. Reitman (1987). *Phys. Rev. B 35.* 5337.

Veal. B. W. et al. (1987). *Appl. Phys. Lett. 51.* 279.

Wada. T. and T. Mihara (1987). *Jpn. J. Appl. Phys. 26.* L1475.

Wells. B. O. et al. (1990). *Phys. Rev. Lett. 65.* 3056.

Wolf. E. L. (1985). *Principles of Electron Tunneling Spectroscopy.* Oxford: Oxford.

Wollman. D. A. et al. (1993). *Phys. Rev. Lett. 71.* 2134.

Wollman. D. A.. D. J. V. Harlingen. J. Giapintzakis. and D. M. Ginsberg (1995). *Phys. Rev. Lett. 74.* 797.

Wu. M. et al. (1987). *Phys. Rev. Lett. 58.* 908.

Yu. J.. S. Massidda. A. J. Freeman. and R. Podloucky (1993). *Physica C 214.* 335.

Zha. Y.. S. L. Cooper. and D. Pines (1995). cond-mat/9503044.

Zhang. K. et al. (1994). *Phys. Rev. Lett. 73.* 2484.

Zhou. C. and H. J. Schulz (1992). *Phys. Rev. B 45.* 7397.